ABSTRACT

The Observation of Phase State and Temperature
Using Noninvasive Ultrasonic Waves

Colin M. Gregg, M.S.M.E.

Mentor: David A. Jack, Ph.D.

There are many ways to obtain temperature measurements and observe phase changes, but most rely on physical contact or a line-of-sight path with the material. Many industries ranging from oil and gas to food and beverage could expand their application space in select scenarios if a noninvasive means were available to identify the internal temperature state of a material within a confined vessel. This thesis investigates the hypothesis that the use of ultrasonic signals and the resulting time of flight and intensity of the high-frequency sound wave may be used to identify a material undergoing a phase change within a confined vessel. A wax melting experiment within a confined chamber has been designed to test this hypothesis. The results presented within this work demonstrate the viability of the method and the results for the speed of sound of a material as a function of temperature are highly repeatable and indicate a clear one-to-one ratio between the speed of sound and the temperature state.

The Observation of Phase and Temperature Change Using Ultrasonic Detection

by

Colin Michael Gregg, B.S.M.E.

A Thesis

Approved by the Department of Mechanical Engineering

_____

Kenneth Van Treuren, Ph.D., Chairperson

Submitted to the Graduate Faculty of
Baylor University in Partial Fulfillment of the
Requirements for the Degree
of

Masters of Science in Mechanical Engineering

Approved by the Thesis Committee

_____

David Jack, Ph.D., Chairperson

_____

Byron Newberry, Ph.D.

_____

Scott James, Ph.D.

Accepted by the Graduate School

May 2017

_____

J. Larry Lyon, Ph.D., Dean

Page bearing signatures is kept on file in the Graduate School.

TABLE OF CONTENTS

LIST OF FIGURES

LIST OF TABLES

CHAPTER ONE

Introduction

The hypothesis of this thesis is that ultrasound and the resulting change in the ultrasonic signal along with the measured speed of sound may be used to estimate the temperature and detect the phase change of a material without physical or visual access to the material. This work focuses on materials such as wax, foods, and polymers that go through a gradual phase change as a function of temperature. The speed of sound for each material tested showed measureable change as the material was heated and cooled as well as a significant change during a phase change event. These changes along with a basic knowledge of the materials are used in this thesis to estimate the instantaneous temperature and phase activity of the material in a confined vessel without using disruptive or invasive techniques like thermocouples.

The specific scenario of interest for this research involves a material which is heated or cooled within a confined vessel such that there is no access to the interior of the vessel and the material cannot be observed visually. With no physical access to the material a thermocouple cannot be used measure the temperature of the material, and without visual access infra-red temperature measurement can only provide container surface temperature measurements. In addition, the material cannot be probed or visually observed for changes in physical state. In this scenario, ultrasound measurements of speed of sound can be used to estimate the temperature and phase of the material non-invasively if the speed of sound to temperature relationship of the internal material is known.

Ultrasonic testing has been used for several decades to assist in quality control by detecting voids or measuring for dimensional accuracy as well as to determine material properties based on wave propagation. These ultrasound methods, discussed fully in Chapter 2, have the advantages of being non-destructive, as opposed to traditional tension testing or cutting cross sections for analysis. Ultrasound is non-invasive, and direct contact with a material of interest is not necessary as long as there is an acoustic path. Chapter 2 highlights that over the past two decades several ultrasound methods have been developed for monitoring changes in temperature or physical properties over time. Current uses of these ultrasound methods are applicable across a range of situations and materials including in-line estimation of polymer melt temperatures, monitoring of resin cures, and monitoring the softening of food products. This project seeks to expand on these methods by including both temperature and phase monitoring for an inaccessible and possibly unknown material.

In order to conduct this testing a custom system was constructed consisting of an acrylic container with up to eight ultrasonic transducers, as many as 29 thermocouples, a 250-Watt heat source, and three different materials. All results from the melting experiment were generated from a custom MATLAB analysis code. The experimental system is described in detail in Chapter 3. The three materials chosen for evaluation are Ecosoya pillar blend (a soy based candle wax), a base paraffin candle wax, and a standard baking chocolate. The Ecosoya wax was chosen for its ability to melt and solidify several times without noticeable damage to the material as well as a significant difference in the solid and liquid speed of sound. The base paraffin has a more complicated melt/ solidification process with a soft solid stage that is detectable in between the hard solid

and liquid stages and a wider gap in the speed of sound between the solid and liquid phases. The chocolate was chosen as a more common material which also experiences a liquid-solid phase change when heated or cooled; unfortunately the full solid phase occurs below room temperature so a phase change could not be detected. Each material was characterized using differential scanning calorimetry on a TA DSC Q20 to determine the temperatures at which phase change occurs, and the results are presented in Section 3.4. The results from the DSC testing give insight as to at what temperatures major changes in the materials speed of sound may occur during the confined container experiments.

The results presented in Chapter 4 demonstrate that as the material melted across the container there is a dramatic drop in the speed of sound and an increase in the signal intensity. Once the material is fully liquid and the heating continues the speed of sound continues to slowly decrease until the heat source was turned off. As the material cools the speed of sound approaches the original solid state value. This pattern is observed in all tests presented in Chapter 4 along with complete analysis of each material and images of the speed of sound measurements. Results demonstrate that the speed of sound can be used to estimate the temperature within 4°C for all materials tested and accurately detect a phase change of a material without having any direct physical contact or visual access.

While ultrasound measurements do provide an effective alternative to traditional temperature measurement methods there are drawbacks. One issue experienced during testing is a loss of acoustic coupling as a material cools and contracts leaving an air gap between the container wall and material that the signal cannot travel through. Another issue is that to quantify the material's temperature it is necessary to create a relational

function or a table of speed of sound at certain temperatures; conversely if a material is unknown, the results still show that by monitoring the changes in speed of sound over a short period of time it is possible to identify if a material is being heated or cooled. This later conclusion may not be applicable to materials that do not fit these trends. Even with these issues the ultrasound methods presented in this thesis may prove useful in applications including food and beverage production such as monitoring the temperature of the materials during production without the risk of contamination from opening containers, monitoring the temperatures and degree of cure during the curing process of composite materials in real time, and estimating the temperature of flows with in a pipe without disrupting the flow.

CHAPTER TWO

Literature Review

This chapter will cover the previous research performed in the areas of ultrasound as a means of monitoring temperature or changes in material properties as well as a background of the basics of ultrasound techniques. The use of ultrasound as a non-destructive, or in the case of this project non-invasive, measurement instrument has been steadily increasing in recent years. Recent applications have been researched and implemented such as; temperature measurements of polymer melts during extrusion [5, 7, 23-25] and injection molding [27], monitoring of the change of physical properties such as fruit softening [29, 30], plastic pellets melting [26], and epoxy resin curing [18-22]. These nondestructive testing techniques continue to advance and provide alternatives to traditional destructive or invasive measurement methods.

The effects of temperature on ultrasound have been investigated for many materials and the changes in signal can be used to predict temperature in many situations. Brown *et al*. [6] introduce a new method using through transmission ultrasound to measure the time of flight for a signal to monitor the temperature of polymer flow in a single screw extruder by placing ultrasound transducers on either side of the polymer melt mounted to metal wave guides. The time of flight measurements were used in tandem with a second temperature measurement method such as thermocouples or infra-red to estimate the temperature of the melt. Praher *et al*. [7] expanded on temperature monitoring of single screw extrusion by employing several receivers oriented radially around the ante-chamber to provide a 2-d temperature profile of the polymer melt. Jia and

Skilar [10] apply pulse-echo ultrasound methods to develop a temperature distribution and measure heat flux through a solid layered cement sample.

Phase change has a significant effect on the speed of sound, as well as the signal attenuation and intensity, of any material, which makes ultrasound methods a candidate for monitoring melt or solidification processes such as a melting polymer or a curing resin. Whitney and Green Jr. [18] use the resonant ultrasound frequency spectrum to monitor the cure of carbon fiber epoxy composites and possibly improve the laminate properties by reducing the number of voids present. Cheng *et al*. [26] applied pulse-echo ultrasound methods to determine the melt time and presence of air bubbles for polymer pellets within a mixer. Zhao *et al*. [27] examined the use of pulse-echo time of flight methods to monitor the melt flow arrival, the solidification, polymer properties, and ejection time of an injection molded part in-situ by incorporating an array of high-temperature ultrasound transducers directly into the mold.

Chapter Two, Section 1: Basics of Ultra Sound

Ultrasonic testing is a broad and useful tool that can be applied in several forms and used in many different scenarios. The basics of ultrasound measurements and equipment used in ultrasound testing are available in [1, 2]. Tuziuti et al. [3] as well as Rae and Brown [4] described the common practice of measuring the speed of sound for some polymers and composites. Rommetveit et al. [5] discussed a more advanced ultrasound technique utilizing a multilayered transducer model, that may be useful in future works. Similar practices and equipment are put to use in the experiments discussed in Chapter 3.

In his 1998 book “Fundamentals of Ultrasonic Nondestructive Evaluation: A Modeling Approach,”[1] Lester W. Schmerr, Jr. covered the basics of ultrasonic testing and computational modeling of ultrasound propagation. The first Chapter of the book covers the basic instrumentation typically used, such as ultrasound transducers, signal pulser and receiver, and signal viewing device (computer software or oscilloscope) as well as how and when to use certain techniques such as pulse/echo (single transducer) and through transmission (two transducers facing each other) methods. This heavily influenced the design of the experimental system described in Section 3.2 by providing information on how to set up an ultrasound measurement system as well as which measurement method would best fit the needs of the project (through transmission was selected). The Chapter also covers the three ways ultrasound information is presented, including the A-scan (a simple plot of the signal in terms of voltage vs. time), which is heavily used in this project.

Nde.ed.org [2] is a website formed as a collaboration between the NDT Education Resource center, The Collaboration for NDT Education, and Iowa State University as a resource for teaching the basics of nondestructive testing and ultrasonic methods. The site’s ultrasonic testing section covers everything from the basic principles and history of ultrasound as a tool in flaw detection to basic equipment and measuring techniques. The site also has a section on the physics of ultrasound that covers the basic equations of wave motion as well as attenuation, reflection, refraction, and some ultrasound material properties. In particular the process for calculating the speed of sound (shown in (3. 1)) based on the time of flight measurements was used heavily in this project.

Tuziuti et al. [3] explored the speed of sound through different areas of an injection molded PLA-clay composite part using the same through transmission methods selected for this project. The composite was created by mixing in a twin screw extruder followed by injection molding into a rectangular sample. The sample is then divided into three square segments of approximately 10 x 10mm. Ultrasound measurements are taken at the middle of each sample across the width (shorter side) and at three places across the length (longer side). Results show higher speeds of sound with higher %wt. of clay (0, 5, and 10%wt. were tested) as well as higher speeds of sound in areas where the polymer flow path (and inferred crystallinity) aligned with the wave path. This measurement process is the basis of the test method applied to the solid Ecosoya wax (as is described in Chapter Three, Section 5) to determine the effect of random voids formed during solidification by measuring the speed of sound of wax blocks in three directions.

Rae and Brown [4] outlined a similar process to Tuziuti et al. [3] for testing the longitudinal and shear speeds of sound in several materials using through transmission ultrasound and make observations as to how to improve the accuracy measurements. Materials testing include PEEK, PEEK with 10% carbon fiber, PTFE, HDPE, UHMWPE, polycarbonate, 6061-T6 aluminum, and copper. A single sample of each material was created that had five thicknesses organized in steps ranging from 3mm to 19mm. The speeds of sound were measured and used to calculate elastic constants for all samples except the PEEK with carbon fiber with an error of <1% for poisons ration (ν), <2% for Young's (E) and shear modulus (G), and <5% for bulk modulus (K). The experiment showed that the greatest accuracy is achieved when measuring samples of at least 9mm,

which is much smaller than the sample dimensions for this project given in Chapter Three, section 2.

Rommetveit et al. [5] developed a finite element model of a multi-layered transducer system in an effort to characterize a wax layer deposited on a steel plate. The multi-layered method consists of a maximum of six layers; from top down these were wax, steel, a coupling agent, the active piezo transducer, an isolation layer, and a passive ceramic. The transducer sends a signal in each direction with one wave reflecting off of the steel-wax interface and the wax-air interface, and the other reflecting off of the passive ceramic. This setup allowed the signal from the steel to be suppressed to isolate the wax signal. The wax signal was then used to estimate the properties of the deposited wax layer. It was determined that if density, thickness, or speed of sound is known, then the other two can be accurately estimated by the model.

Chapter Two, Section 2: Temperature Monitoring

Traditional temperature measurement methods such as thermocouples or infra-red measurements require either direct contact or visual access to the material of interest, but in some scenarios this access is undesirable (thermocouples altering the flow of a liquid in a pipe, or unavailable (a confined container or hard to reach area). For these situations ultrasound measurements can provide a useful non-invasive alternative to estimate the temperature of the material of interest. The following articles discuss several methods for monitoring the temperature of different materials in situations such as polymer extrusion [8, 9], solid materials like metals and ceramics [10-13], liquid materials like water and oil [14-18], and also air [19].

Brown et al. [6] proposed and tested a new method for measuring the temperature profile of a polymer melt flow by using through transmission ultrasound methods during single screw extrusion where conventional temperature measurement methods either provide a limited penetration of the melt flow (Infra-red) or disrupt the flow and cause shear heating (thermocouples). Through transmission ultrasound measurements were made by attaching transducers to wave guides that make direct contact with the melt flow in the extrusion die. Results showed that time of flight had a similar profile to the changing melt temperature over the course of the experiment with considerations made for pressure change. It is concluded that using ultrasound in tandem with another temperature measurement method will allow a temperature profile to be estimated, and that ultrasound provides the advantage of being non-invasive to the melt flow.

Praher et al. [7] utilized a method similar to that of by Brown et al. [6] and expanded the method to estimate the 2-d temperature distribution at the screw ante-chamber of an injection molding machine. A simulation was created to estimate the effects of temperature and pressure on the speed of sound through polypropylene and an experiment was performed to demonstrate the effectiveness of the design. The set up involved six ultrasound transducers, one transmitting and five receiving, attached to waveguides and arranged around one side of a cylinder at several angles. Three types of front surface geometries, flat front, half cylinder, and thin slit, were tested for the wave guides. The thin slit being chosen as the best for beam spread and non-invasiveness (the half cylinder would interfere with the internal material). The set up was tested on water with a heating element placed in the center of the cylinder to create a small temperature

gradient. It was determined from the experiment that the temperature distribution could be estimated within a reasonable error.

Christidis and Gunarathne [8] developed a temperature correction function for ultrasound measurements taken outside of a lab environment where temperature change can be a concern. The study focused on pulse-echo ultrasound method with an oil coupling medium with materials including marble, glass, Perspex, aluminum, brass, and steel. The function corrects for temperature by normalizing results to a pre-determined base temperature and takes the form of a third-order polynomial. It is stated that the correction would be valid for most materials that have a high acoustic impedance relative to the coupling medium.

Jia et al. [9] introduced a method for measuring a temperature distribution in a segmented solid material using pulse echo ultrasound methods. The material chosen for this experiment was a cylindrical ceramic rod. Holes were drilled through the rod to provide reflection points causing echoes. The rod was placed partially in a cylindrical furnace such that the end farthest from the transducer was at the center of the furnace and the transducer would not be harmed by heat. Time of flight was recorded as the furnace heated up to 1200°C and created a temperature distribution across the ceramic rod. The varying speeds of sound across each section allowed for an estimation of the temperature distribution of that segment. The temperatures are presented as piecewise functions (either piecewise constant or piecewise linear) that display the temperature across each segment of the ceramic rod. It was also suggested that this method could be used to estimate other properties that could vary by segment such as density.

Jia and Skilar [10] continued to develop the research described in [16] by applying similar methods to a layered cement sample. The sample is placed in an insulated container that houses heating elements to create a temperature distribution across the sample. The time of flight is measured as the echoes from each layer interface return to the receiver and the difference in speed of sound from a base temperature (20°C was used for this test) is related to the temperature distribution through the sample. An equation for the time of flight as a function of temperature distribution was derived and is fully explained in the paper.

El-Sariti et al [11] used through transmission ultrasound in order to monitor the speed of sound through bovine bone marrow over a temperature range of 17 to 44°C. The bone marrow was extracted from bovine femurs and bone fragments and other contaminates. The marrow is then inserted into a cylindrical bung and transducers are fitted to each side of the sample. The apparatus is then submerged in a water bath used to control the temperature of the sample (monitored by thermocouples). It was found that the relation of the speed of sound to temperature was linear with a coefficient of approximately -4.21 as the speed of sound decreases from 1456 m/s at 17°C and 1342 m/s at 44°C. Values stated are averages from the five animals tested.

Benedetto et al. [12] examined the changes in the speed of sound in pure water for changes in temperature (274-394 K) and pressure (0-90 MPa). A double reflector pulse echo apparatus was created in which a piezoelectric transducer was mounted offset from the center such that one acoustic path was 30.5mm and the other was 46mm. The apparatus is submerged in a temperature controlled water bath and a pressure control device is used to create a high pressure environment. Results show an approximately

linear increase in speed of sound as pressure is increased and temperature is held constant. As temperature is increased for constant pressures the speed of sound increased to a maximum around 350K decreases slightly up to 394K. Measured speed of sound values agree with values predicted by IAPWS-95 formulation within 0.1%.

Hoche et al. [13] describe a method for measuring critical process parameters (CPP) and critical quality attributes (CQA) of yeast fermented beverages. To simulate the fermentation process several ternary sample liquids were prepared with varying levels of water, maltose (0-12%), and ethanol (0-6%). An experimental set up was created using pulse/echo ultrasound methods to monitor the speed of sound through the sample liquid as the temperature was increased. A U-tube density meter was also used to monitor changes in density. The collected data was then used to form a series of polynomials which model the speed of sound behavior as temperature increases (5-30 °C) and ethanol values increase or maltose values decrease.

Zou et al. [14] create an effective density fluid model in order to examine the effects of temperature and varying permeability (which in this context can be thought of as the small pores of the sediment which are filled with water) on the acoustic properties of seafloor sand sediment. The study observes temperature from 0 to 30°C, frequencies from 0 kHz to 1000 kHz, and permeability from 0 to 1 ($10^{-10}m^2$). Trends show that at 40 kHz as temperature and permeability increase so does the speed of sound, and that attenuation increases as temperature increases and decreases as permeability increases. These trends change slightly for 200 kHz model; the speed of sound increase with temperature is much less drastic, and attenuation increases slightly with increased

permeability. This would indicate that a lower frequency transducer is more sensitive to changes in material temperature.

Oliveira et al. [15] investigated the speed of sound in soybean oil over the temperature range of 20-50°C. To do this a cylindrical sample cell of soybean oil was submerged into a thermally controlled water bath and a 1 MHz transducer was attached to the sample cell. The temperature of the bath was increased from 20 to 50°C in 5°C increments as ultrasonic time of flight was measured using a pulse-echo method. Speed of sound was then calculated from time of flight measurements along with the signal path distance. Results showed that over the tested temperature range the speed of sound decreased linearly as temperature was increased with the speed of sound ranging from 1484 m/s (20°C) to 1383 m/s (50°C). A simple linear regression was used to form a relational equation that can be used to predict the speed of sound in the soy bean oil for a given temperature.

Yebra et al. [16] automatized an experiment for measuring the speed of sound through several liquid materials over a pressure range of 0.1 to 95 MPa and a temperature range of 283.15 to 343.15 K. The experimental setup utilizes a cylindrical pressure vessel in which a sample liquid is placed with transducers on either side, one pulser and one receiver. Temperature is controlled by placing the vessel in a thermally controlled water bath. The entire experiment is automatized by computer controllers and data acquisition resulting in a full experiment time of 15 hours. Tested materials include water, methanol, hexane, heptane, octane, toluene, ethanol, and 1-propanol. Results show a general increasing speed of sound with increasing pressure, which is linear in the case of water and a slight curve for the other materials. The increase in temperature shifts the speed of

sound vs. pressure curves up for water and down for all other materials. These results were compared and are consistent with previously published values.

Kon et al. [17] develop a method for measuring dry bulb temperature and relative humidity using airborne ultrasound. The experimental setup used a sealed temperature and humidity chamber with a speaker and microphone inside (similar to the through transmission method used in this project) and a thermometer-humidity sensor to confirm any ultrasound measurements. Speed of sound measurements are made at temperatures ranging from 283.15 to 323.15 K and at relative humidity ranging from 30%, to 100%. Results show that the speed of sound increases with increasing humidity and temperature. Also for a higher set temperature the rate at which the speed of sound increases with increasing humidity also increases. The ultrasonically measured values of temperature and relative humidity agreed with the values from the thermometer-humidity sensor within 16.4% for relative humidity and within 0.7 K for temperature. It is concluded that although there is decent agreement between the traditionally measured values and the ultrasonically measured values. More accurate testing is needed to improve the effectiveness of the proposed method.

Chapter Two, Section 3: Physical Property Monitoring

The real time monitoring of changing material properties during processes such as polymer melting or resin curing is a difficult process. The occurrence of polymer melt is traditionally determined either off-line using differential scanning calorimetry (a method using a small material sample heated/cooled in a small chamber with a reference material to compare the heat flow into or out of the material), by measuring the resistance to rotation in a mixer or extruder, or by visual observation. The degree of cure for

thermosets is commonly tested destructively post manufacturing. Ultrasound can be used as an alternative in both scenarios to provide in-line real time measurements of the speed of sound to detect the change in the stiffness of materials resulting from a phase change. The articles below demonstrate the use of ultrasound properties such as time of flight, speed of sound, and attenuation to monitor the physical properties of materials such as curing thermoset resin and resin composites [18-22], melting polymers [23-28], and ripening food products [29, 30].

Whitney and Green Jr. [18] examined the use of resonant ultrasound spectroscopy to monitor the cure state of carbon fiber epoxy composites. The experiment was performed by passing signals through the metal tooling that the composite laminate is vacuum bagged to during cure. The resonant ultrasound spectrum was captured every 90 seconds during cure at frequencies ranging from 50 kHz to 85 kHz in 50 Hz steps. It was determined that the curing resin had a significant effect on the frequency spectrum that can be used to monitor the curing process. This process is also beneficial to the laminate creating a part with lower porosity (confirmed by post cure C-Scans of these parts compared to other laminates).

Thomas et al. [19] described a method for monitoring z-direction resin flow for a carbon fiber composite part. The parts tested consisted of a single layer of plain weave carbon fiber fabric with a thin resin film covering the top of the fabric. The part is vacuum bagged and placed in a 70 °C water bath to infuse. The resin film penetrates the carbon fiber weave and flows downward towards the aluminum tool. C-scan pulse/echo ultrasound methods are used to monitor this process with images generated every three minutes for 21 minutes. Images show that as the resin penetrates the fabric the carbon

fiber tows become more visually evident and the measured reflectivity increases (drastically through the first 3 minutes and slowly after that). This reflectivity is then used to calculate through-thickness flow velocity. C-scan images are paired with images gathered by microscopy in order to display the non-uniform flow pattern of the resin and confirm possible voids detected by the ultrasound scan.

Svilainis et al. [20] explore the errors associated with the monitoring of epoxy resin cure using through transmission ultrasound. Four signal types were tested including pulse, continuous wave tonebursts, chirp 0.5-5 MHz, and chirp 0.7-3.5 MHz Cure was monitored at room temperature (20°C) over the course of several days by constantly measuring the speed of sound. The largest change in speed of sound (1800-2600 m/s) occurred over the first day and a half of testing as gelation occurred. After gelation the speed of sound increased slowly as the resin solidified, but would never reach complete cure as if the resin were cured at an elevated temperature (speed of sound approximately 2700 m/s). It was determined that the signal energy was a major influence on error which decreases with higher signal energy making the chirp 0.5-5MHz the lowest error signal and the pulse signal the highest error, though their difference in accuracy is small. It was also determined that further study is needed in order to account for all possible errors in these measurements.

Lionetto and Maffezzoli [21] summarize a decade of experimentation performed by their research group in monitoring the cure of thermoset resin using ultrasound. Two experimental setups were explored. The first was a through transmission contact method and the second was an air-coupled angled reflection method. The curing process was monitored by assessing changes in the speed of sound, attenuation, and longitudinal/loss

modulus. It was determined that gelation of the resin began at the onset of the speed of sound increase, and that the onset of vitrification corresponded to the peak of the measured attenuation. Calculated values of longitudinal and loss moduli were used to determine the end of the curing process which corresponds to the longitudinal modulus stabilizing at its maximum value. The speed of sound in the air-coupled experiment showed to be in agreement with the speed of sound from the contact experiment. The air contact method allows the transducers to be on the same side of the part making it easier to apply in-line measurements within an oven.

Jaunich and Stark [22] examined the use of through transmission ultrasound as a means of monitoring the cure progress during vulcanization of rubber. A transmitting and a receiving probe were imbedded into a mold, and speed of sound of the material, a carbon black filled natural rubber, is captured throughout the vulcanization process. This study examined a semi-efficient-vulcanization method. For cure temperatures of 150, 160, and 170°C the speed of sound showed an initial decrease as the material entered the mold. The speed of sound reached a minimum and then began to increase due to crosslinking reactions. The value then stabilizes signaling the curing process is nearly complete. The speed of sound values were then normalized in order to be compared to the storage torque measured by curemeter in accordance with ISO 6502. Similar trends were detected by both methods, where cure time decreased with increasing temperatures, and measured cure times were also in agreement. The ultrasound results were also able to confirm that as sample thickness increased the cure time increased.

Abu-Zahra [23] employed pulse-echo ultrasound methods along with dielectric sensor measurements to measure the real time density and viscosity of a PVC melt.

Through testing the density of the PVC was varied using AZO and K400 compounding agents. Measurements were taken near the exit of a steel extrusion die. The density is estimated by taking the difference of the calculated acoustic impedance and measured speed of sound. Results were about 1.5 times the value of the measured densities. The dielectric measurements also resulted in a reasonable estimation of the viscosity compared to values measured by rheometry.

Abu-Zahra [24] developed a method for monitoring the density of a polymer melt during the polymer extrusion using a shear wave pulse/echo methods. For this study the polymer used was a PVC compound. The transducer was attached to a delay line and incorporated into an extrusion die such that the delay line would be in contact, but not interfere, with the flow. Measurements of the reflected wave pressure from the delay line to polymer interface were taken and divided by the pressure of the reflected wave of an empty extrusion die (delay line to air interface). This pressure ratio was then used to calculate the acoustic impedance of the polymer melt, and the melt viscosity is estimated by the Poiseuile equation. These values along with the excitation frequency can then be used to calculate the density (see equation 8 from the paper). These density values had a statistical correlation of 96% when compared to extruded material density measurements with the melt density always greater than the extruded material density

Wang and Min [25] applied pulse-echo ultrasound techniques to monitor the melting process of LLDPE pellets and four formulations of powdered PVC within a twin screw extruder (with two different screw selections) at several feed rates and screw speeds. Measurements were taken near the middle of the extrusion barrel, at flight and C-chamber regions, meaning that the rotating screw had to be accounted for in these

measurements. An ultrasonic transducer attached to a delay line was fitted into a custom barrel segment such that waves would echo off of the screw base or threading. Measured ultrasonic attenuation was used to calculate a normalized amplitude ratio to characterize the melt degree and uniformity. It was concluded that higher screw speeds result in lower uniformity melts, and higher feed rates increase the degree of melt.

Cheng *et al*. [26] examined the use of pulse-echo ultrasound methods as a means to monitor polymer melt within an internal mixer. A single ultrasound transducer attached to a delay line is integrated into a side wall of an internal mixer and is aimed at one of the rotating blades. The signal's time of flight is measured from the echo which reflects off the wall of the delay line as well as the reflection off of the blade, assuming the polymer has melted enough to provide acoustic coupling. The amplitudes of the echoes are used to determine the presence of air bubbles and un-melted pellets/addition of new material, both of which lower the amplitude of the signal for a short time. Melting time is determined by taking the moving standard deviation of the time between echoes, when these times stabilize full melt has been achieved. These methods were tested for three melt temperatures of 170, 200, and 230°C, and for three blade rotations speeds of 14, 18, and 42 rotations per minute.

Zhao *et al*. [27] developed and tested a new technique for in situ monitoring of the injection molding process using high temperature ultrasound transducers. The technique employs an array of four transducers in a pulse-echo mode (two longitudinal probes and two longitudinal/shear probes) which are integrated into the mold. The melt arrival and part ejection times are found by monitoring the amplitude of echoes at the insert/polymer interface and from the back surface of the polymer. Upon melt arrival the signal echo at

the insert/polymer interface decreases as the polymer fills the air space and introduces a new echo off its back surface. These signals return to their previous values upon part ejection. Time of flight of the longitudinal and shear waves are also monitored in order to detect solidification and polymer properties (Young's and Shear Moduli).

Walker *et al*. [28] monitor the speed of sound through poly(N-isopropylacrylamide) (PNIPAm) hydrogels around the phase transition at 33°C where the hydrogel expels it's liquid content. Through transmission ultrasound is employed across a PNIPAm sample which was submerged in a water bath which controlled the temperature of the sample. Initially the speed of sound of the hydrogel begins around 1350 m/s, a value far lower than the gels main constituent, water (1480 m/s). The speed of sound decreases slightly as the temperature reaches 27°C, but once the phase transition (33°C) is reached the speed of sound spikes to near 1400 m/s.

Mizrach [29] proposes a method for nondestructive determination of avocado fruit ripeness using through transmission ultrasound. This was accomplished by placing a transducer and receiver in contact with the fruit at a 120° angle with respect to each other. Wave velocity and attenuation were measured and related to measured firmness and oil content (two parameters for determining fruit ripeness) for fruit stored at 2, 4, 6, 8, and 20°C. A linear relationship was observed when relating firmness to attenuation where attenuation increases as the fruit softens. The slope for this relationship varied with storage temperature allowing for determination of firmness if the storage temperature is known. Oil content was also related to attenuation, and in tandem with the relation to firmness the maturity of the fruit may be determined. It was also proposed that these methods would be suitable in evaluating the maturity of mangofruits.

Llull *et al*. [30] propose a method for evaluating the ripeness of sobrassada (a cured pork product from Mallorca, Spain) using ultrasound. The textural properties of sobrassada can be related to moisture content which decreases during the curing process. An experiment was created where the speed of sound of a cylindrical sample of sobrassada is obtained using through transmission ultrasound. The textural properties of hardness, compression work, maximum puncture force, and puncture work are then measured using compression testing and a puncture test, moisture content was also measured. Two sets of samples were observed; samples 1, 2, and 3 were ripened for 45 days, and sample 4 was ripened for 100 days. Two distinct period of ripening were observed, 0-40 days and 40-ripened. The trends over the first 40 days show similar relations, but after 40 days the trends differ. A set of equations was developed relating the ultrasound velocity (as $1/v^2$) to the moisture content, and therefore ripeness, of the sobrassada over the course of ripening. The equation was used to predict velocities that were then compared to the experimental data and exhibited a percentage of explained variance of greater than 94.3%.

Chapter Two, Section 4: Literature as it Relates to the Project

As the above articles show there is ongoing research into the use of ultrasound as an alternative means of non-invasive temperature estimation and phase/physical property monitoring when physical and visual access may be restricted or undesireable. As previously stated the goal of this project is to assess the ability of ultrasound techniques [1, 2] such as time of flight and speed of sound measurements to simultaneously monitor the temperature [8-17] and detect phase change [18-30] of a material non-invasively. Several articles [3, 4, 6, 7, 11, 16, 17, 20-22, 28-30] utilize through transmission

ultrasound methods similar to the method employed in this experiment as described in Chapter Three, section 2. The materials chosen for this project were waxes, but could also have been polymers [3, 4, 6, 7, 18-27] as were tested in several of the above articles or any other material that changes phase/physical properties as it changes temperature, or in the case of food products [29, 30] change with time.

CHAPTER THREE

Foundational Material

This Chapter will introduce the basics of the ultrasound methods used in this project as well as give an over view of the experimental set up and analysis. Two material containers of different sizes were created to confirm that the speed of sound results were not dependent on geometry. The materials of interest, Ecosoya pillar blend wax, base paraffin wax, and baker's chocolate will be introduced in detail using results from differential scanning calorimetry to qualify the phase change as a function of temperature and two supplementary ultrasound experiments on solid wax and acrylic will also be discussed.

Chapter Three, Section 1: Basics of Ultrasound

Ultrasonic testing is a common method of non-destructive testing that utilizes pressure waves (in liquids) or elastic waves (in solids); ultrasonic frequencies are often described as having frequency components greater than 20 kHz [2]. Many applications (see e.g. [2-5]) use ultrasound to examine properties such as flaw/void detection, dimensional measurements, and other material properties without the use of destructive measures such as cutting or breaking. A typical ultrasonic evaluation used for such an application consists of a pulser (shown in Figure 3. 2), an electronic device that creates and interprets electrical signals, a transducer (several examples shown in Figure 3. 3) which creates the physical wave from the electrical signals sent by the pulser by vibrating an internal piezoelectric ceramic, and/or receives the physical wave and converts it to an

electrical signal for the pulser to interpret, and a device that can display electrical wave forms such as an oscilloscope or specialized computer software (shown in Figure 3. 4). This process is also detailed in the flow chart shown in Figure 3. 1.

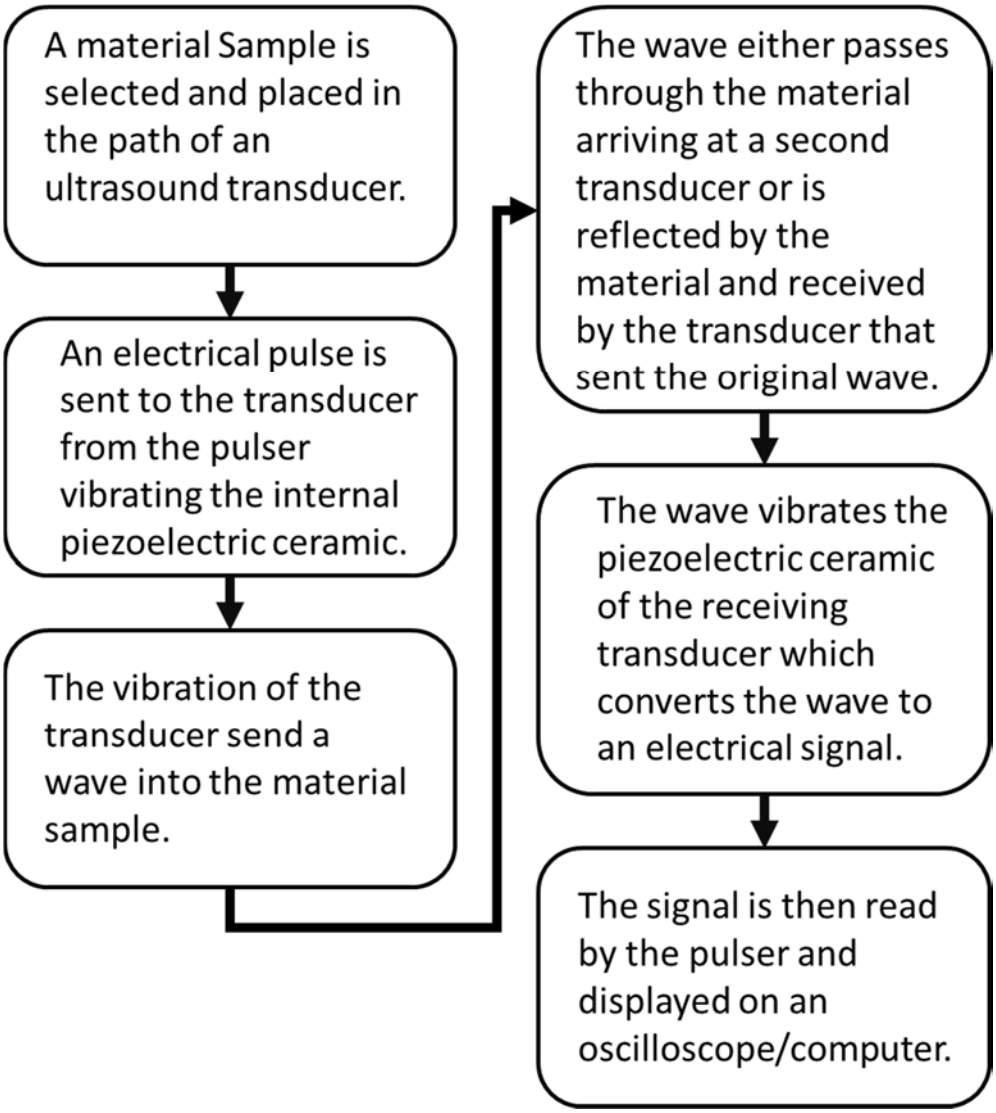

Figure 3. 1: A flow chart describing a typical ultrasound testing set up.

Figure 3. 2: Image of a typical ultrasound pulser.

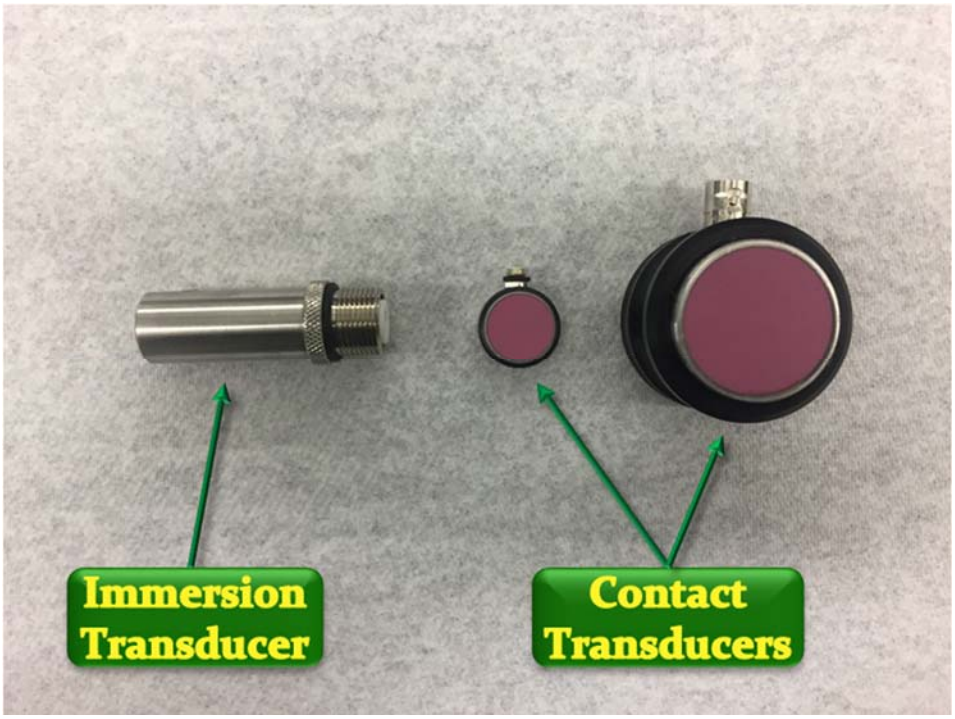

Figure 3. 3: Image of typical ultrasound transducers, one immersion transducer and two contact transducers.

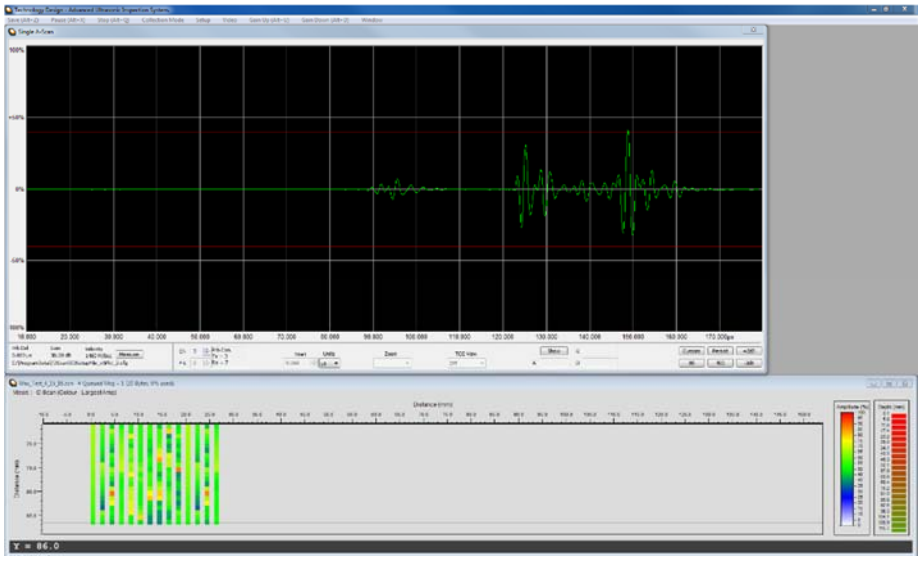

Figure 3. 4: View of an ultrasound signal through the use of an oscilloscope software

There are three commonly employed scan categories for analyzing a structure with ultrasound [1]. The first of these is an A-scan (shown in Figure 3. 5), which is the image of the sound intensity taken at a single point. This sound intensity is plotted as a function of time in order to monitor echoes reflecting from the sample, to measure the time of flight through a sample, or to measure the dimension of samples based on how long it takes from the time the signal is sent to when the signal is received. Next is the B-scan (shown in Figure 3. 6), a two dimensional plot of the amplitude values for several A-scans taken along a line if the transducer is moving or at the same point over time if the transducer is fixed. The B-scan's main use is to detect changes in the amplitude of signals to help identify defects, changes in thickness across a sample, or changes in amplitude over time. Finally, there is the C-scan (shown in Figure 3. 7) a two-dimensional plot of signal intensity measured over an area over a finite range of time. The C-scan provides an area image around a point of interest allowing the detection of defects and the dimensions of those defects.

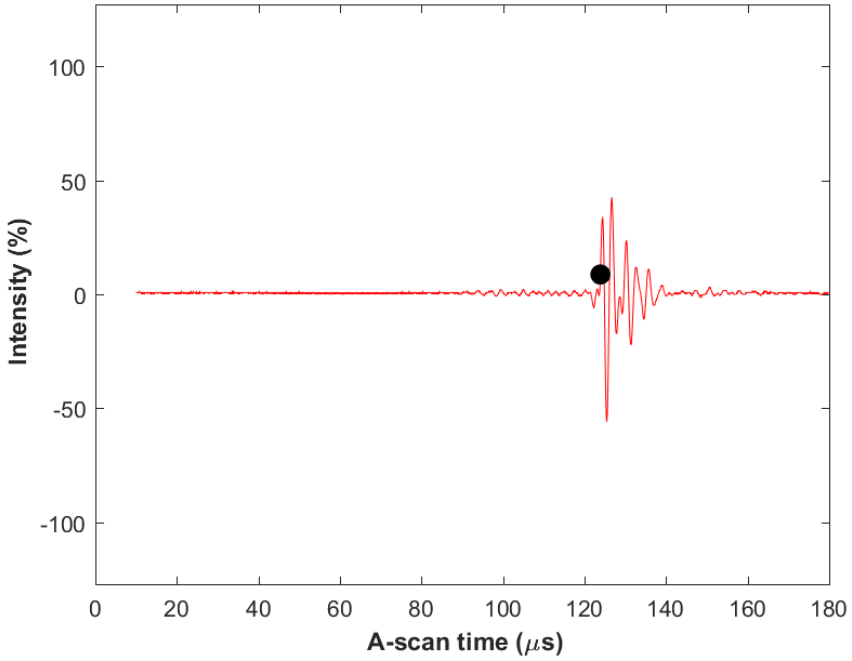

Figure 3. 5: A typical A-scan with the time of flight marked by the black dot.

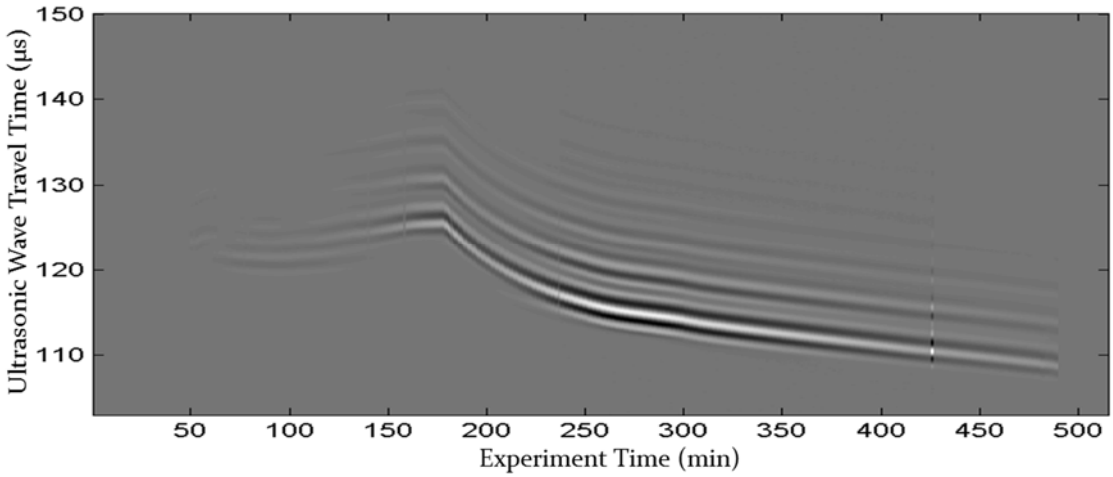

Figure 3. 6: A typical B-scan image with lighter color corresponding to higher wave intensity.

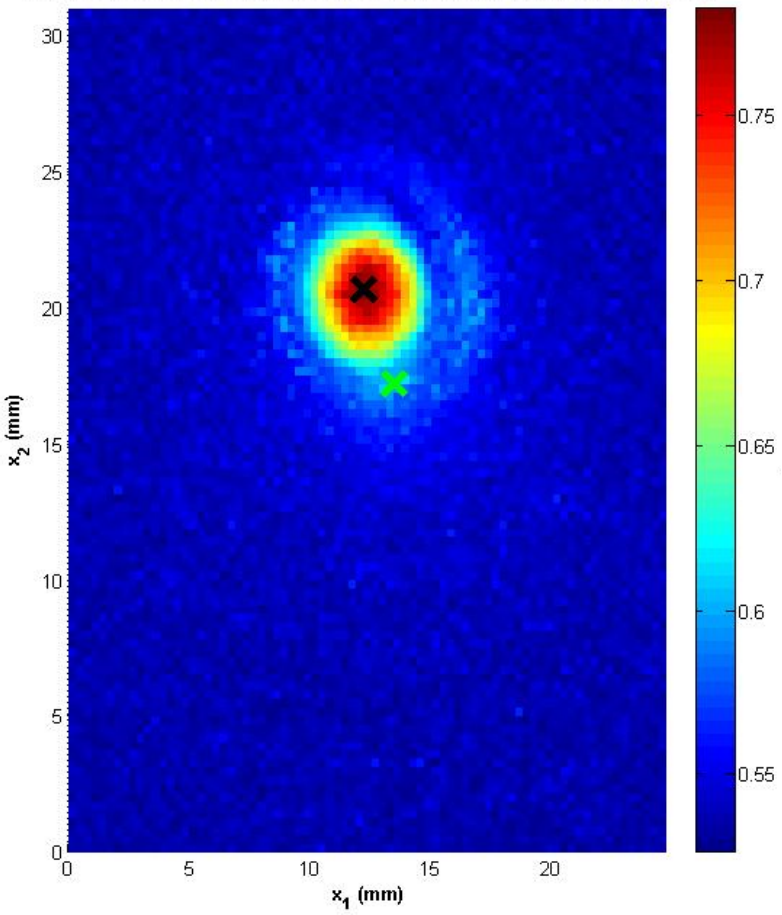

Figure 3. 7 A typical C-scan image of a through transmission ultrasound test where the color scale corresponds to signal intensity.

There are two main methods of ultrasound that are commonly used. The first is pulse-echo ultrasound during which a single transducer is used to both transmit the wave signal and receive echoes that are reflected back by discontinuities such as an internal crack or the back wall of a sample. Pulse-echo methods are extremely useful for situations where only one side of a material is accessible. The second method is through transmission ultrasound which utilizes two transducers, one to transmit the signal and one to receive the signal on the opposite side of the part. Unlike the pulse-echo method which monitors for changes by reflected echoes, through transmission monitors the strength of a

signal for changes that would indicate part of the wave being reflected or absorbed and not transmitting. Through transmission ultrasound is useful for thick or attenuative materials which would make it difficult for pulse echo methods to receive information from deep within a material. A diagram of each method is shown in Figure 3. 8.

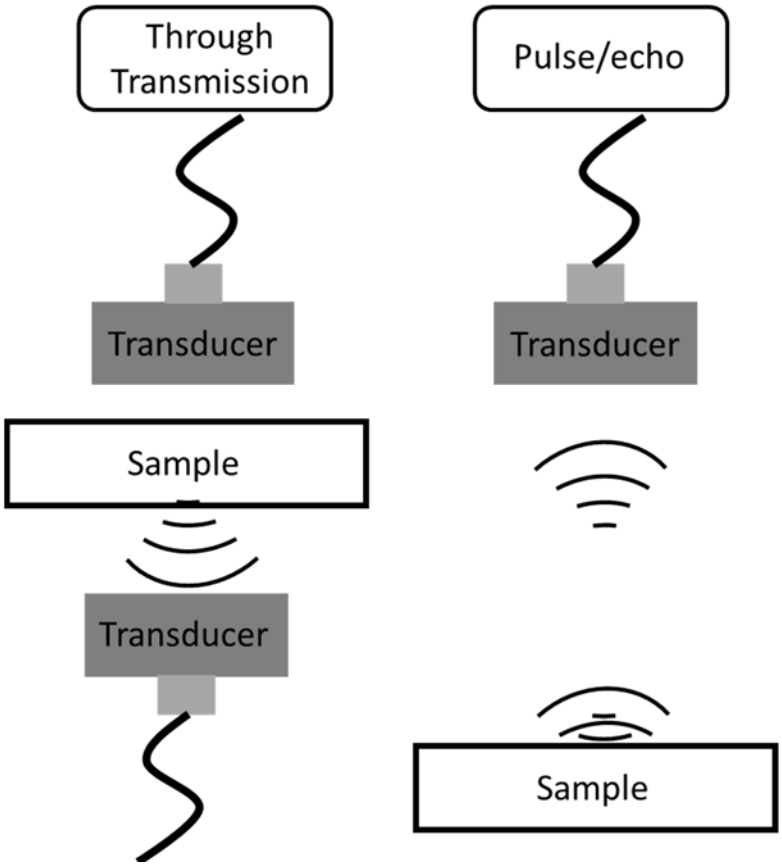

Figure 3. 8: A depiction of the through transmission and pulse/echo methods.

Ultrasonic wave propagation necessitates ultrasonic coupling to solids because ultrasound waves cannot travel through air. This is often done using a liquid medium such as water or specially made gels, but can be done with something as simple as super glue. This allows the wave to pass from the transducer into the solid part.

One typical ultrasound measurement is time of flight (TOF), or the amount of time a signal takes to travel from the transmitting to the receiving transducer whether it is directly through the sample (through transmission) or reflected off of a discontinuity (pulse-echo). Normally this value is measured in microseconds (μs). Figure 3. 9 shows a typical A-scan with a black dot indicating the measured time of flight occurring at approximately 115 μs, where the onset of the signal occurs when the first part of a wave exceeding a threshold, in this case 10%, is achieved. The purpose of the threshold is to prevent capturing a wave generated by random noise.

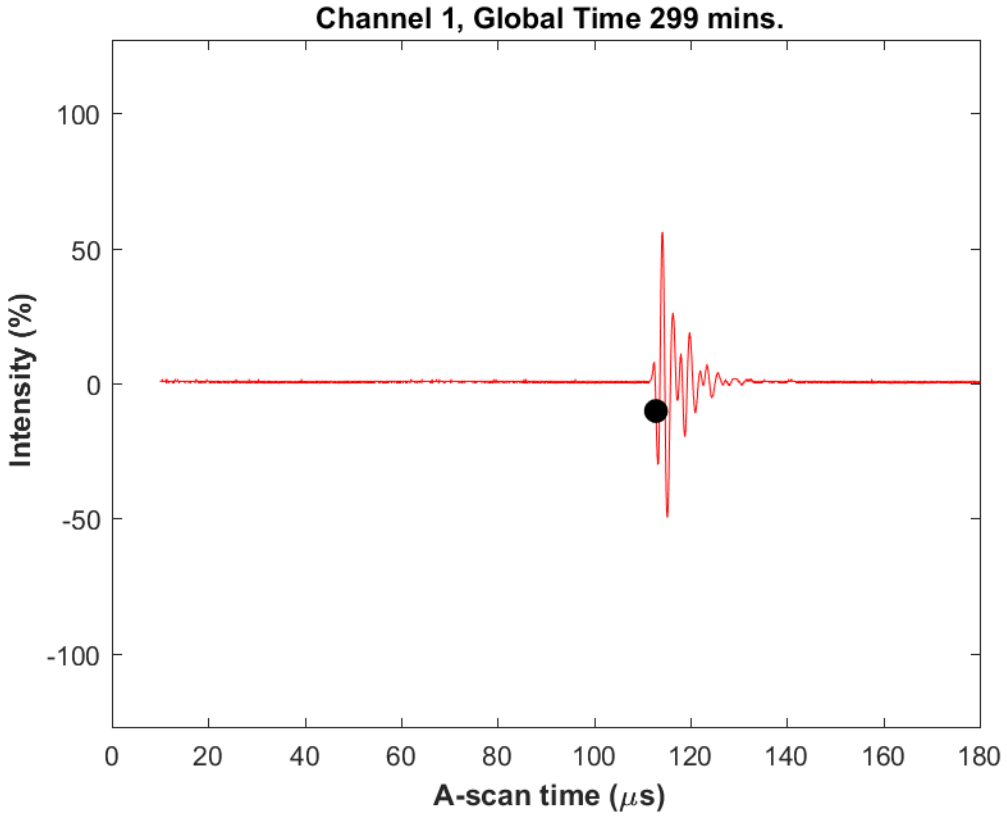

Figure 3. 9: A typical A-scan with the time of flight marked by the black dot at 115 μs.

The measured time of flight can be used to calculate the speed of sound for a material: Also called the wave velocity (v_w) this value is calculated by dividing the

length of the wave path (l) by the measured time of flight to determine the velocity of the wave. This value is normally reported in meters per second (m/s) or millimeters per microsecond (mm/μs) and is defined as:

$$v_w = \frac{l}{TOF} \tag{3. 1}$$

The ultrasound signal's attenuation may also be of interest. Attenuation is the rate of decay for a signal as it travels through a material caused by absorption or scattering. This value is calculated from the change in amplitude (A) as a signal travels farther through a material in the z direction. This value is often reported as a dimensionless coefficient of attenuation (α) and is defined as:

$$A = A_0 e^{-\alpha z} \tag{3. 2}$$

Equation (3.2) shows the calculation where A is the signal amplitude, A_0 is the signal amplitude at some other depth into the material, and z is the change in depth.

Acoustic impedance (Z) is a material property calculated by the product of a materials density (ρ) and speed of sound (v_w). Acoustic impedance is useful in the determination of how a signal will reflect/transmit when crossing a boundary of two materials with different acoustic properties and is expressed as:

$$Z = \rho v_w \tag{3. 3}$$

In the case of this current research, through transmission ultrasound is used to detect changes in the speed of sound of a material due to changes in temperature or physical properties. Of the properties discussed above the time of flight and speed of sound are used extensively.

Chapter Three, Section 2: Experimental Set Up

This section discusses the equipment used, experiment design, and the experimental procedure. In order to measure the speed of sound across the melting materials an experimental set up was created with several custom pieces made in house and other items readily available for purchase. The experiments performed typically consisted of six to nine hours of continuous observation.

Chapter Three, Section 2.1 Equipment Used

The first major piece of equipment is a container for holding the material of interest depicted in Figure 3. 10. This container had to be water tight, hold up to the heat of the fully liquid material (often up to 100°C), and have temperature independent contribution to the time of flight to allow for accurate speed of sound measurements (see Chapter Three, Section 5 for verification). It was also desirable to use an optically transparent material for the container so that the melt could be visually monitored, and that its geometry be such that the transducers could be easily attached and aligned. Acrylic (1/4" sheet) was chosen for the box based on its ability to with stand the temperatures of this test, simplicity to machine, and transparency. The acrylic sheets were cut to the dimensions for a rectangular box as is described in Chapter Three, section 2.2.2. The segments were held together by Loctite Super Gel adhesive and the interior and exterior edges were sealed using high temperature RTV sealant. After several scans failed due to leaking, the container was reinforced by applying pressure with compression clamps. Aluminum thermocouple brackets, shown in Figure 3. 11, were fabricated from 1/2" square aluminum stock to span the width of the container. Holes were drilled at intervals of 1.5" (1" for the small geometry system) for the thermocouples to sit in held at

the desired height by a set screw as shown in Figure 3. 10. Additional holes were added to each side of the originals to accommodate a three dimensional temperature array. The transducers were attached to the exterior walls of the container by Loctite Super Gel adhesive. Diagrams and images of both the large and small geometry containers are shown in Section 3.2.2.

Figure 3. 10 Image of the assembled acrylic container used in testing.

The heating blocks used in this testing, shown in Figure 3. 11 and Figure 3. 12 consist of a block of aluminum of 4”x1”x1” dimensions for the large geometry container and 4”x4”x1” dimensions for the small geometry container, with a ½” hole drilled into the long axis to house a heating element. One (large geometry system) or two (smaller geometry system) smaller holes are also drilled into the top center of the aluminum block to hold thermocouples used for temperature controller feedback or temperature

monitoring. The blocks are attached to a ½" thick aluminum square stock piece, similar to the pieces used as thermocouple mounts, by threaded rods with nuts located above and below the square stock piece used to control the height of the heating element. The heating element used was the Watlow 250-Watt, 3/8" outer diameter, 2 7/8" long heater shown in Figure 3. 13. This heating element can hold the set temperatures of 250 to 300°C consistently. The large geometry heating block uses one of these heating elements and the small geometry heating block uses two. The larger heating block, two heating elements, and smaller cross section of the small geometry system allow the materials to melt with a more uniform melt front than the large geometry box. The completed heating blocks for the large and small geometry systems are shown in Figure 3. 11 and Figure 3. 12 respectively. The heaters are controlled by a Watlow EZ-Zone temperature controller pictured in Figure 3. 14 with a k-type thermocouple providing feedback to the controller.

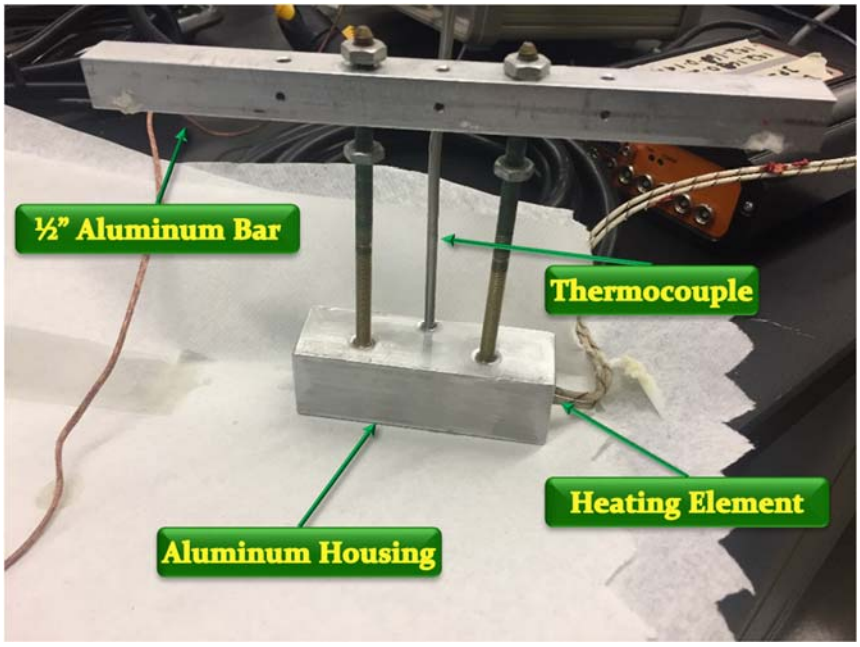

Figure 3. 11: Image of the heater block assembly used in the large geometry testing.

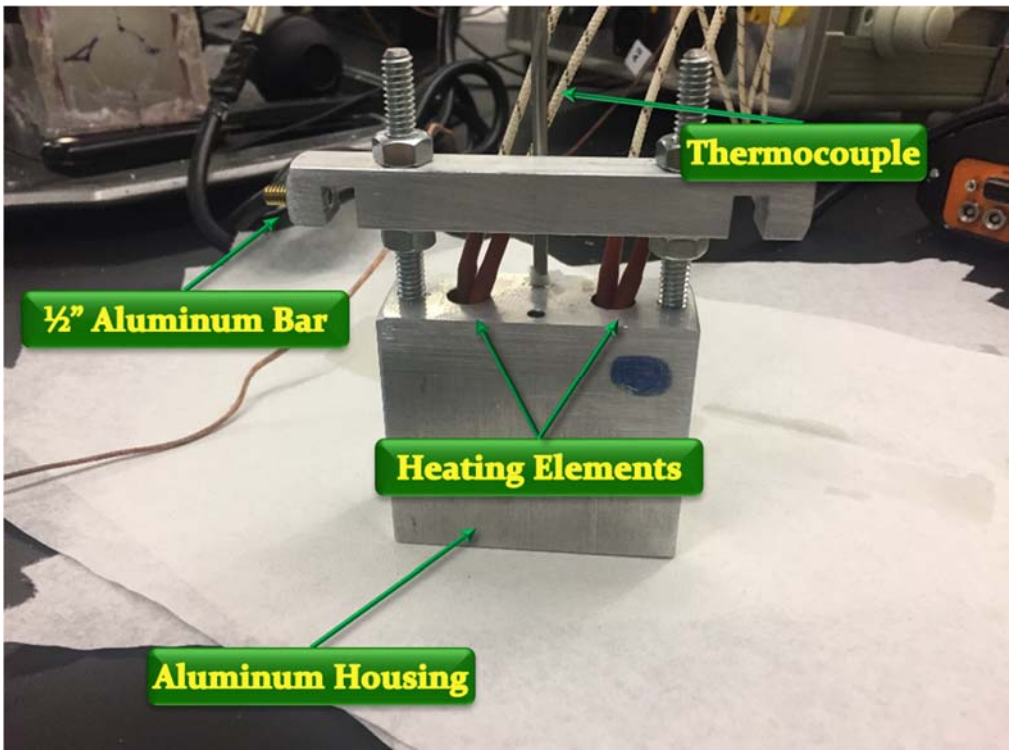

Figure 3. 12: Image of the heater block assembly used in the small geometry testing.

Figure 3. 13: Image of the 250W Watlow heating element used in the experiments.

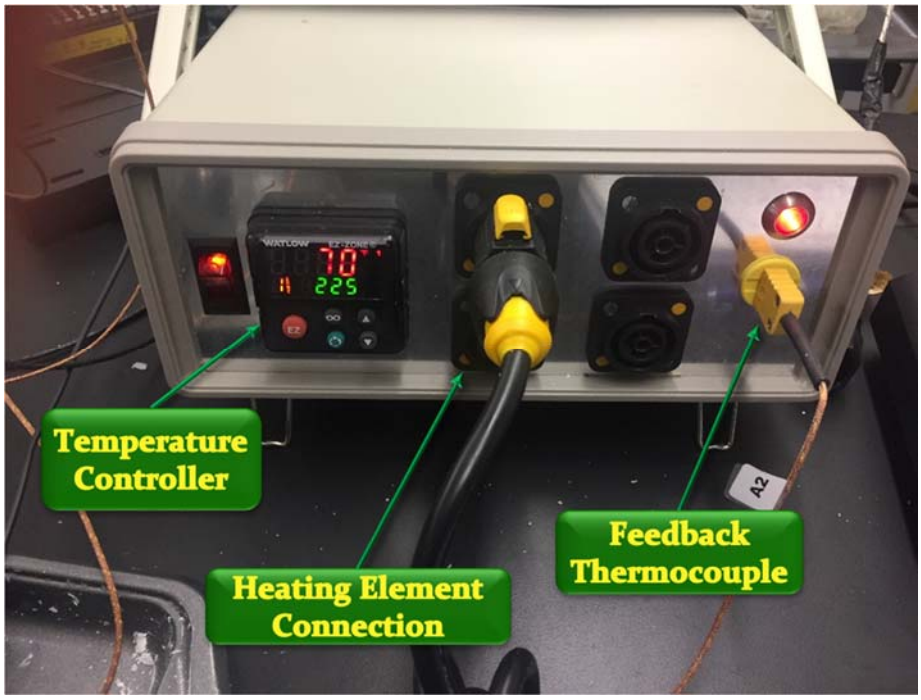

Figure 3. 14: Image of the Watlow heating element controller with the major components labeled.

Temperature monitoring for this experiment uses between 10 and 29, based on the experimental configuration, k-type thermocouples from Watlow to measure temperature at various locations throughout the container. These set ups are discussed and shown in Chapter Three, section 2.2. The thermocouple array was monitored using a Graphtec midi logger GL820, shown in Figure 3. 15, which accommodates up to sixty thermocouples in the current configuration. The GL820 features customizable sample rates and thermocouple naming as well as a large internal memory capacity or the ability to save data directly to a flash drive or computer. The GL820 can be used as a standalone unit (see Chapter Three, Section 4) or can be controlled through a computer as was done for this experiment. It also allowed for real time temperature monitoring through auto refreshing temperature plots and tables.

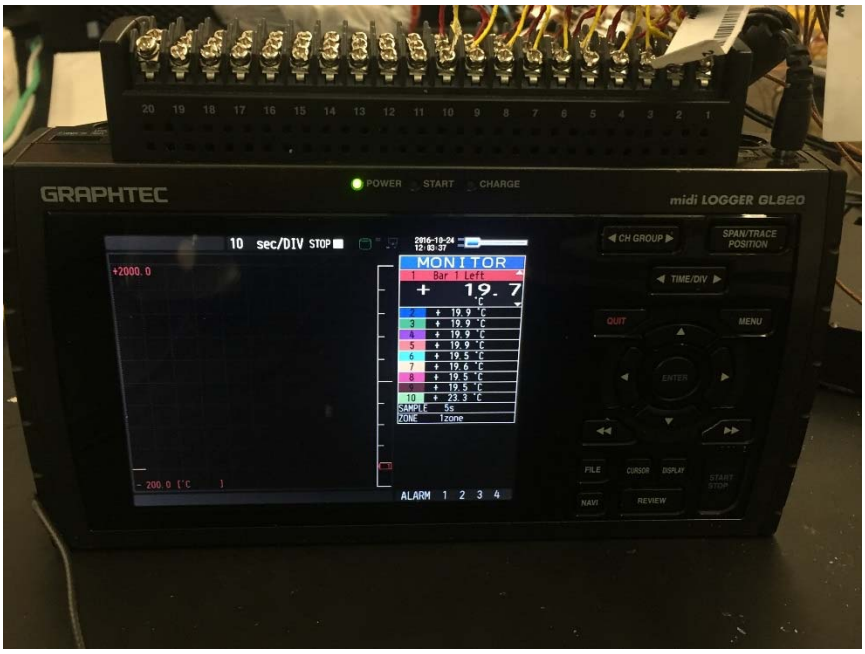

Figure 3. 15: Image of the Graphtec GL820 used to record temperature data during the experiments.

The final component of the experimental set up is the ultrasonic system composed of the pulser, transducers, cabling, desktop system, and software. The pulser used in this experiment is the Technology Design Pocket Scan PS45. This pulser can control up to eight transducers at a time as transmitters, receivers, or both and allows for a large number of transmitter/receiver configurations (the most used in testing was 14 channels). The Pulser is shown below in Figure 3. 16. The ultrasonic transducer selected in this experiment is the Panametrics NDT 0.5MHz, 1 inch diameter transducer (shown in Figure 3. 17). The relatively low frequency of this transducer allows the signal to penetrate through the solid, void filled materials used in testing while still being able to maintain a quality signal when the materials are completely liquid. The software used for data capture is the Technology Design Pockets Scan system. This commercial software must be used with the Technology Design pulser, and allows several different scanning

modes and test parameter customization, and upon completion exports the raw data to a file to allow post processing signal analysis. Data exported form the Pocket Scan software is then analyzed using custom MATLAB script files created as part of the research in support of this thesis described in Chapter Three, Section 4.

Figure 3. 16: Image of the Technology Design Pocket Scan PS45 pulser.

Figure 3. 17: Image of the Panametrics contact transducer used in testing.

Chapter Three, Section 2.2 Container Designs

For this experiment three distinct container designs were fabricated, a large geometry, a small geometry, and a heater-less small geometry. The large geometry set up is shown in Figure 3. 18 with exterior dimensions 11.5”x 6”x 6” and a wall thickness of ¼” composed of acrylic. The heater block is located along one side of the container such that the material will melt asymmetrically within the box. The height of the heater is such that it aligns with the midpoint of the box height. Transducers are spaced roughly 2” apart beginning about 2” past the heater block and are placed with the center of the transducer face half way up the side of the container (3” from the top or bottom edges). The orange dots on the image represent thermocouple placement with a row of thermocouples placed 1” inside the walls on either side, one row down the centerline of the container, and 2 on the heater block. For the standard test all of these thermocouples are aligned such that their tips align with the midpoint of the container’s height (3” from the top or bottom edges) as shown from the side view in Figure 3. 19. The ultrasound channels, or each desired transducer to transducer path, are laid out as shown in Figure 3. 20 with channels 1-4 traveling directly across the box and 11-14 traveling the reverse path. For example, channel 1 is composed of transducer 1 transmitting and transducer 5 receiving with channel 11 being the reverse. Channels 5-10 were set up to monitor the signal scattered diagonally through the material as shown in Figure 3. 21, though these channels did not yield any useful results and will not be discussed further or used on the small geometry testing. The fully assembled container is shown in Figure 3. 22.

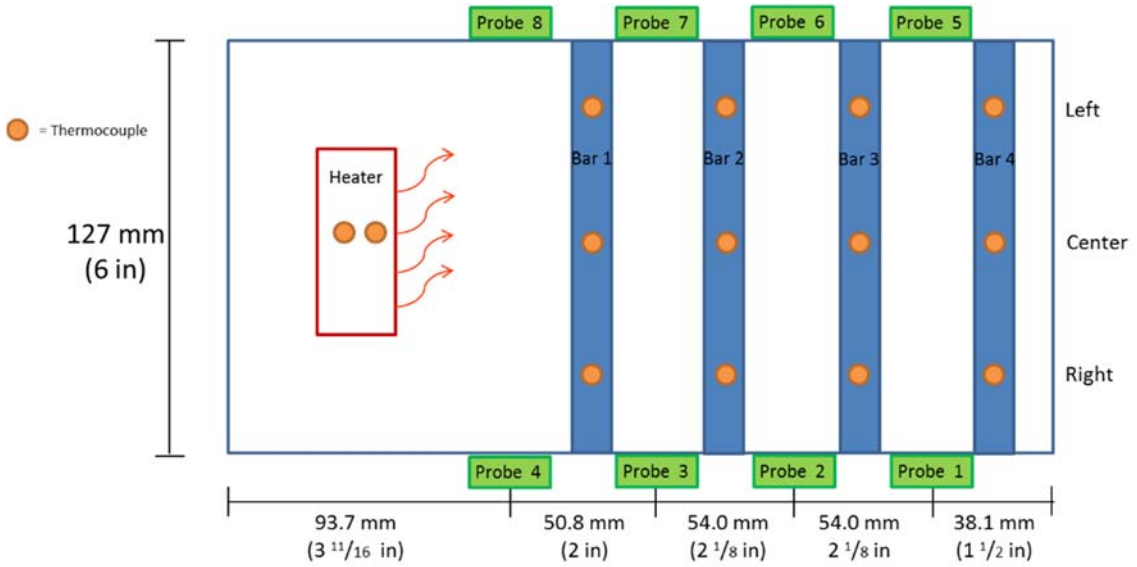

Figure 3. 18: Top view diagram of the large geometry container.

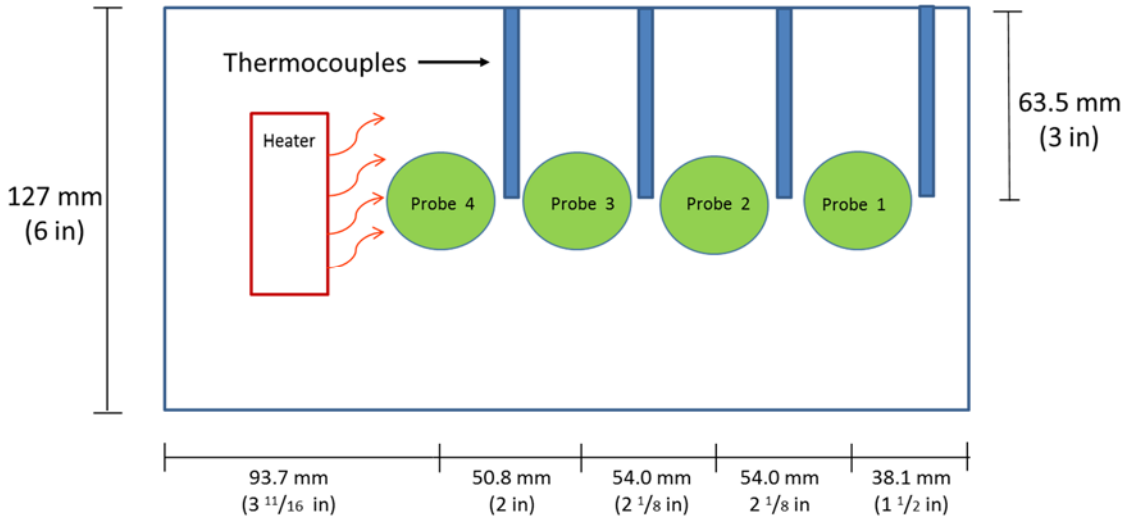

Figure 3. 19: Side view diagram of the large geometry container.

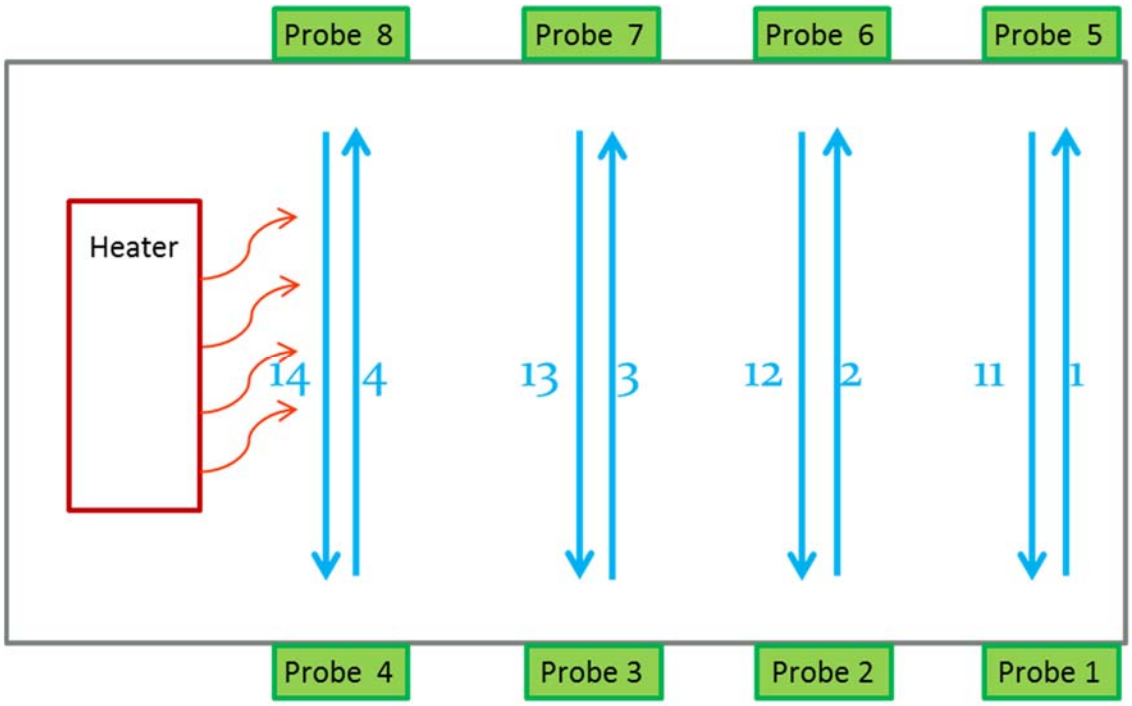

Figure 3. 20: Direct path ultrasound channel guide for the large geometry system.

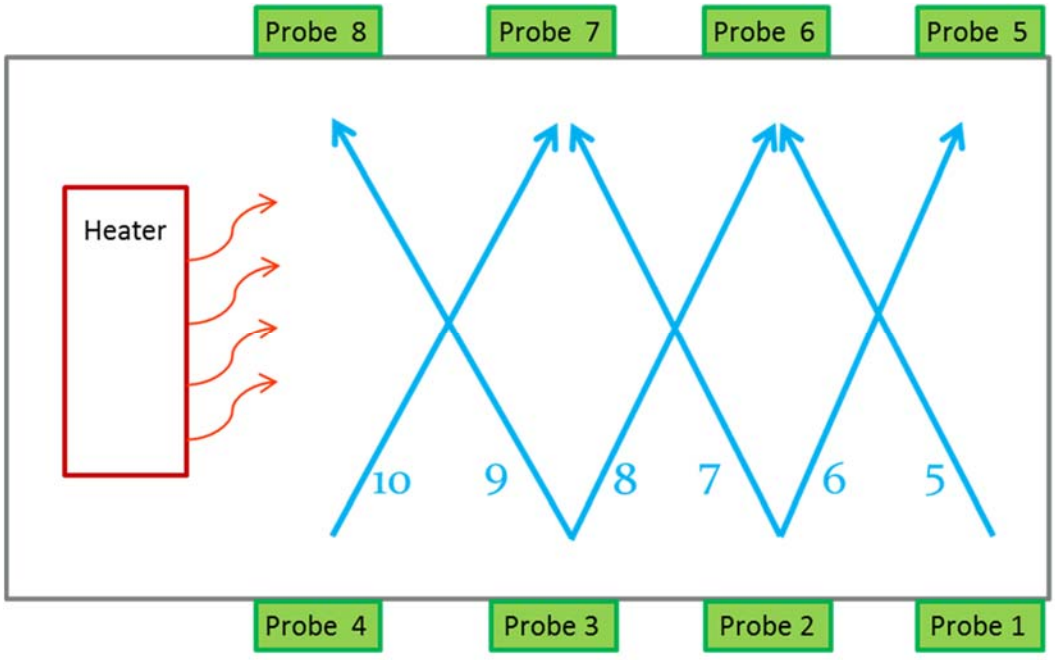

Figure 3. 21: Off axis ultrasound channel guide for the large geometry system.

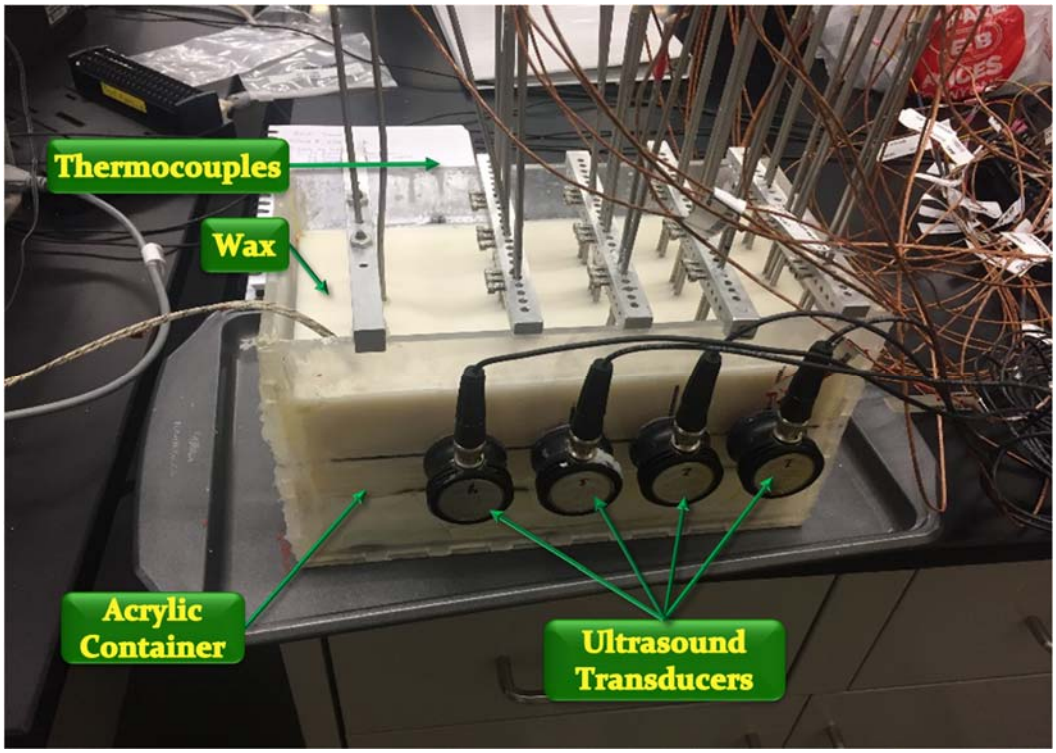

Figure 3. 22: Fully assembled large geometry system with major components labeled.

The small geometry system with exterior dimensions 9”x 3.5”x 4” and a container wall thickness of ¼”, is depicted in Figure 3. 23, and was created in order to confirm the speed of sound results of the large geometry on a smaller through thickness path as well as shorten the duration of a test from greater than eight hours to between six and seven hours. The layout of the small geometry system is shown in Figure 3. 23. This design utilizes only four transducers with two on each side spaced 2.5” apart beginning 2.5” from the heater block. The thermocouple layout is similar to that of the larger geometry with the exception of a thermocouple bar between the heater and first set of transducers as well as one fewer bar of thermocouples. The thermocouple bars are located roughly 1 ¼” on either side of the transducer pairs. The center of the transducer faces and the tips of the thermocouples are located half way up the container (2” from the top and bottom

edges) as shown from the side view in Figure 3. 24. The heater block used in this system is much larger than the one used in the large geometry system and takes up most of the container's width and height. The ultrasound channel diagram for this system are shown in Figure 3. 25. Channels 1 and 2 travel directly across the container and channels 3 and 4 travel the reverse path. This system does not feature any off axis channels because the shorter through thickness path and the wider spacing of transducers allow very little scatter to reach the off axis transducer. The fully assembled system is shown in Figure 3. 26.

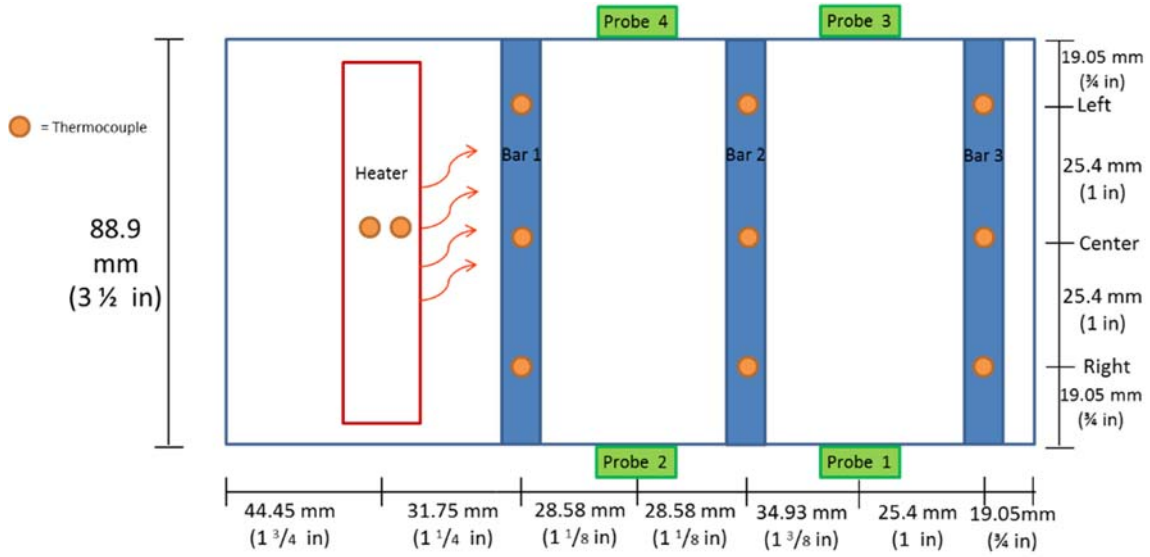

Figure 3. 23: Top view diagram of the small geometry container

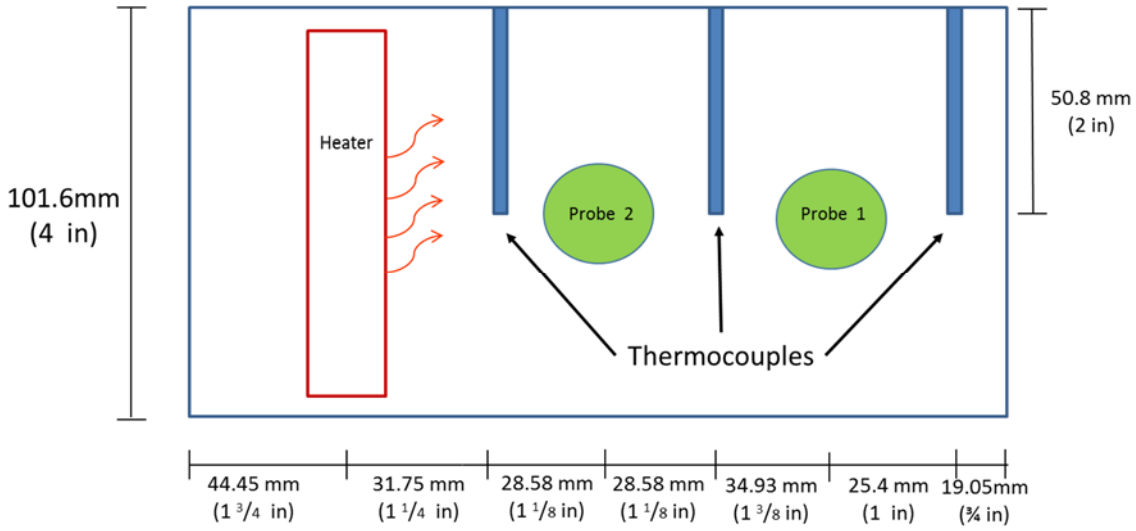

Figure 3. 24: Side view diagram of the small geometry container

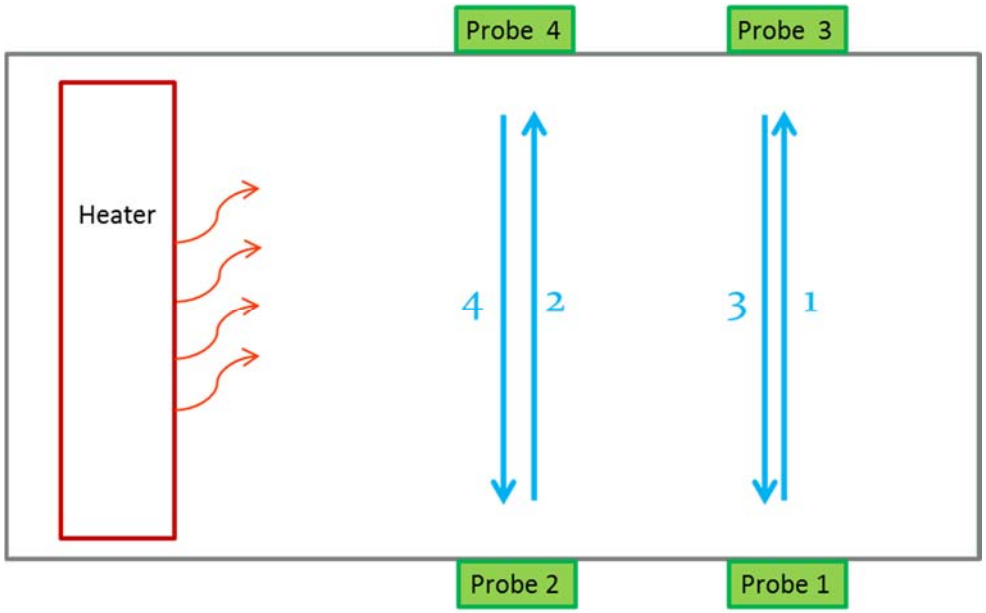

Figure 3. 25: Ultrasound channel guide for the small geometry system

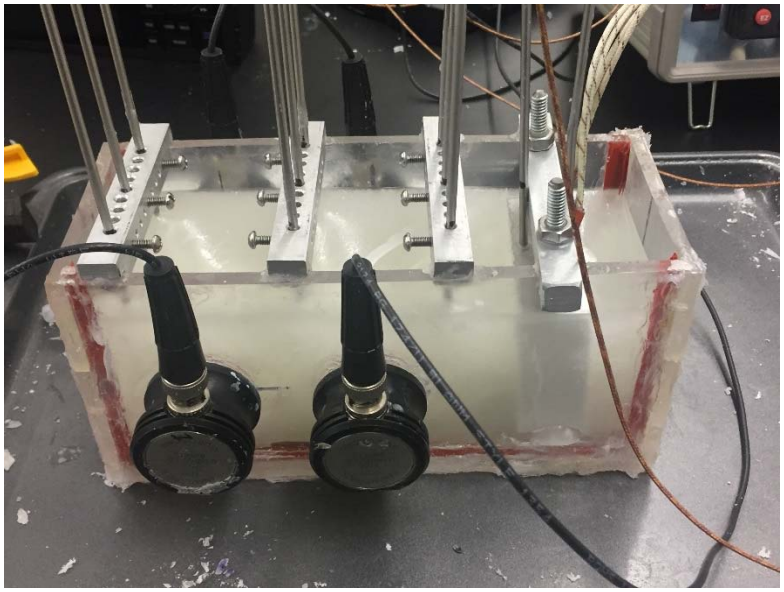

Figure 3. 26: Fully assembled small geometry container

A modified version of the small geometry system without a heater block was created in order to execute a test on chocolate. Initial tests tried to melt the chocolate using the heater, but were unsuccessful. The heater block was removed and a third transducer pair was installed, and the entire system was placed in a convection furnace for heating and the cooling of the chocolate was monitored. The layout of the transducers and thermocouples for this system are shown in Figure 3. 27 and Figure 3. 28 and the ultrasound channel layout is shown in Figure 3. 29.

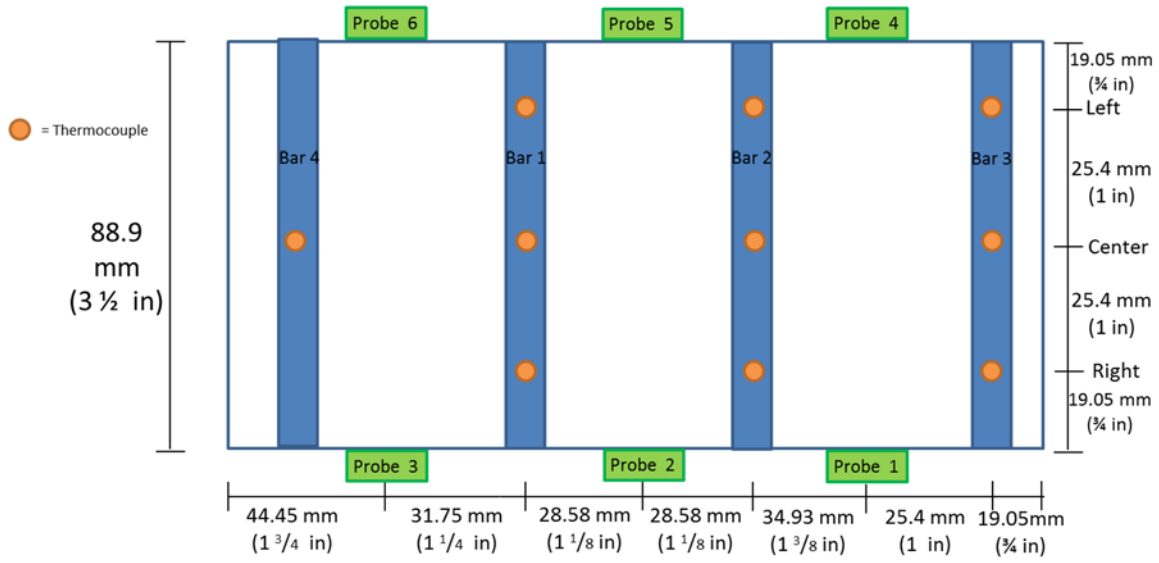

Figure 3. 27: Top view diagram of the small geometry chocolate testing container

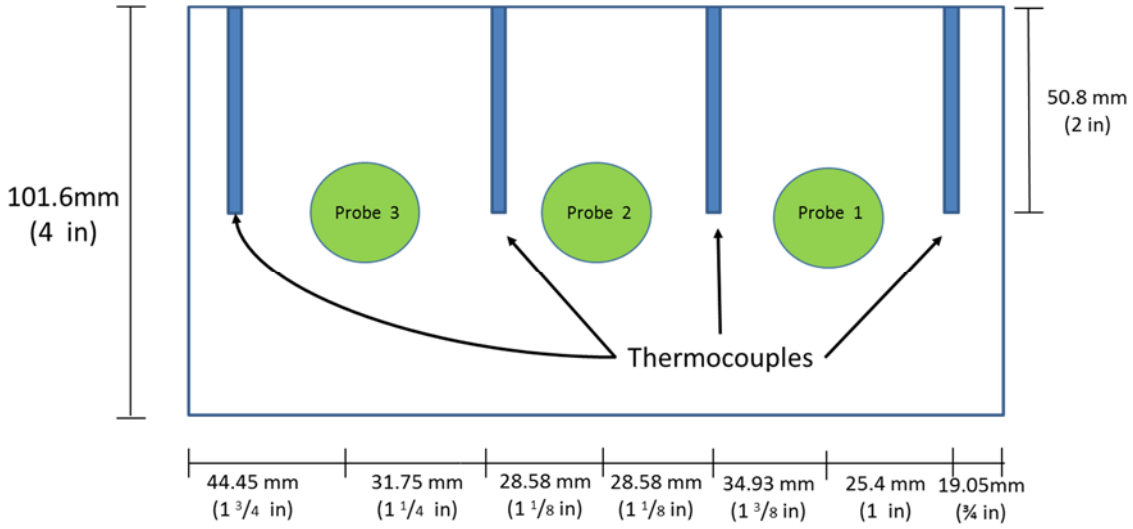

Figure 3. 28: Side view diagram of the small geometry chocolate testing container

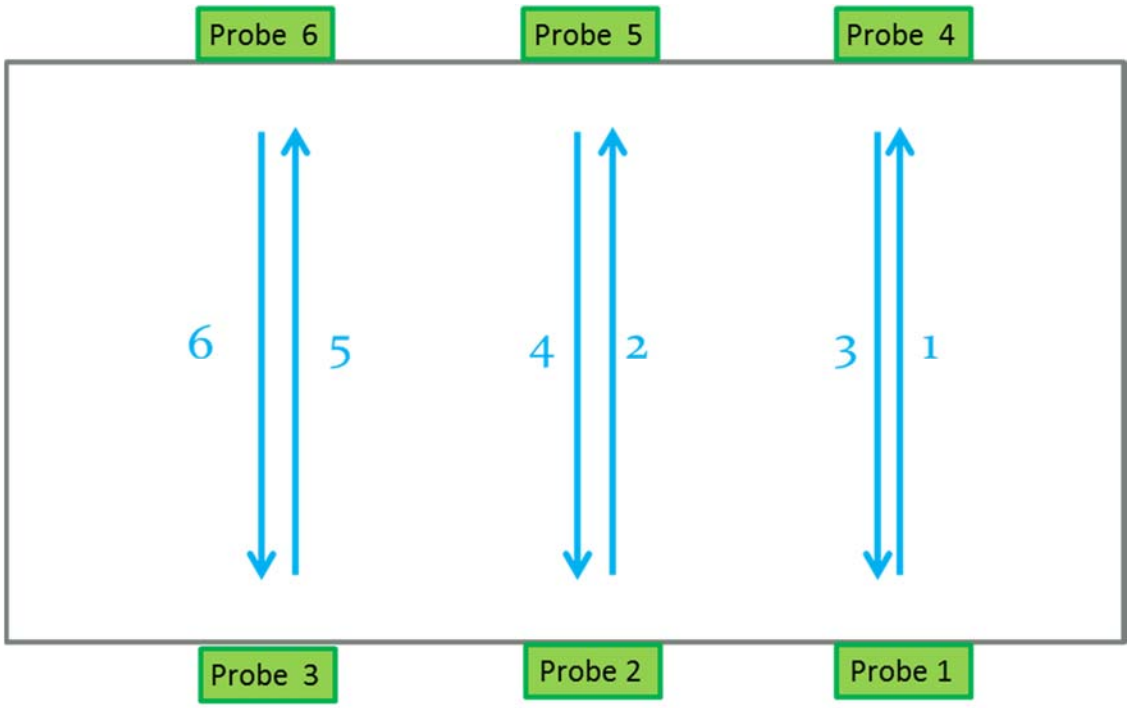

Figure 3. 29: Ultrasound channel guide for the small geometry system used in chocolate testing

Chapter Three, Section 2.3 Thermocouple Calibration

The thermocouples involved in testing were calibrated using an AMETEK ETC calibration instrument, shown in Figure 3. 30, which has a temperature controlled chamber with slots for differently sized thermocouples, along with the Graphtec GL820 data logger described in Chapter Three, section 2.1. The thermocouple is inserted to the correctly sized slot and the temperature is set on the digital display. Once the set temperature has stabilized for 5 minutes, in order to make sure the system had come to equilibrium, the temperature reported on the GL820 was recorded. This was done for a random selection of 5 thermocouples, labeled TC1-TC5, (four from the first batch ordered and one from the second batch) out of the 40 thermocouples used for temperatures of 30-70°C in 5°C increments. The results of calibration testing are shown

below in Table 3. 1. All thermocouples measured proved to be accurate within 0.3°C of the set temperature and within 0.1°C of each other.

Table 3. 1: Results from temperature calibration.

Source	Measured Temperatures (°C)								
Set Temp	30	35	40	45	50	55	60	65	70
TC 1	29.9	35.0	40.0	45.0	50.1	55.1	60.2	65.1	70.2
TC 2	30.0	35.0	40.0	45.1	50.1	55.1	60.2	65.3	70.3
TC 3	30.0	34.9	40.0	45.0	50.0	55.1	60.1	65.2	70.2
TC 4	30.0	35.0	40.1	45.1	50.1	55.1	60.1	65.2	70.3
TC 5	29.9	34.9	40.1	45.0	50.0	55.1	60.1	65.1	70.2

Figure 3. 30: Image of the Graphtec GL820 and Ametek ETC during the thermocouple calibration process

Chapter Three, Section 2.4 Ultrasound time of flight Calibration

The ultrasound time of flight was calibrated for this experiment by measuring the speed of sound of water at room temperature, which has an established speed of sound of 1484m/s. This was done by filling the small geometry container with water and using ultrasound channel 1 to measure the time of flight for the signal through the water as shown by the A-scan in Figure 3. 31. The speed of sound was then calculated using the equation shown in (3.1) with the time the signal spent in the container walls subtracted off the total measured time of flight, and their thickness subtracted from the acoustic path length. The calculated speed of sound was 1466m/s a difference of 1.2% from the established value. From this it is reasonable to conclude that the ultrasound measurements are accurate.

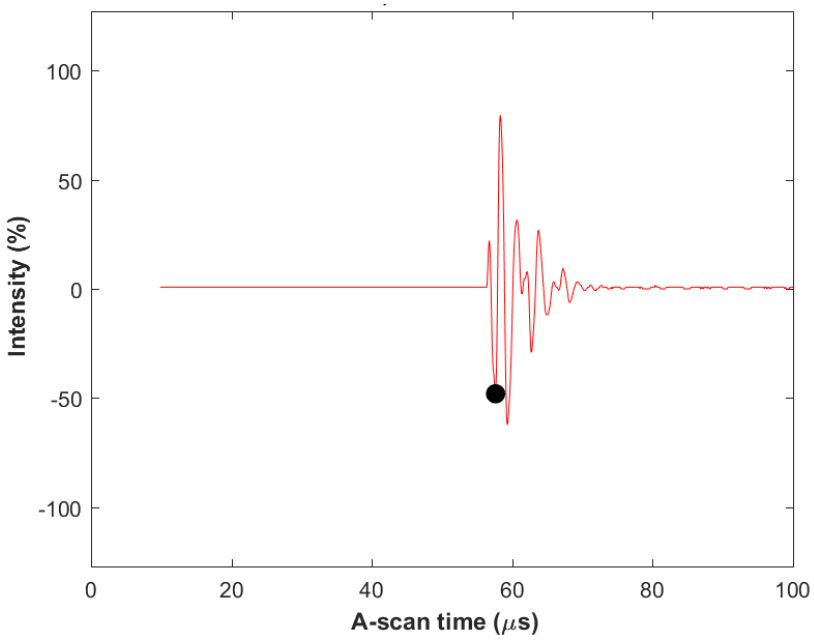

Figure 3. 31: A-scan recorded through water using the small geometry system ultrasound channel 1. Time of flight is marked by the black dot.

Chapter Three, Section 2.5 Experimental Procedure

The procedure for conducting the experiment are as follows. The first item that needs to be addressed is ultrasonically coupling the solid wax to the walls since a gap forms during cooling. This was done by pouring water into the gap until it covered the faces of the transducers. The 14 channels are initialized as in 3.2.2, the pulser is turned on and linked to its operating software. The low and high pass filters are set to 1 and 0.25 MHz, respectively, and initial gain of 70 db. The gain of each channel is then adjusted manually during the test such that the peak of signal is maintained near 50% saturation; gains are normally between 64 and 72 db. Before the ultrasound measurement is started the thermocouple collection is initialized. The GL820 computer application is opened and all thermocouples in use are set to monitor temperature in degrees Celsius for k-type thermocouples. The thermocouples are named according to their location, and the sample rate is set to one sample every 30 seconds. The ultrasound measurements started immediately after the temperature measurements are started. The heater block is switched on and set to the desired temperature 5 to 10 minutes after the ultrasound measurement has begun so that the speed of sound of the solid wax at room temperature can be captured before the wax begins heating. The heater is turned off when the melt front is no longer advancing or the material is completely liquid. While the material is in its fully liquid state the water added at the beginning of the test is removed from the bottom of the container using a large syringe. Care is taken to not interfere with the acoustic paths during water removal.

The peak amplitude of each ultrasound channel must be monitored throughout the test to ensure that the signals do not reach saturation or die off as the material heats and

cools. The gain is changed manually in 2 db increments to maintain the signals in an appropriate amplitude range throughout the test. Generally the gains need to be decreased as the material heats and increased as it cools. The total gain range for the test spans 8-72 db.

The test is considered complete when the material has fully solidified after melting, and contact with the wall is lost due to the material shrinking. At this time the ultrasound and thermocouple systems are stopped and the data file is saved for later analysis.

Chapter Three, Section 3: Basics of MATLAB Code

A custom MATLAB code was created to analyze the results generated by the Pocket Scan and Graphtec software (the code summarized in the flow chart shown in Figure 3. 32). This code is divided in to seven steps and is composed of nine total script files. The first step is to take the Pocket Scan text files and convert them from Unicode, a commonly used encoding system, to useable numeric arrays. This is completed by a trio of script files. The first script simply executes the others, allows the user to set the total number of ultrasound channels and asks whether or not the user would like to watch the A-scan as the data file is converted. The second script assigns a name to each channel's data in the form of "ch01_probes_01_to_05." The third script then interprets the Unicode data file and converts it to an array of numerical values, which is stored into a vector for each ultrasound channel, creates an A-scan plot, and saves the data as a *.mat file. This script also creates a test parameter vector consisting of the number of points in an A-scan, the number of A-scans per channel, the starting time, and the frequency. These vectors will be used in steps 2-4.

The second step is to read the converted data and parameter files in order to calculate and plot the speed of sound. The geometric properties are manually input and change based on which container is being used. These properties are used to account for the additional time of flight added by the container walls and include the signal path distance (shown in Figure 3. 18 and Figure 3. 23 as the width of the container), the thickness of the container walls, the speed of sound for the container material (2700 m/s for acrylic). The time of flight was then measured as the time with the first peak of the ultrasound signal above a 30% sound intensity threshold when the signal has been scaled such that the maximum of the signal is at 95% sound intensity. This method was chosen because it gave the smoothest results with the point of measurement moving from signal peak to signal peak less than the signal on set, or max of the signal methods. The time the signal spent in the walls of the container is then subtracted off, and the speed of sound is the computed by dividing the total path length (minus the wall thickness) by the time of flight as is shown in (3.1). This value is recorded for every A-scan performed and a plot is created showing the speed of sound throughout the test for each ultrasound channel.

The next two steps each use a single script file to create videos of the A-scan and its fast Fourier transform. Both scripts load the .mat and parameter files and calculate the time of flight as described for step two. The A-scan is then plotted and a video is created for each ultrasound channel. In step four the fast Fourier transform is computed using a building MATLAB function “fft,” and is plotted for each scan throughout the test to create a video.

Steps five and six involve the temperature data from the Graphtec GL820 saved as a .csv file. The data is loaded directly into MATLAB so that it can be rearranged for

ease of use in step six. The GL820 save the date and time rather than the run time for a data set, the values are organized into year, month, day, hour, minute form and used to calculate a time in the form of minutes since the start of a test for each measurement taken. A final array of the time vector and temperature vector for each thermocouple is created and saved as a .dat file. Step six uses this .dat file to create several plots of the temperature profile throughout the test including plots of the temperatures recorded for each bar of thermocouples, a two dimensional temperature profile video, and a one dimensional temperature line video from the center thermocouple of each bar.

The final script file uses the data created in the previous steps to calculate and plot the speed of sound as a function of temperature and the derivatives of the temperature profiles, the speed of sound as a function of time, and the speed of sound as a function of temperature. The derivatives were estimated using the slope of a group of fifteen data points forward from the current data point repeated for each point in the test. The temperature used in the plots of speed of sound as a function of temperature are selected as the linear average of the measurements from the center thermocouples located adjacent to the path of the ultrasound signal.

Chapter Three, Section 4: Differential Scanning Calorimetry

The materials of interest for this project were all analyzed for phase change temperatures using differential scanning calorimetry (DSC) using a TA instruments DSC Q20 (shown in Figure 3. 33). DSC works by placing the material of interest (contained within an aluminum pan) into a heating chamber with a reference sample (in this case an empty aluminum pan) as shown in Figure 3. 34.

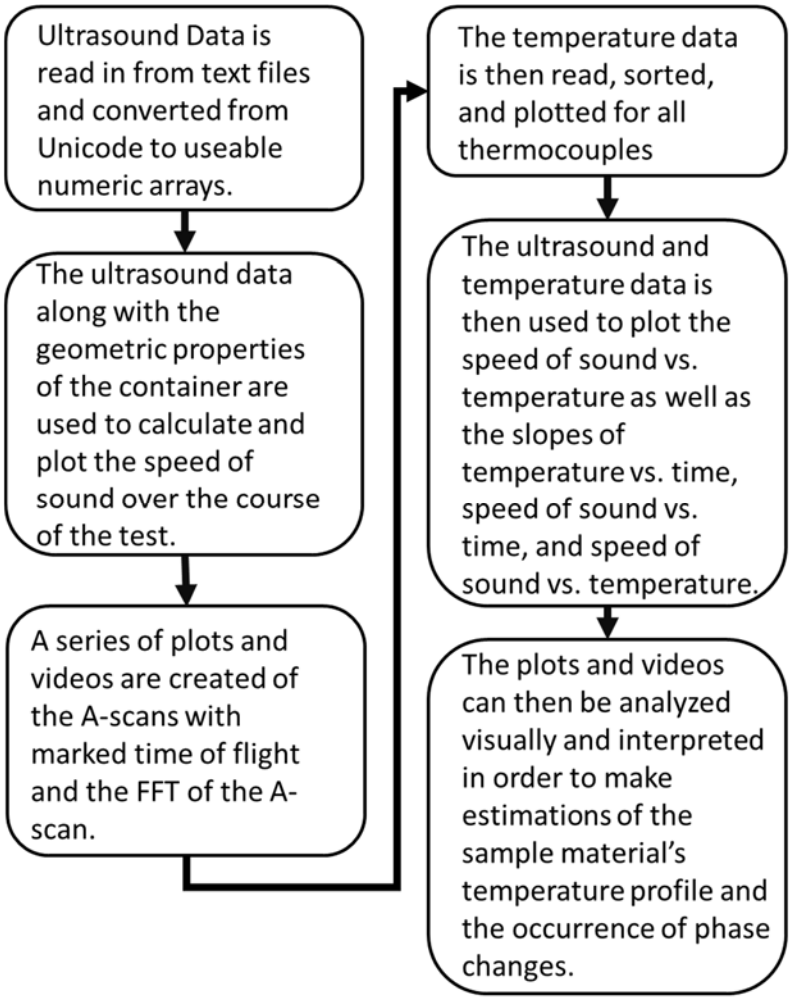

Figure 3. 32: A flowchart describing the data analysis performed in MATLAB

The chamber is heated over a specified temperature range at a specified temperature rate and the heat flow is measured as a temperature range at a specified temperature rate and the heat flow is measured as a function of temperature. For these tests all materials were tested for a temperature range of -50°C to 150°C which covers the entirety of melt and solid phases for all materials. The tests were performed at temperature ramps of 1, 2, and 5°C per minute to identify any dependence on heating rate, and each test consisted of two heating and cooling cycles. This test is used to

determine the temperature at which sample property changes occur, such as melting or glass transition temperatures.

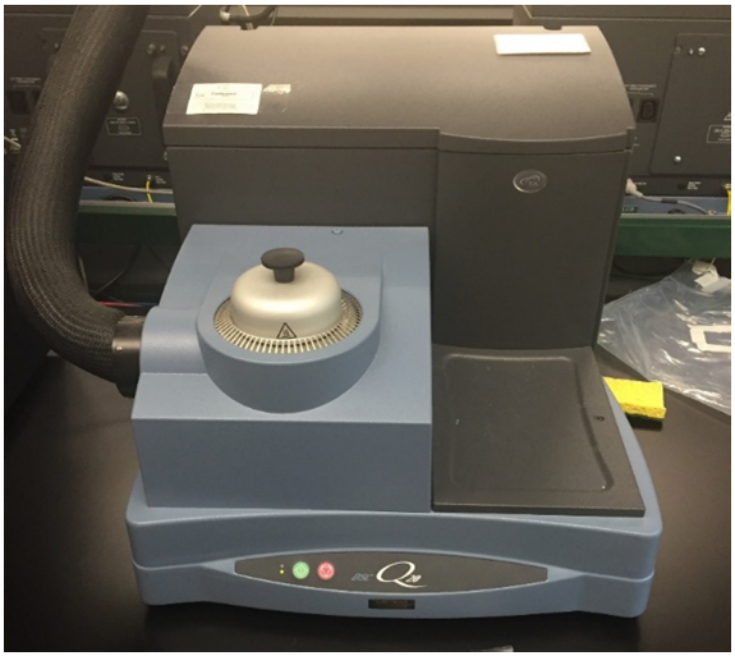

Figure 3. 33: Image of the TA instruments DSC Q20.

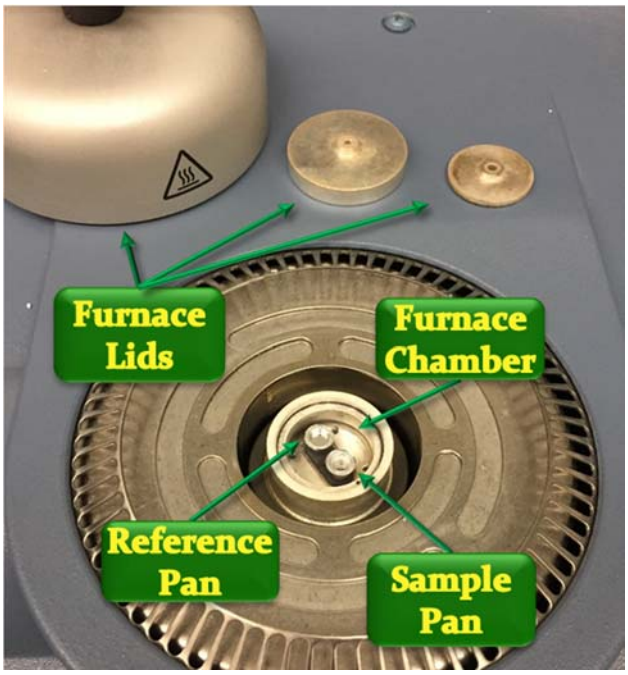

Figure 3. 34: Close up of the DSC Q20 furnace with major components labeled.

Chapter Three, Section 4.1 Ecosoya Wax

The Ecosoya pillar blend soy based wax is the first material that was used for testing. It is a standard candle wax with a smooth, oily texture and is easily marked or scratched. When melted, the liquid wax is similar in consistency to motor oil. As the wax solidifies small voids form at random and range in size from the tip of a pen to about ½". This wax tends to pull away from its container as it cools, but tends to keep the shape of the container after solidifying and maintains a smooth, flat top surface after cooling completely. Figure 3. 35 shows the results of DSC testing on the Ecosoya wax for a 1°C per minute temperature ramp. The heat flow as a function of temperature plot generated from a DSC test is generally read beginning from the lower left to the lower right and back around the upper curve following the heating and cooling cycles around twice. It can be seen that the heat flow begins to drop quickly at 40°C until 53°C where the heat flow increases sharply. This can be observed more clearly in the zoomed in plot of heat flow vs. temperature shown in Figure 3. 36. Over this temperature range an increasing amount of energy is needed to raise the temperature of the material indicating a phase change event. From this the melt temperature of the material is defined by the peak of the heat flow at 53°C. These same features are observed on the cooling cycle as the liquid wax solidifies with the solidification temperature shifted about 5°C to the left from the melt temperature. This hysteresis is a result of the wax being a crystalline material and some energy being used to form the crystalline structure during cooling. Figure 3. 37 shows the effects of different temperature ramps at 1, 2, and 5°C/min. The plots show the same melt temperature and solidification temperature regardless of temperature ramp indicating that these properties are independent of the heating rate. The only difference

between the three heating rates is the magnitude of the heat flow value which increases with increasing temperature ramps due to higher amounts of energy being needed to make the larger temperature increase.

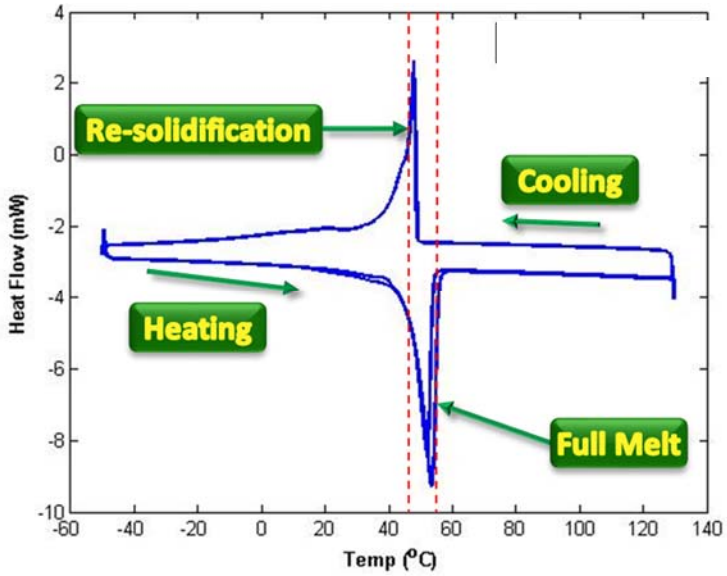

Figure 3. 35: Heat flow as a function of temperature for the Ecosoya wax with a 1°C per minute temperature ramp.

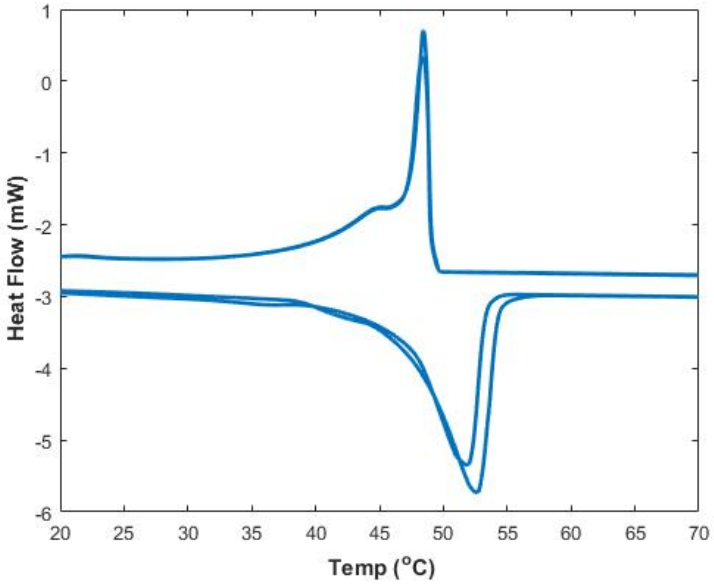

Figure 3. 36: Close up of the heat flow as a function of temperature for the Ecosoya wax with a 1°C per minute temperature ramp during phase change.

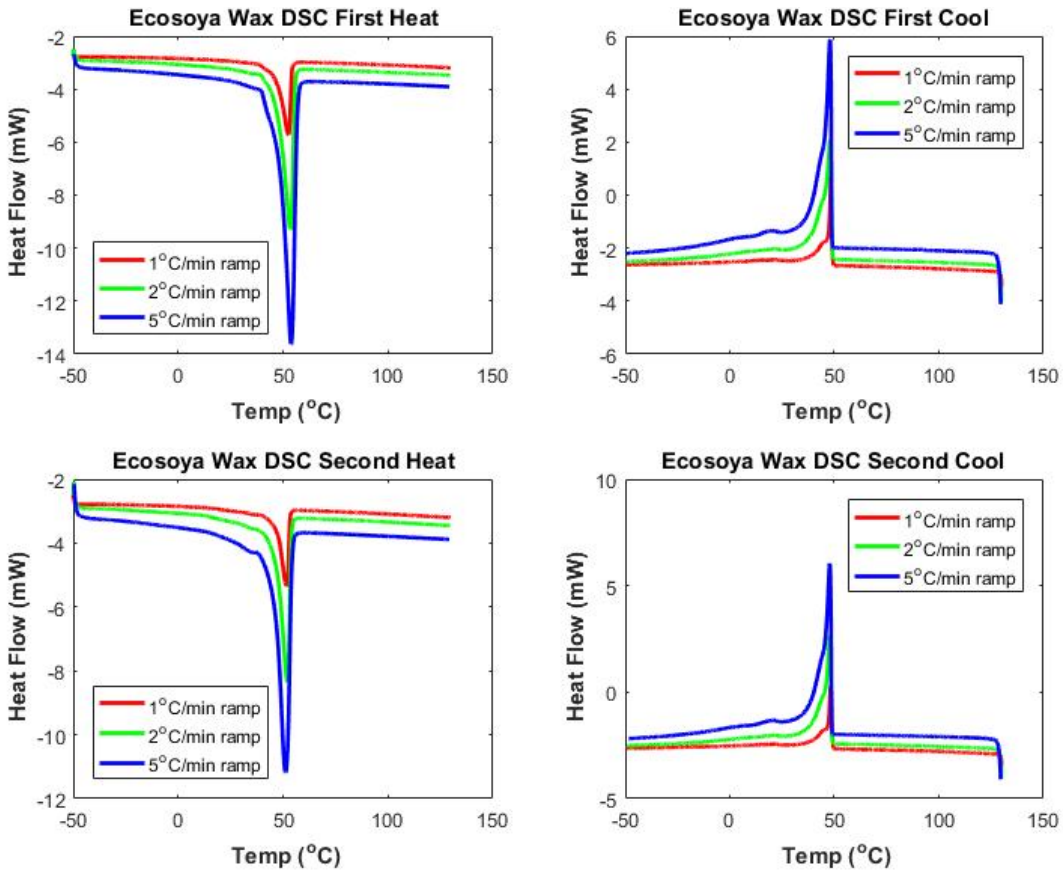

Figure 3. 37: Heat flow as a function of temperature for the Ecosoya wax at temperature ramps of 1, 2, and 5°C per minute broken into the heating and cooling cycles.

Chapter Three, Section 4.2 Base Paraffin Wax

A base paraffin wax was chosen so that a similar but different material could be tested. This wax is much harder in its solid state compared to the Ecosoya, and less stiff in its liquid state. Similarly to the Ecosoya this wax also forms small voids as it cools and pulls away from the container, but this wax also forms large depressions towards the middle of the container with high points around the walls and at the thermocouple locations. This behavior does effect the melting process by providing areas for the hot liquid wax to flow into and pool on the top surface resulting in a slightly more top down melt as opposed to the side to side melting of the Ecosoya. The DSC results for the base

paraffin wax with a 1°C per minute heating rate are shown in Figure 3. 38. The plot of heat flow as a function of temperature shows two major events for this wax during the heating and cooling cycles rather than just one as was seen with the Ecosoya wax. The first occurs at 38°C marked by the small spike in heat flow indicating that some phase change like event has occurred, but it is unlikely melt due to the second larger spike in heat flow occurring at 56°C. This can be observed more clearly in the zoomed in plot of heat flow vs. temperature shown in Figure 3. 39.The first temperature event seems to be a glass transition temperature where the hard wax becomes more soft and gummy before fully melting at the second event at 56°C. The same events are also observed during the cooling cycle shifted left by 3°C, a similar hysteresis as was observed with the Ecosoya wax. Figure 3. 40 shows the results from each of the three temperature ramps, 1, 2, and 5°C/min. Just as with the Ecosoya the major temperature events occur at the same temperature regardless of the heating rate indicating that these events are independent of heating rate with the only differences being the magnitude of the heat flow values. These results were also confirmed qualitatively by heating a small sample of the paraffin wax in a small metal bowl, pictured in Figure 3. 41 from 30°C to 60°C in 5°C increments, and prodding the sample to check for any change in stiffness. The wax remained hard and rigid for 30°C and 35°C, but once the material reached 40°C the material yielded when pressure was applied. At this temperature the sample was not melted and could hold the shape of an indent without breaking as shown in Figure 3. 41. This state was maintained for the 45°C and 50°C measurements, and the sample began to melt at 55°C.

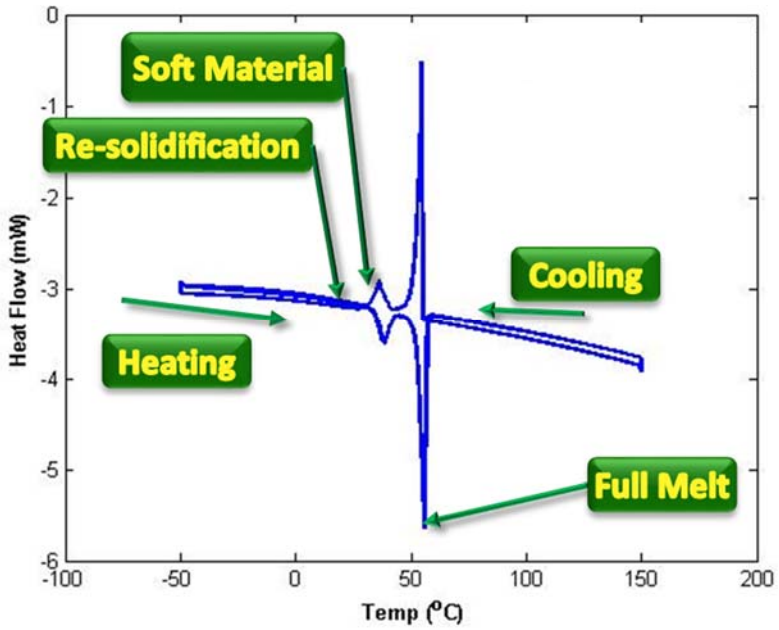

Figure 3. 38: Heat flow as a function of temperature for the base paraffin wax with a 1°C per minute temperature ramp.

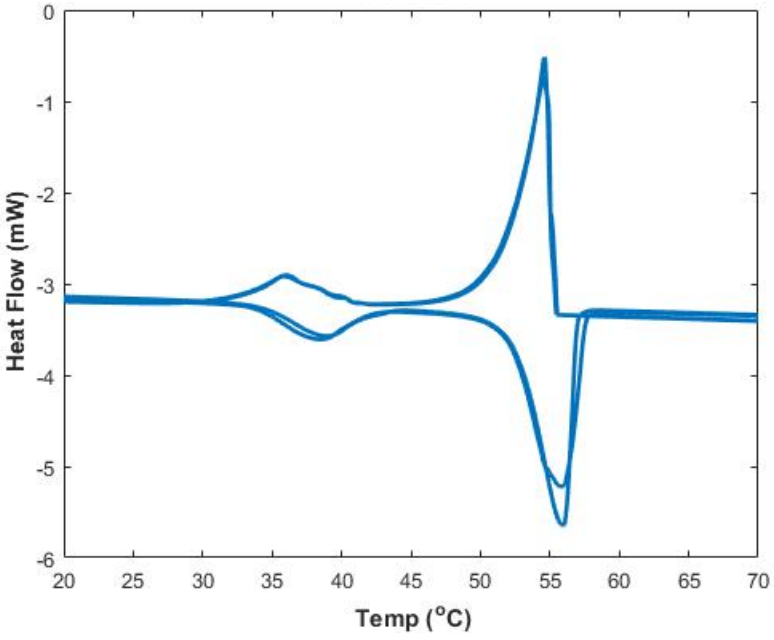

Figure 3. 39: Close up of the heat flow as a function of temperature for the base paraffin wax with a 1°C per minute temperature ramp during phase change.

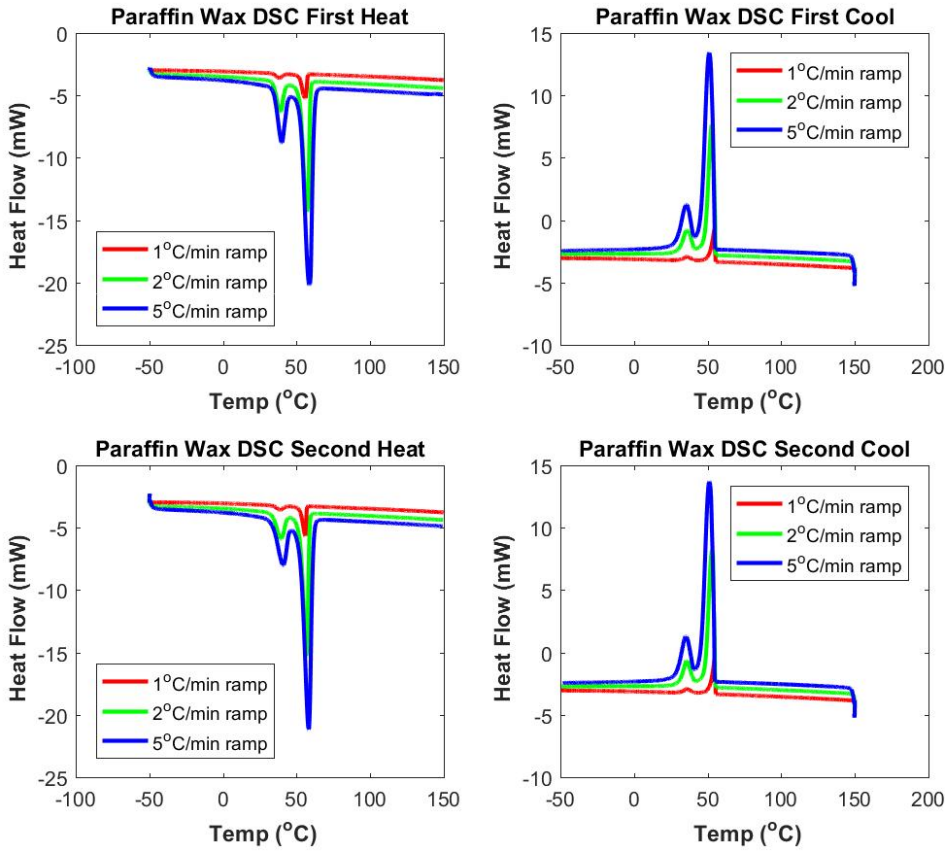

Figure 3. 40: Heat flow as a function of temperature for the base paraffin wax at temperature ramps of 1, 2, and 5°C per minute heating and cooling cycles.

Figure 3. 41: Image of the base paraffin wax in a metal bowl heated above the glass transition temperature at 40°C.

Chapter Three, Section 4.4 Baking Chocolate

The final material examined is a standard 86% cacao bakers chocolate. Chocolate was chosen as another material that experiences a solid to liquid phase change when heated and a liquid to solid phase change when cooled. This particular chocolate is low in sugar content meaning there are few sugar crystals to interfere with the signal, though there may be some. When melted the chocolate is much stiffer than either of the melted waxes. The DSC results for chocolate at a heating rate of 1°C per minute are shown below in Figure 3. 42. The plot of heat flow as a function of temperature shows what appears to be one major temperature event for melt which occurs at 20°C during the heating cycle with an offset between the first and second heating cycles, but zooming into this area, as shown in Figure 3. 43 it is apparent that there are actually two temperature events occurring over a short temperature range which are slightly different from one heating cycle to the next. One event occurs at approximately 18°C and the other at approximately 23°C. The cause of the first of the events is unknown, but could possibly be a hard to soft transition as appears in the base paraffin wax, or could be a melting point of a particular component of the chocolate. The second event signals the full melt of the chocolate as the heat flow stabilizes after this peak. This is only the case for the heating chocolate as the cooling cycle only shows one temperature event at 15°C, about 5°C cooler than the melting temperature. Figure 3. 44 shows the results from each of the three temperature ramps 1, 2, and 5°C/min. The two described events during the heating cycle occur for the 1°C/min and 2°C/min temperature ramps, but not the 5°C/min temperature ramp likely lost due to the quick heating rate. All other events occur independent of the heating rate. One major item of note is that the chocolate fully

solidifies below room temperature (15°C) meaning that the solidification of the chocolate will not be observed during the ultrasound testing.

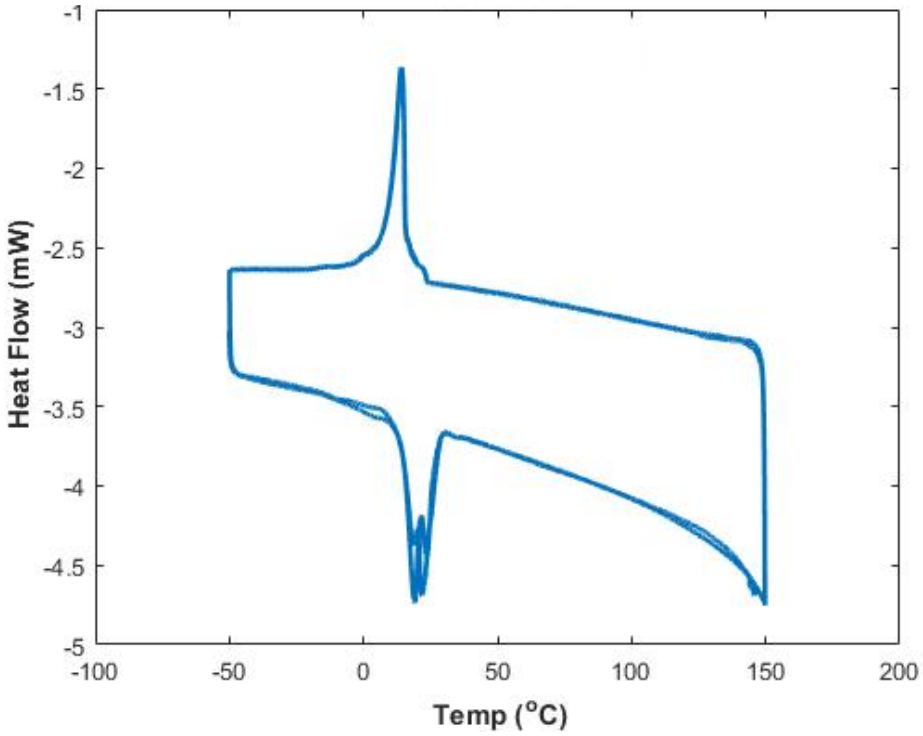

Figure 3. 42: Heat flow as a function of temperature for the chocolate with a 1°C per minute temperature ramp.

Chapter Three, Section 5: Other Ultrasound Testing

In addition to the experiment described in Chapter Three, section 2 some supplemental testing was needed to verify the experiment design. The first of these is a test on a solid block of the Ecosoya wax at room temperature to determine any directional effects of small voids filled with air caused during cooling on the resulting time of flight within the structure. The second test evaluates the effect of elevated temperatures on the speed of sound of the acrylic wall to determine whether or not these changes should be accounted for in the wax measurements for speed of sound.

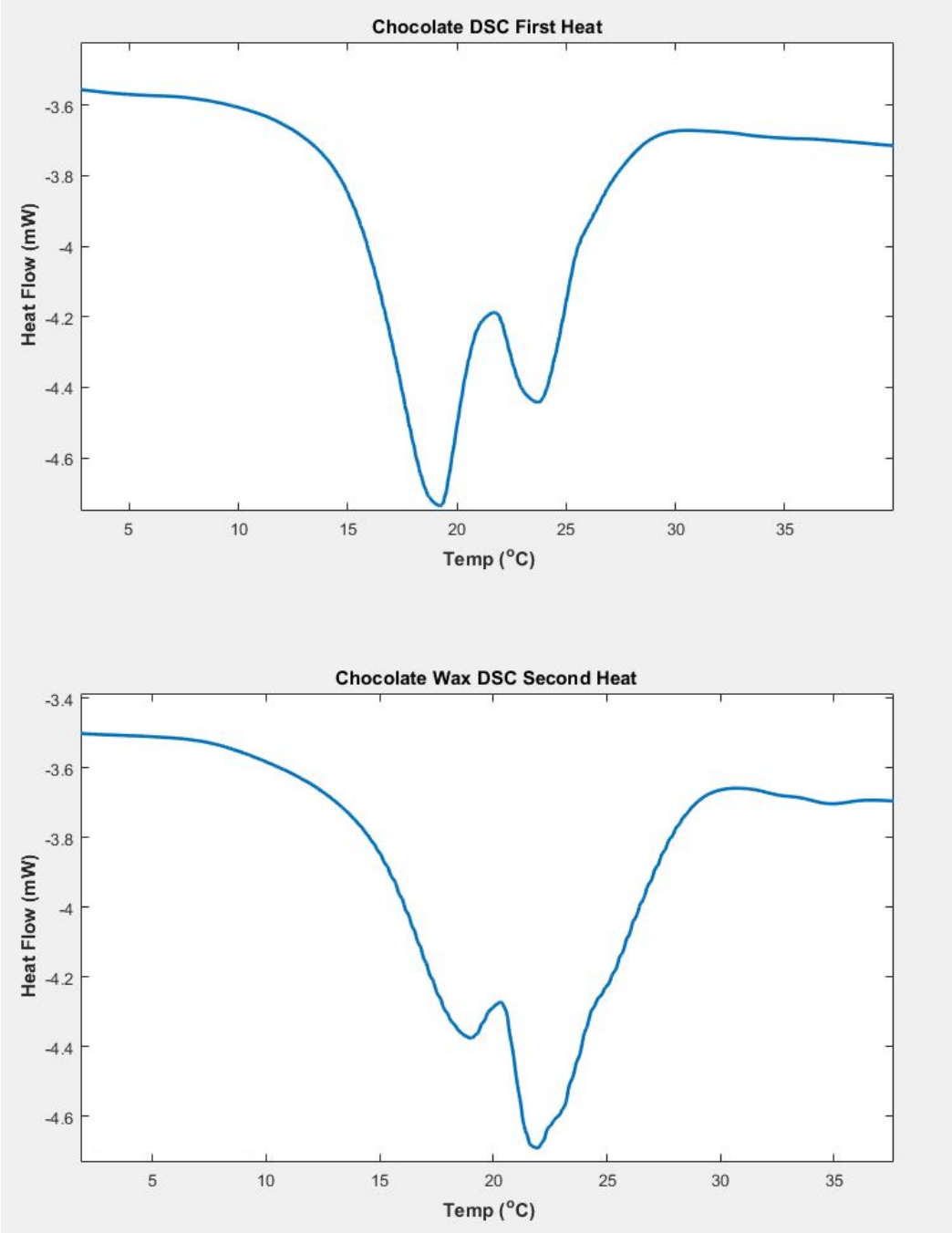

Figure 3. 43: Close up of the heat flow as a function of temperature for the chocolate with a 1°C per minute temperature ramp during phase change for both heating cycles.

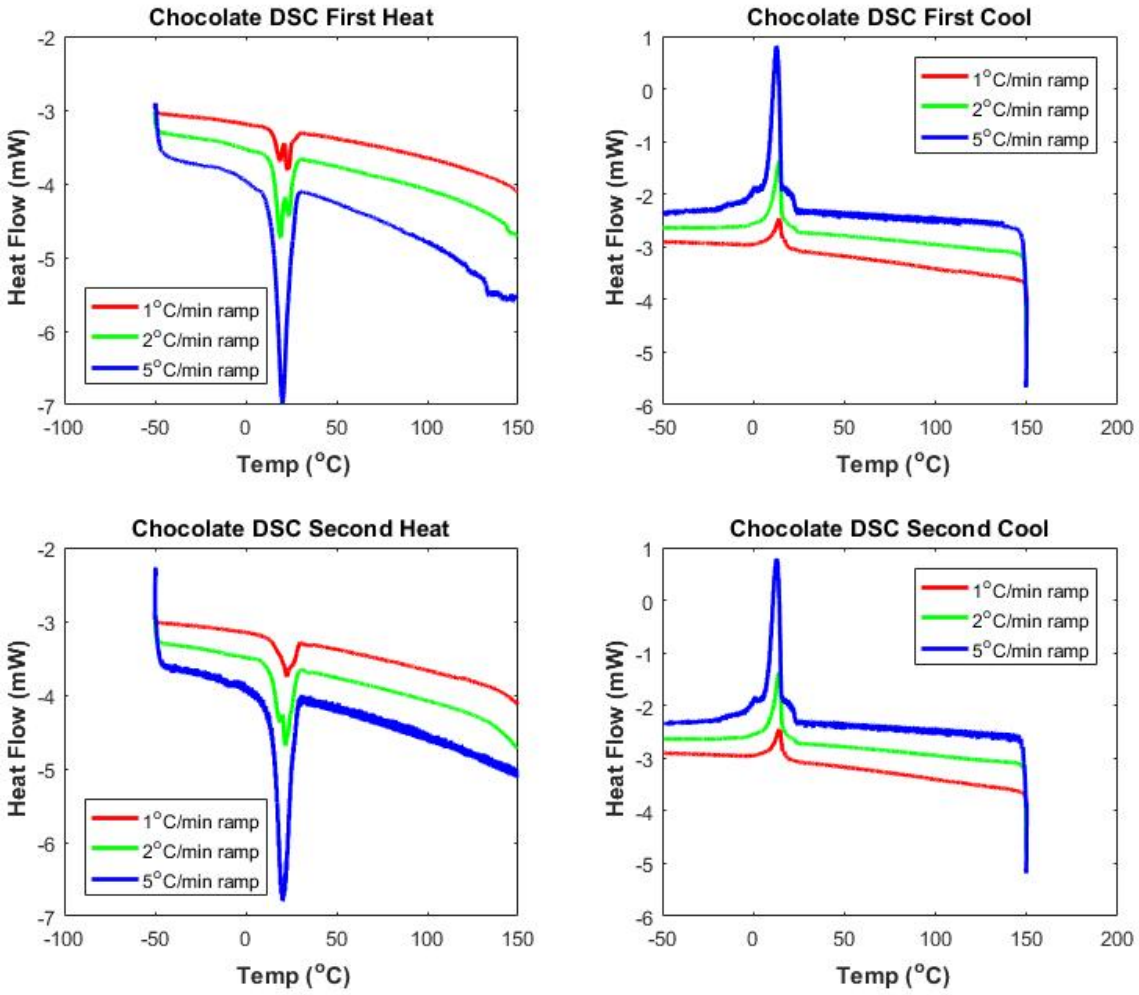

Figure 3. 44: Heat flow as a function of temperature for the chocolate at temperature ramps of 1, 2, and 5°C per minute broken into the heating and cooling cycles.

Chapter Three, Section 5.1 Ecosoya Directionality Testing

Due to the formation of voids during cooling there was reason to suspect that the Ecosoya pillar blend wax in a solid form would be acoustically anisotropic. This is not to say the material itself has any anisotropic properties, only that the random formation of voids would have directional biases, thus causing differences in the speed of sound depending on which direction the measurement was taken. A test was preformed to investigate this hypothesis. A large block of cooled wax was cut into seven smaller

blocks using a hand held coping saw with care taken to keep the blocks in their original orientation as shown in Figure 3. 45 and Figure 3. 46. The top surface was marked with a "T" to ensure the measurements were taken in the correct direction. Speed of sound measurements were then performed using through transmission methods. A 0.5 MHz transducer, coupled to the wax with ultrasonic gel, was manually held to each side of the wax blocks (as shown in Figure 3. 47) and a series signals were captured once per second over a five second window. This was repeated for all three directions x, y, and z where x is the direction along the length of the original large block, y is the direction across the width of the original large block, and z is the vertical direction. Figure 3. 48 shows the results of the testing with the speed of sound of each block in each direction and Table 3. 2 provides the average speed of sound measured in each direction as well as the average bulk speed of sound along with the standard deviation of these measurements. From the data collected there is no distinguishable pattern or any one direction with a distinctly different speed of sound from the others. The speed of sounds measured range from 1.7mm/μs to 2.3mm/μs with an average speed of sound of 1.91mm/μs. This varying speed of sound with direction rejects the theory of ultrasonic anisotropy caused by voids created during cooling but indicated that the random formation of voids can have a significant effect on the measured speed of sound. This also shows up in the plot of multiple box tests shown in Chapter Four, Section 1.5 where the beginning speed of sound in the solid wax varies with each test.

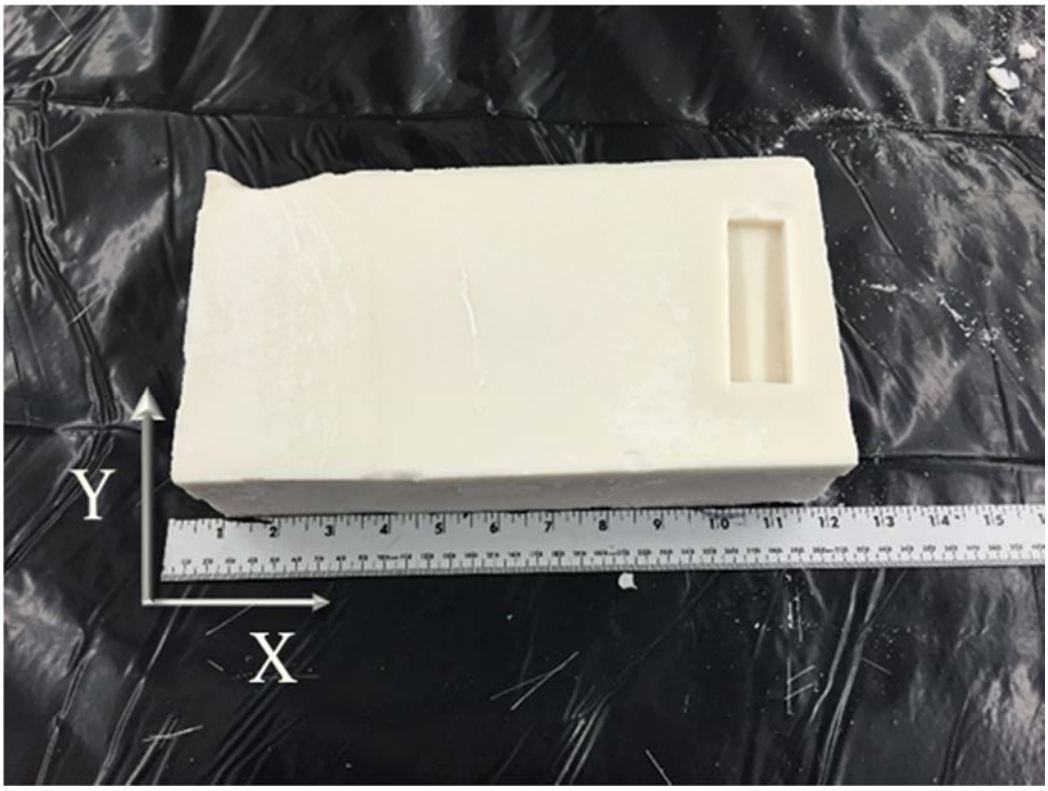

Figure 3. 45: Image of the large wax block with defined orientation before it was cut into smaller blocks.

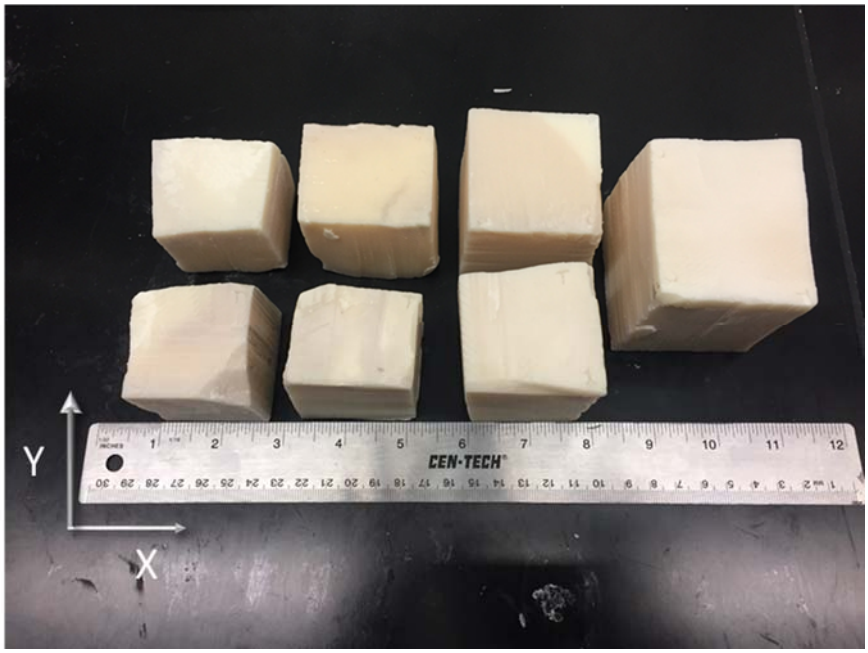

Figure 3. 46: Image of the small wax blocks with defined orientation arranged in the area from which they were taken.

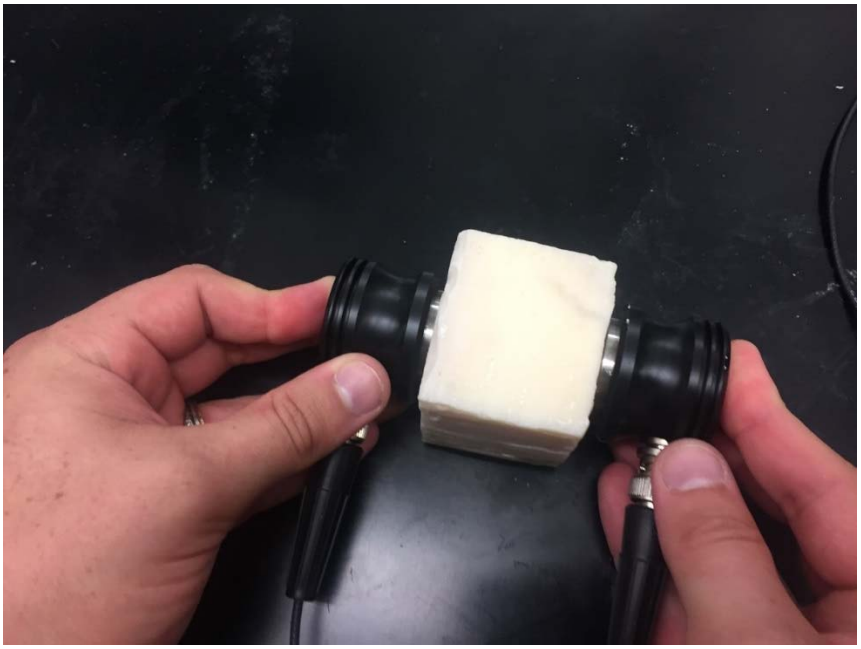

Figure 3. 47: Image depicting the process of manual application of the contact transducers during solid Ecosoya speed of sound measurements.

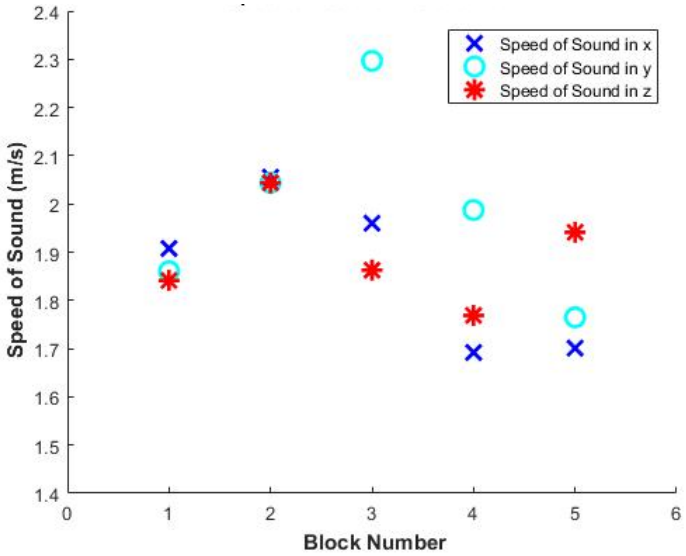

Figure 3. 48: Measured speed of sound in each direction for all wax blocks.

Table 3. 2: Calculated average speed of sound values and the standard deviation for measurements taken in each direction and for the bulk material.

Direction	Average Speed of Sound (mm/μs)	Standard Deviation
X	1.86	0.16
y	1.99	0.20
Z	1.89	0.10
Bulk Average	1.91	0.16

Chapter Three, Section 5.2 Acrylic Speed of Sound Testing

Because the ultrasound transducers were attached to the outside of the container and the signal will travel through the acrylic walls it was necessary to determine if the temperature change of the acrylic would affect the speed of sound calculations. A small experiment was set up consisting of an acrylic block 5/8" thick with two holes drilled for thermocouples being heated in a furnace over a temperature range of 35 to 65°C in 5°C increments. The block was left to sit in the furnace at the set temperature until the thermocouples at the interior of the block registered the set temperature. The block was then briefly removed from the furnace and a transducer was manually held on each side of the block coupled with acoustic gel as shown in Figure 3. 49. At each temperature a series of 10 A-scans were taken at equal intervals over a 10 second period and the mean time of flight value was tabulated. The block was then returned to the furnace at the next set temperature and the process was repeated. The results of the test are shown in Figure 3. 50. The plot shows some change in the speed of sound as the temperature increased with a high measurement of 2645m/s and a low of 2560m/s, a range of about 3%. From these results it is determined that the speed of sound results will not be significantly affected by the temperature change in the acrylic walls.

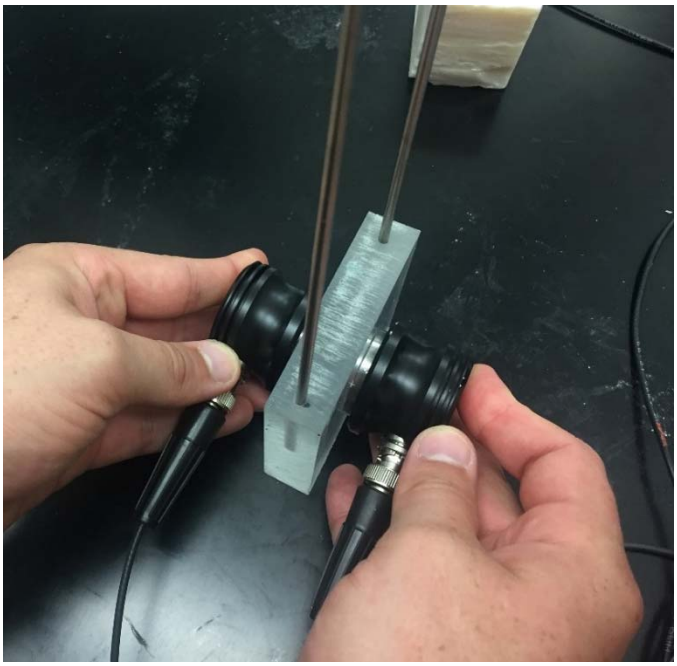

Figure 3. 49: Image depicting the process of manual application of the contact transducers during acrylic speed of sound measurement.

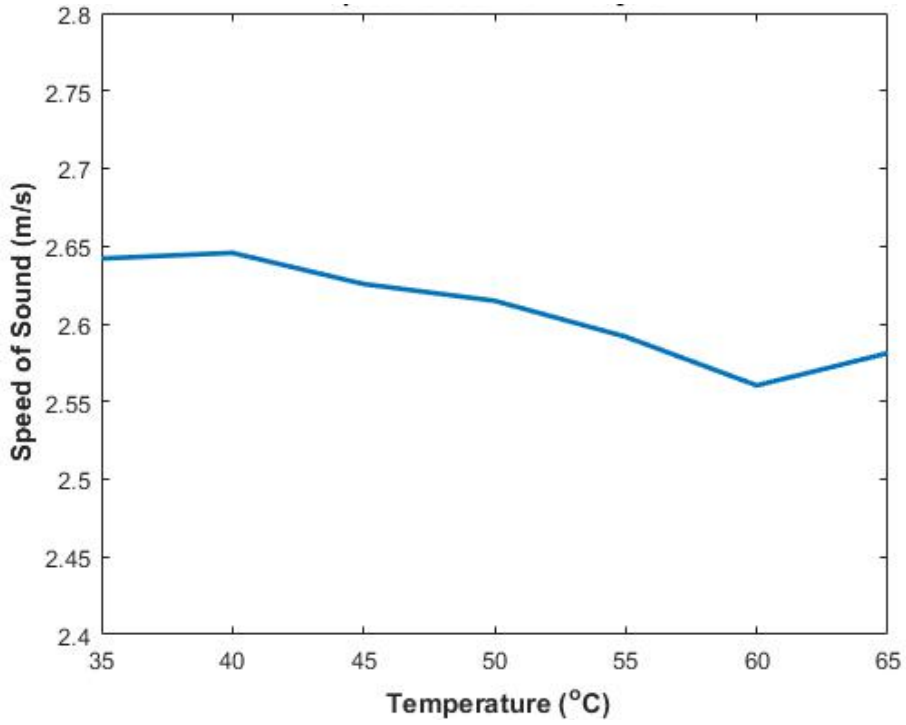

Figure 3. 50: Measured speed of sound in acrylic from 35-65°C

CHAPTER FOUR

Results

The following sections will discuss the results obtained from the large and small geometry confined container testing performed with the Ecosoya wax, base paraffin wax, and baking chocolate. The speed of sound of each material is analyzed as described in Chapter Three, Section 3, and temperature profile estimations are made using the measured speed of sound.

Chapter Four, Section 1: Large Geometry Testing, Ecosoya Wax

This section will review the large geometry test set up shown in Figure 3. 18 - Figure 3. 22 with the Ecosoya wax. The set temperature of the heating block for these tests was 149°C (300°F); at this temperature the wax melts fully across the box without the risk of thermal degradation of the wax directly adjacent to the heater.

Chapter Four, Section 1.1 Temperature Profile Results

This temperature was maintained until the wax had melted to the point where all transducers were above the melt line. The box was then allowed to cool until the wax had solidified and pulled away from the walls. Figure 4. 1 shows the trends for all thirteen thermocouples over the duration of a test. The first thermocouple to spike in temperature is thermocouple 13 monitoring the heater block followed by the other thermocouples as the melt front arrives at their locations. After the melt front has passed all of the thermocouples the temperature of the liquid wax continues to increase until the wax is completely melted. With full melt achieved the heater is turned off and the cooling cycle

begins; all of the thermocouples show a rapid decrease at first that levels out as the wax approaches room temperature.

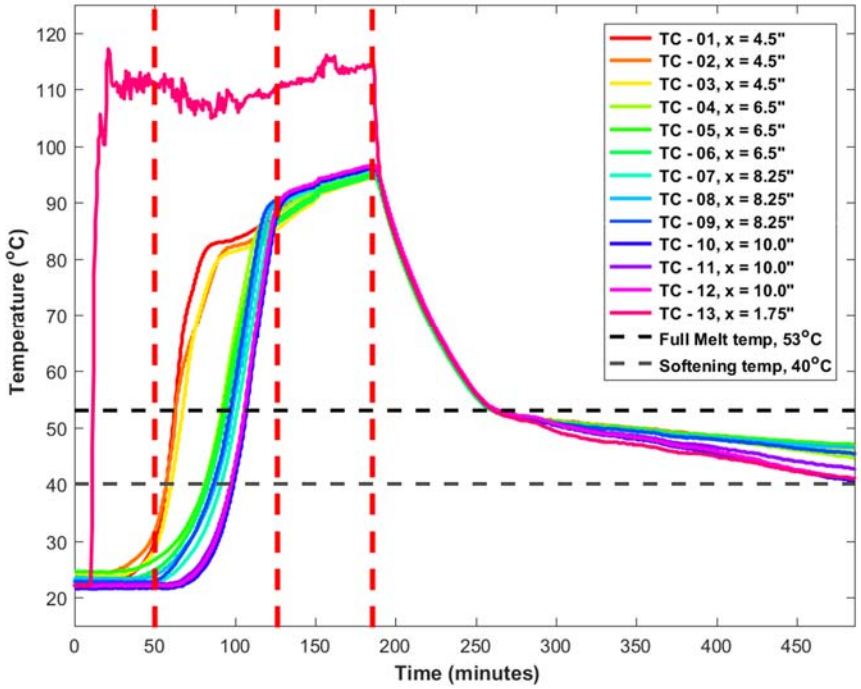

Figure 4. 1: Typical thermo couple measurement results from the large geometry Ecosoya wax testing

The dashed vertical lines shown in Figure 4. 1 delineate the various stages of the heating and cooling cycles. The far left section is the initial heating of the material. During this stage the wax is still mostly solid except around the heater block as is shown in Figure 4. 2. The next stage is melt progression, shown in Figure 4. 3. During this period the melt line is traveling across the container but the wax has not completely melted. The third stage is the full melt (Figure 4. 4). At this point the melt front has passed all of the transducers and the liquid wax is continuing to heat. The final stage is

the cooling cycle (Figure 4. 5), this occurs after the heater is turned off and lasts until the wax contracted and separated from the container walls.

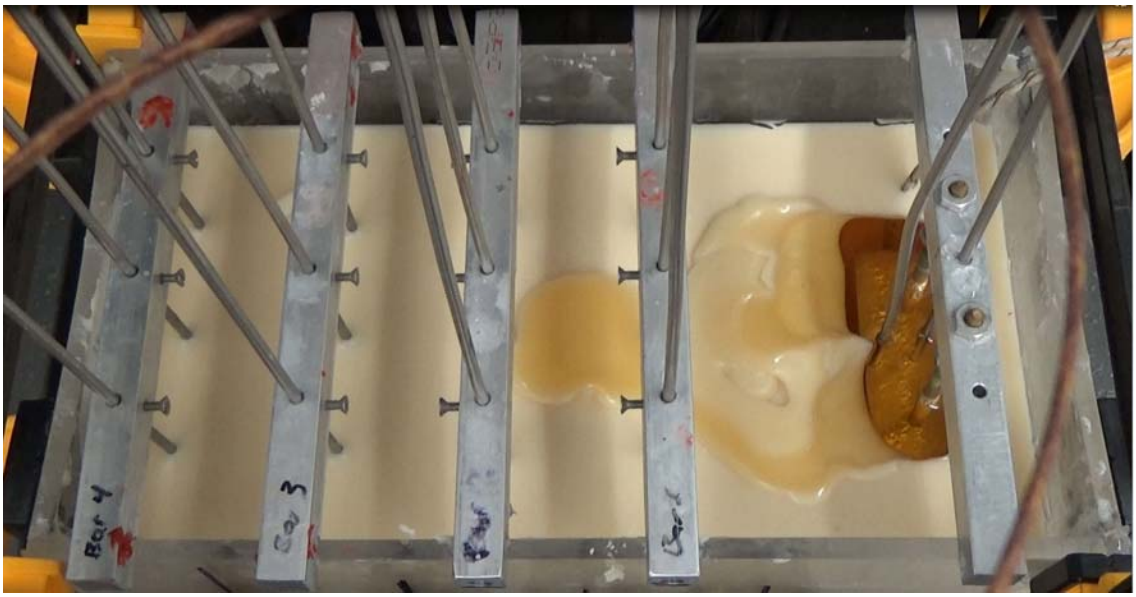

Figure 4. 2: Image of the large geometry Ecosoya wax test shortly after the heater was turned on.

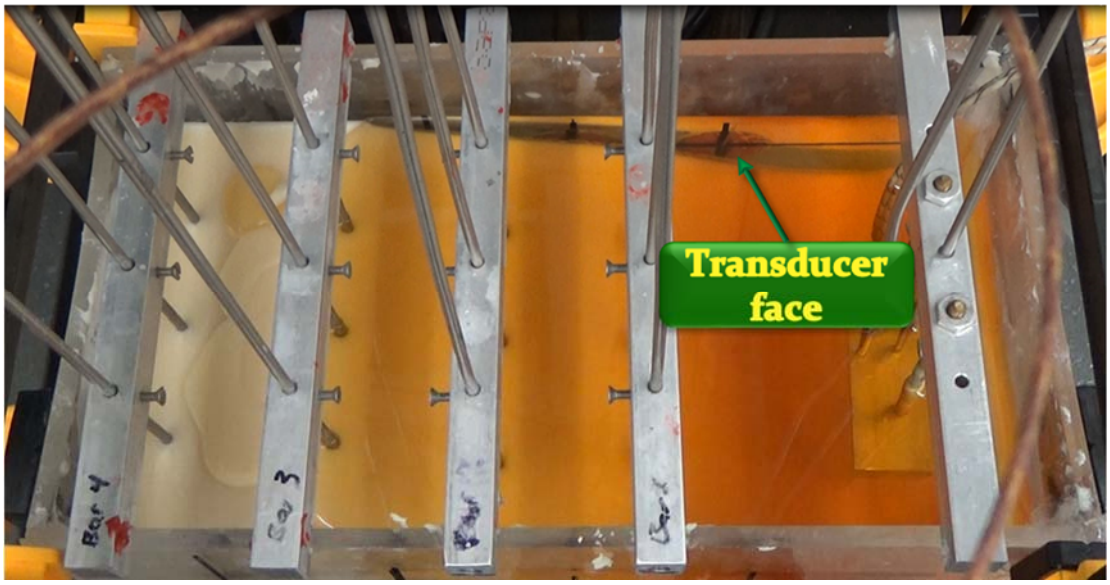

Figure 4. 3: Picture of the large geometry Ecosoya wax test as the melt front progresses partially revealing some of the transducer faces.

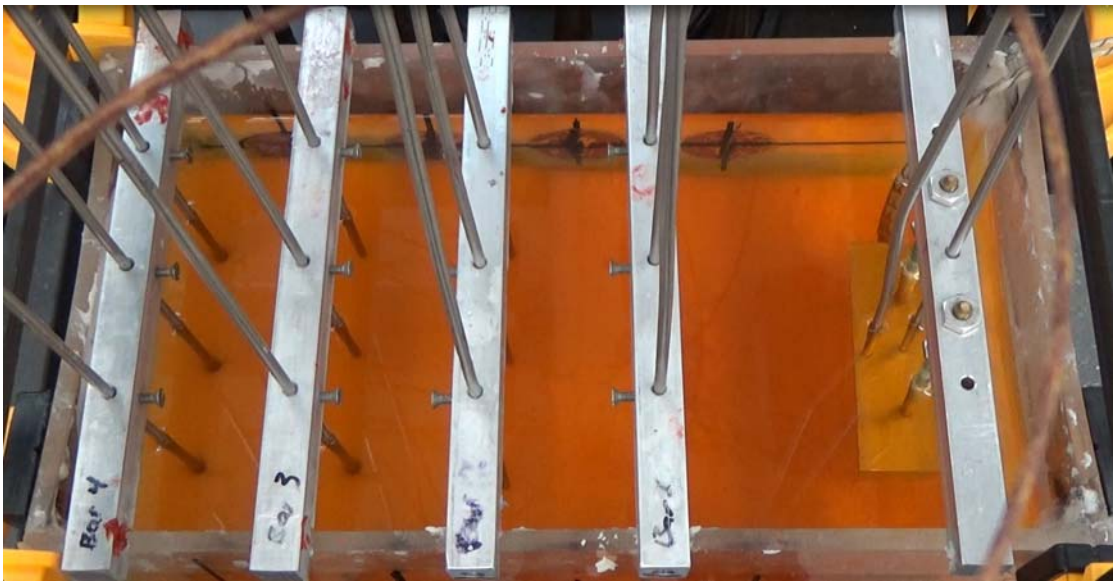

Figure 4. 4: Image of the large geometry Ecosoya wax test near full melt.

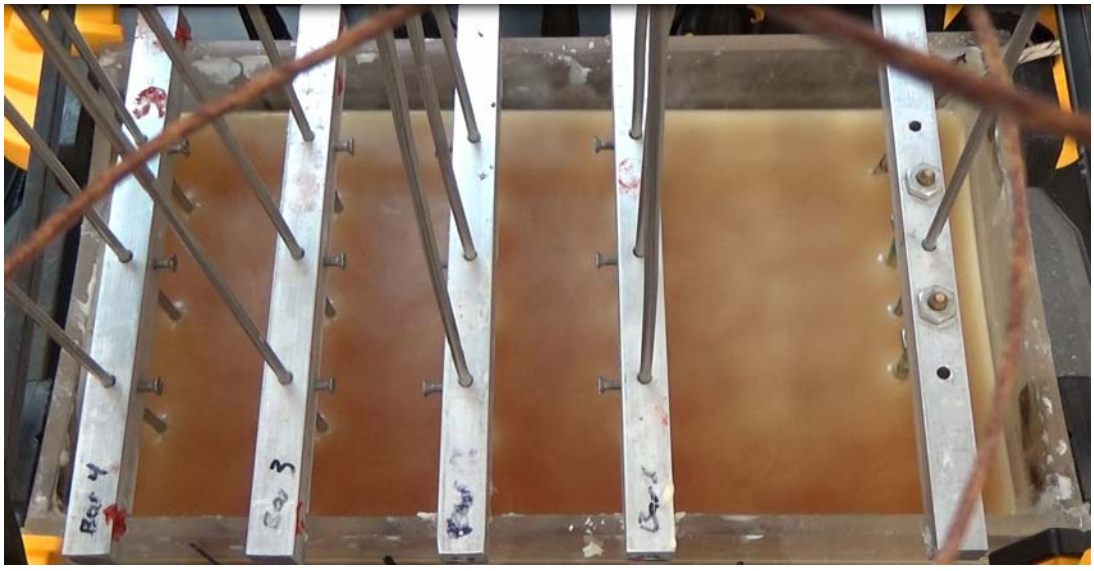

Figure 4. 5: Picture of the large geometry Ecosoya wax test during cooling as the surface layer of wax is solidifying.

In order to better understand the temperature profiles, Figure 4. 6 shows the temperature profiles recorded at bar 1 (thermocouples 01-03) at 4.5 inches from the from the box wall behind the heater as shown in Figure 3. 18. The melt temperature is marked

by the horizontal dotted line at 53°C as was determined by DSC testing shown in Figure 3. 35. This is the first set of thermocouples to react to the heat and has a slightly different profile than the other sets of thermocouples during the initial heating section. During this time the melt progresses past the bar 1 thermocouples and the thermocouples heat quickly followed by a short stall at approximately 80 minutes where the melt front expands across the width of the container before progressing further across the length. Once the melt front progresses along the length of the container again the temperature increases on a near linear slope until the heater block is turned off (180th minute of this test).

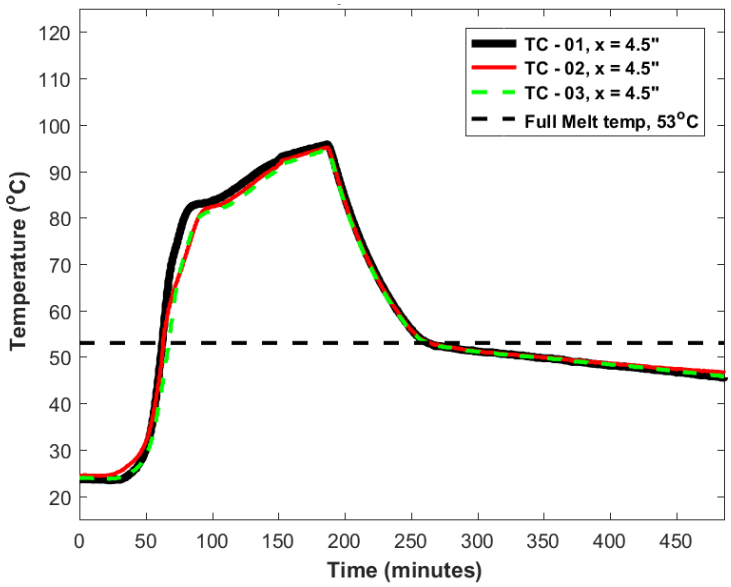

Figure 4. 6: Typical temperature profiles measured by the bar 1 thermocouples during a large geometry Ecosoya wax test.

The other thermocouple groups (bars 2-4) all have similar trends. There is a spike in temperature as the melt front passes the thermocouples followed by an approximately linear increase until the heater block is turned off. These temperature profiles are shown in Figure 4. 7, Figure 4. 8, and Figure 4. 9. The melt temperature is marked by the horizontal dotted line at 53°C as was determined by DSC testing shown in Figure 3. 35.

These trends in the temperature profile are consistent for all large geometry tests performed

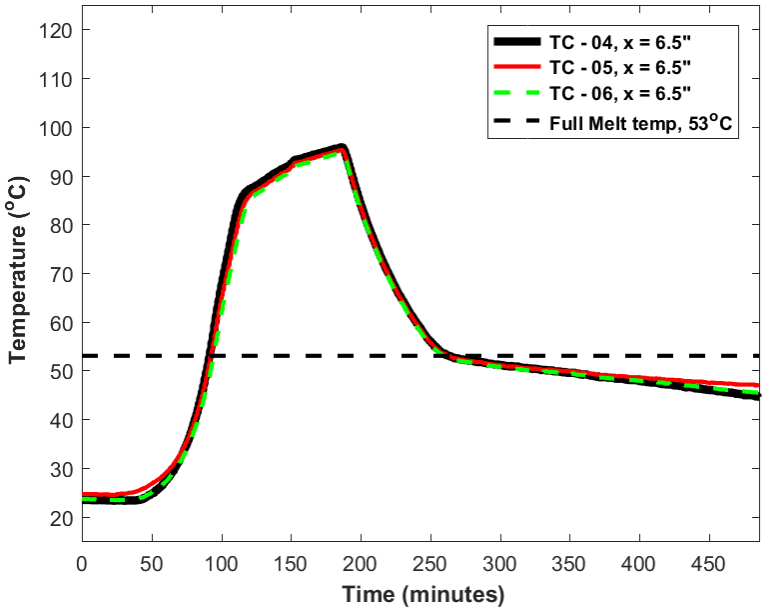

Figure 4. 7: Typical temperature profiles measured by the bar 2 thermocouples during a large geometry Ecosoya wax test.

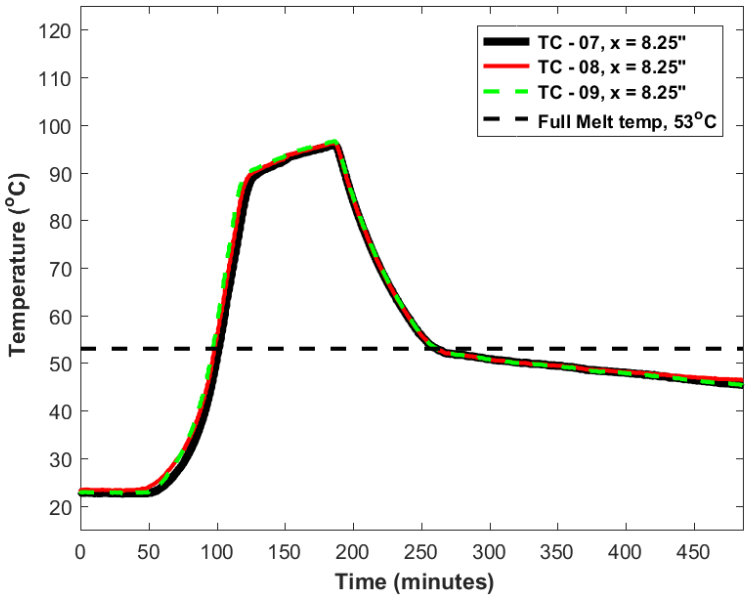

Figure 4. 8: Typical temperature profiles measured by the bar 3 thermocouples during a large geometry Ecosoya wax test.

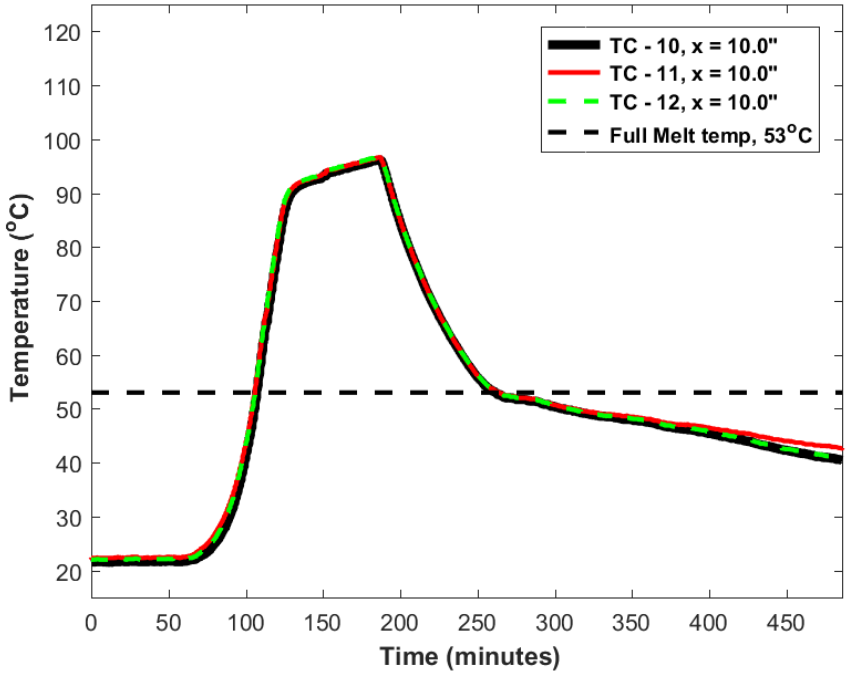

Figure 4. 9: Typical temperature profiles measured by the bar 4 thermocouples during a large geometry Ecosoya wax test.

Chapter Four, Section 1.2 Speed of Sound Results

Ultrasound data is captured according to the large geometry box channel guide show in in Chapter Three, section 2. Typical A-scan results are shown in Figure 4. 10 - Figure 4. 14. These A-scan images show the change in the time of flight as well as signal shape throughout the test. Figure 4. 10 shows an A-scan taken 4 minutes into the test, at this point the A-scan generated has a maximum at the third signal peak after which the signal decays quickly. At this time the wax is still completely solid and the heater has not been turned on yet. The speed of sound is computed as described in Chapter Three, Section 3 and shown below in (4.1). At this time the speed of sound is calculated at 1.7mm/μs.

$$v_w = \frac{l_{total} - 2 * l_{wall}}{TOF - t_{wall}} = \frac{0.1463\ \text{m} - 2 * 0.0112\ \text{m}}{89.35\mu\text{s} - 4.32\mu\text{s}} = 1.72\frac{\text{mm}}{\mu\text{s}} \quad (4.\ 1)$$

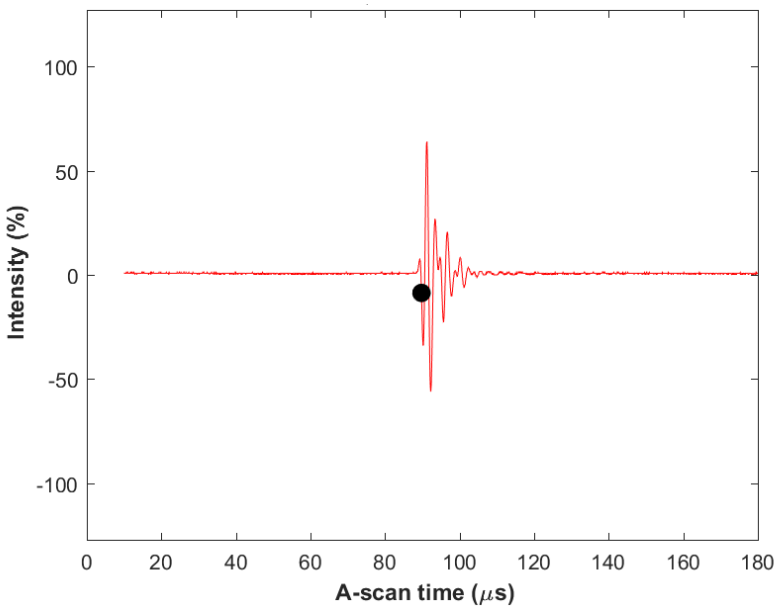

Figure 4. 10: Typical A-scan for the solid Ecosoya wax at ultrasound channel 1 at 4 minutes into the large geometry test. The time of flight is marked by a black dot.

Figure 4. 11 shows an A-scan taken 94 minutes into the test. At this point the melt front has arrived at the transducer face (see Figure 4. 3) but has not completely passed it resulting in a split signal where part is traveling through a solid wax path and part is traveling through a liquid path. This is shown in Figure 4. 11 by the occurrence of two distinct signals, one at 90μs and the other at 135 μs. These signals have significantly different shapes with the faster signal having a similar shape to the solid wax A-scan shown in Figure 4. 10 with a longer decay time, and the slower signal having a smaller amplitude with the signal max at the front of the signal followed by a slower decay with more activity in the tail of the signal. At this time the speed of sound is recorded based on the first normalized signal with a peak grater that 30% saturation (as described in Chapter

Three, Section 3 and shown in (4.1), which in this case is the solid signal, providing a speed of sound of 1.7mm/μs. This will continue until the melt front progresses far enough that the slower becomes dominant and the speed of sound drops abruptly to approximately 1mm/μs. This signal is not always strong enough to be captured as the time of flight, but it is present in all scans.

As the wax continues to melt the fully liquid signal becomes apparent between the other two waves at around 125μs as shown in Figure 4. 12. This scan shows the signal from the solid material has decreased in intensity but maintained its shape while the signal from the indeterminate material has increased in intensity. The fully liquid signal will increase in intensity as the melt front passes the transducer pair and the other signals slowly decay.

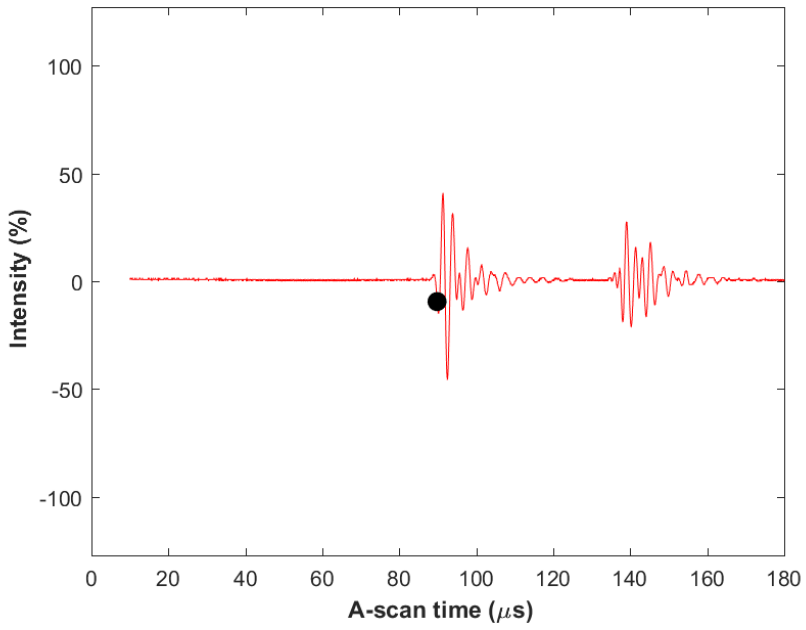

Figure 4. 11: Typical A-scan for the transitioning Ecosoya wax recorded at ultrasound channel 1 at 94 minutes into the large geometry test. The time of flight is marked by a black dot.

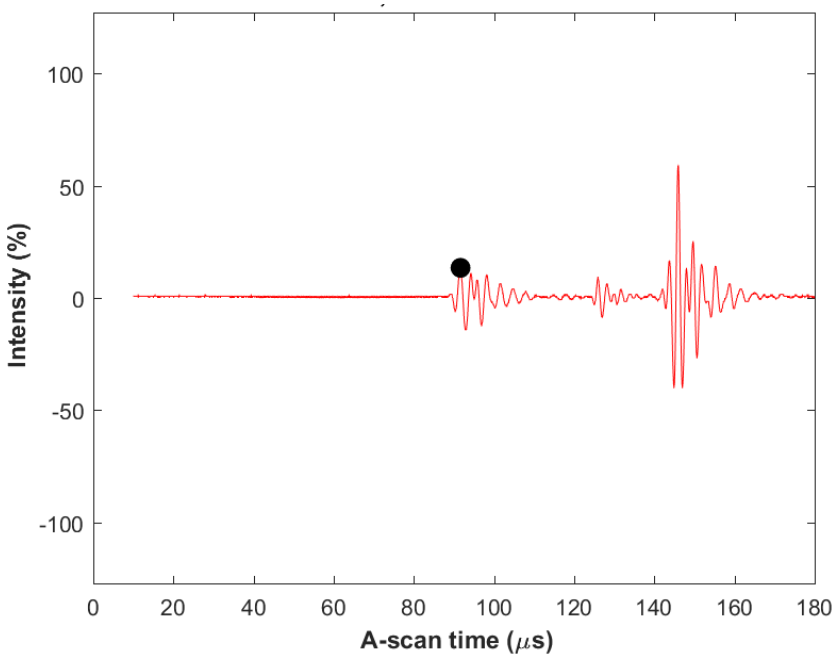

Figure 4. 12: Typical A-scan for the transitioning Ecosoya wax recorded at ultrasound channel 1 at 103 minutes into the large geometry test. The time of flight is marked by a black dot.

Figure 4. 13 shows an A-scan taken 149 minutes into the test. At this time the wax is nearly fully melted as shown in Figure 4. 4 and the signal shows a fully liquid path with a time of flight of 125μs. The signal shape at this point is a mix of the two signals show in Figure 4. 11 where the signal maximum is still the third peak like the solid signal, but the signal has a bit more noise toward the tail like the slower mixed phase signal. At this time the speed of sound is calculated at 1.2mm/μs using equation (4.1).

Figure 4. 14 shows an A-scan taken 399 minutes into the test (about an hour before the end of the test). The wax has now had several hours to cool and has re-entered the solid phase. The signal has returned to the same shape as the solid signal shown in Figure 4. 10 with the shorter decay and signal maximum at the third peak, but with the material still at an elevated temperature the time of flight is longer at approximately 105μs. At this time the speed of sound is calculated to be 1.4mm/μs using equation (4.1).

From this point the wax will continue to cool and contract until it pulls away from the container wall and ultrasonic coupling is lost.

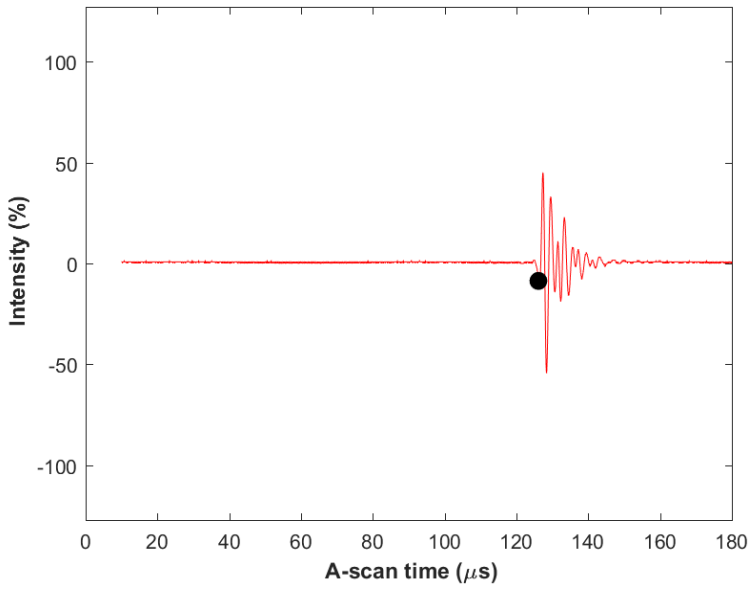

Figure 4. 13: Typical A-scan for the liquid Ecosoya wax recorded at channel 1 at 149 minutes into the large geometry test. The time of flight is marked by a black dot.

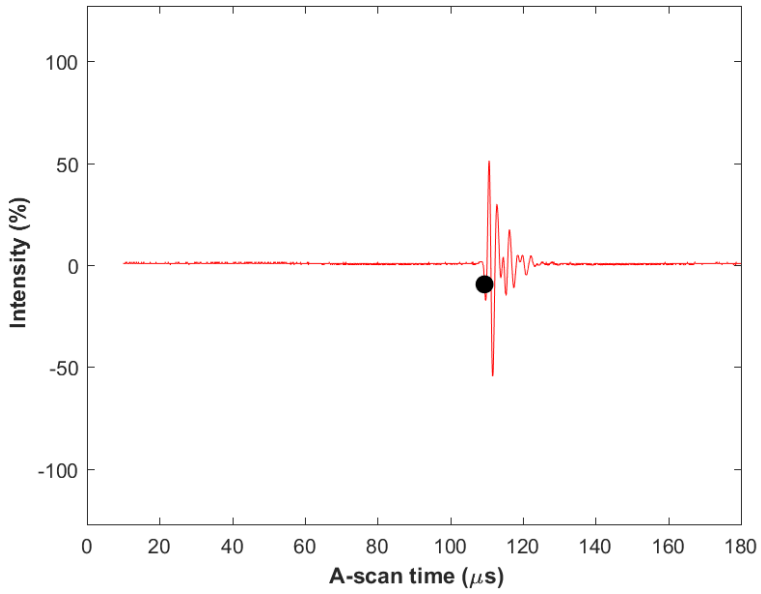

Figure 4. 14: Typical A-scan for the cooling Ecosoya wax recorded at channel 1 at 399 minutes into the large geometry test. The time of flight is marked by a black dot.

The speed of sound is calculated based off of the recorded time of flight and the path length shown in the large geometry box diagram in Figure 3. 18. An example of this calculation is shown in (4.1). Figure 4. 15 - Figure 4. 18 show the trends of the speed of sound in the wax throughout the duration of the test. Ultrasound channels are laid out as depicted in the diagram for the large geometry box in Figure 3. 20 with channel 1 being farthest from the heater block and channel 4 being closest to the heater block. It is observed that all channels showed similar trends with the only difference being the time of melt, which occurs between 50 and 100 minutes depending on the ultrasound channel, where the speed of sound drops suddenly from its initial value of 1.7mm/μs (as would be typical of the solid region) down to 1.3mm/μs for the liquid region. The speed of sound continues to decrease slowly as the liquid wax continues to heat until the heater is turned off at 180 minutes as indicated by the vertical dotted line in the images. At that point the liquid wax cools over a 300 minute span and the speed of sound increases steadily from 1.2mm/μs to 1.4mm/μs over the first 100 minutes. During this time the wax is beginning to form a solid exterior while the interior remains liquid as is shown in Figure 4. 5. The speed of sound then increases linearly until the wax pulls away from the box. A strange event can be seen in Figure 4. 15 where the signal drops below the fully liquid state value of 1.3mm/μs to near 1mm/μs. This is caused by the slower signal of the dual signals seen in Figure 4. 11 gaining enough intensity relative to the faster signal to be measured as the time of flight. It is not certain what causes this signal to occur, but it may be a Rayleigh wave, a surface wave which propagates along a solid boundary slower than the longitudinal or shear waves, traveling along the solid wax\liquid wax interface as the melt front crosses the transducer path. This will be discussed further in Chapter Five, Section

2. This signal does not always reach the strength where it would contribute to the time of flight, but the signal is present across all ultrasound channels and tests. After the melt front passes the transducer face the liquid speed of sound settles at 1.2mm/μs. The mirroring ultrasound channels (11-14 as shown on the diagram in Chapter Three, section 2) showed identical trends in speed of sound as those displayed by channels 1-4 as showed by Figure 4. 19.

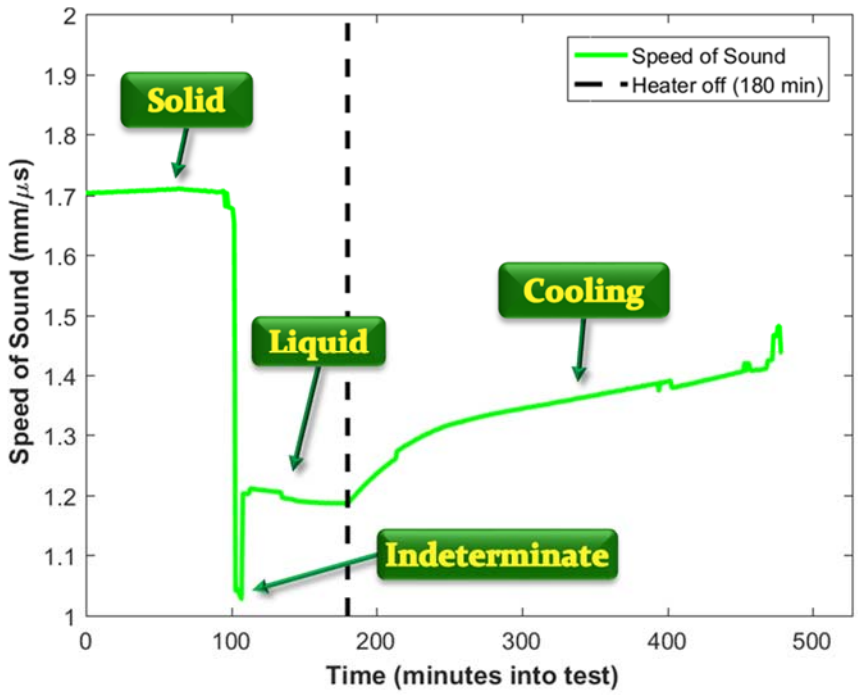

Figure 4. 15: Typical plot of the speed of sound vs. time at ultrasound channel 1 recorded for the duration of the large geometry Ecosoya testing. Major events are labeled.

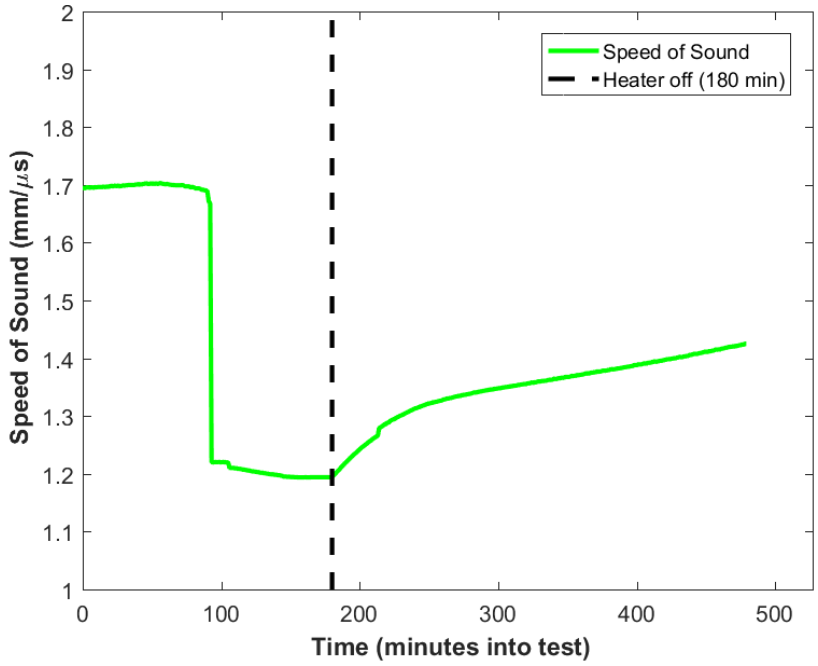

Figure 4. 16: Typical plot of the speed of sound vs. time at ultrasound channel 2 recorded for the duration of the large geometry Ecosoya testing.

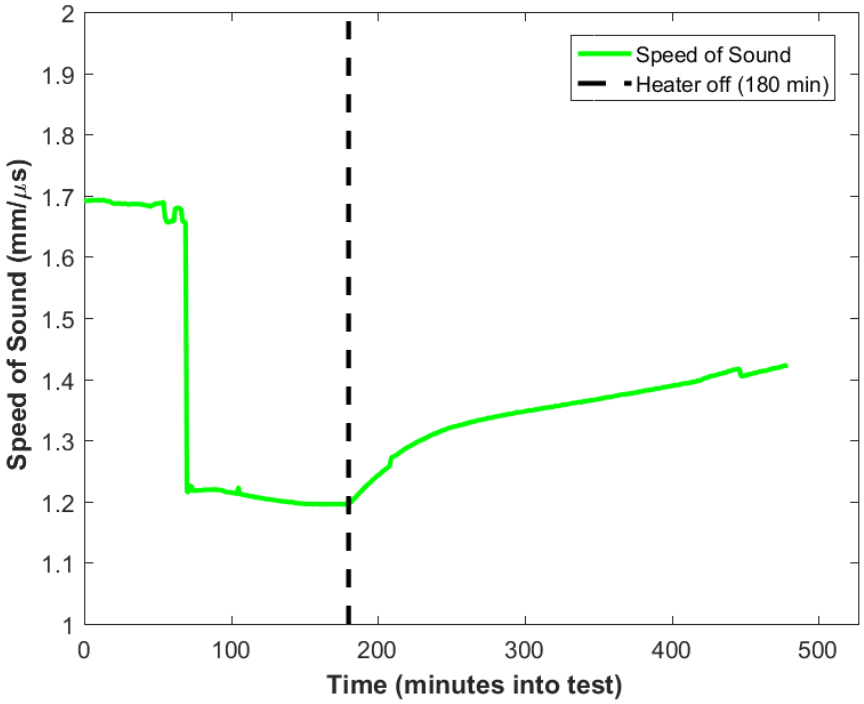

Figure 4. 17: Typical plot of the speed of sound vs. time at ultrasound channel 3recorded for the duration of the large geometry Ecosoya testing.

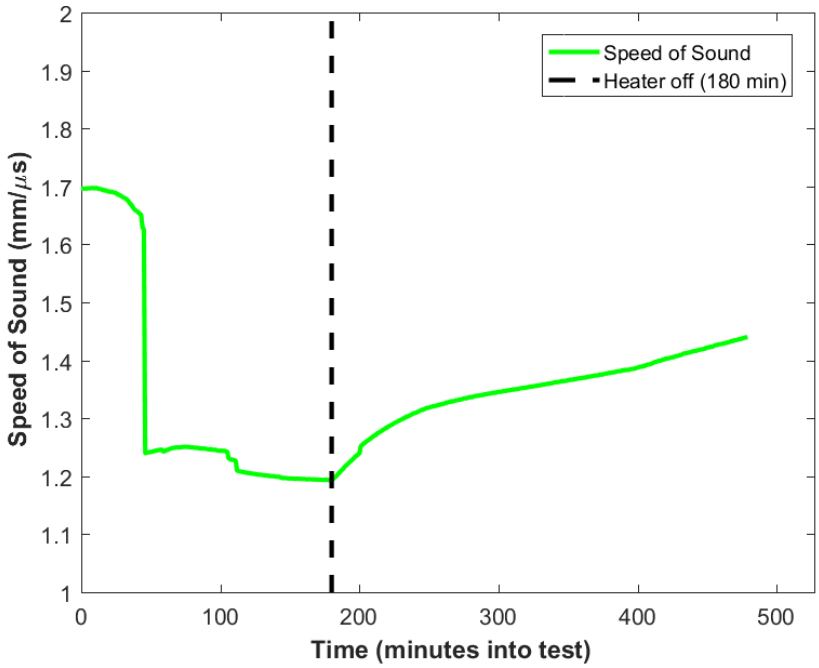

Figure 4. 18 : Typical plot of the speed of sound vs. time at ultrasound channel 1recorded for the duration of the large geometry Ecosoya testing.

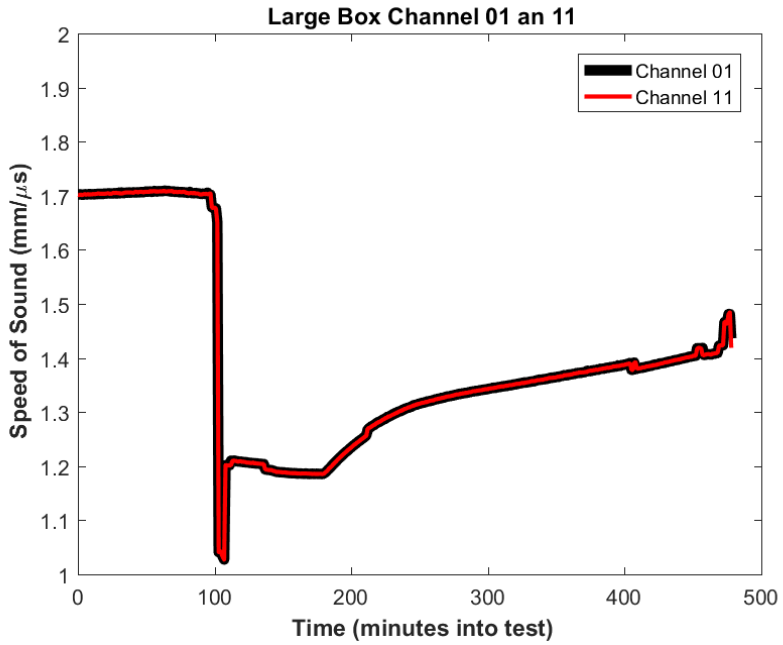

Figure 4. 19: Comparison of speed of sound vs. time results for ultrasound channels 1 and 11 which measure along the same acoustic path

Chapter Four, Section 1.3 Relating Temperature and Speed of Sound

Chapter Four, Section 1.2 illustrated some of the effects of the physical state changes on the speed of sound, but there are also some observations that can be made that relate the speed of sound to the temperature of the wax. Figure 4. 20 shows a plot of the temperature at the center of the ultrasound path (calculated from the linear average of the temperatures measured at the center thermocouples located on either side of the ultrasound path) vs. the speed of sound at ultrasound channel 01 (farthest from the heater block). Notice that the heating portion of the test does not yield much information and just stays the solid speed of sound of 1.7mm/μs until the liquid signal grows enough to dominate the solid signal and causes the sudden drop. This occurs because during the heating portion the wax is melting across the box as a melt front shown in Figure 4. 3. The temperatures just in front of and just behind this melt front are vastly different with the still un-melted wax near 40°C and the liquid wax at approximately 60°C. This leaves a very small window for the solid-liquid phase change and the temperatures around the melt front to be monitored. Conversely, for the cooling portion of the test temperature changes slowly and a clear relationship between the speed of sound and temperature can be observed. It is this cooling portion that will be used in further analysis to determine the instantaneous temperature of a sample using a measured speed of sound.

Figure 4. 21 - Figure 4. 24 show the temperature vs. speed of sound plots for ultrasound channels 1-4 during the cooling portion of the test (the plots read right to left in time following decreasing temperatures during cooling). The temperature portion of each plot is the temperature recorded at the center thermocouple from the bar located directly behind the transducer pair.

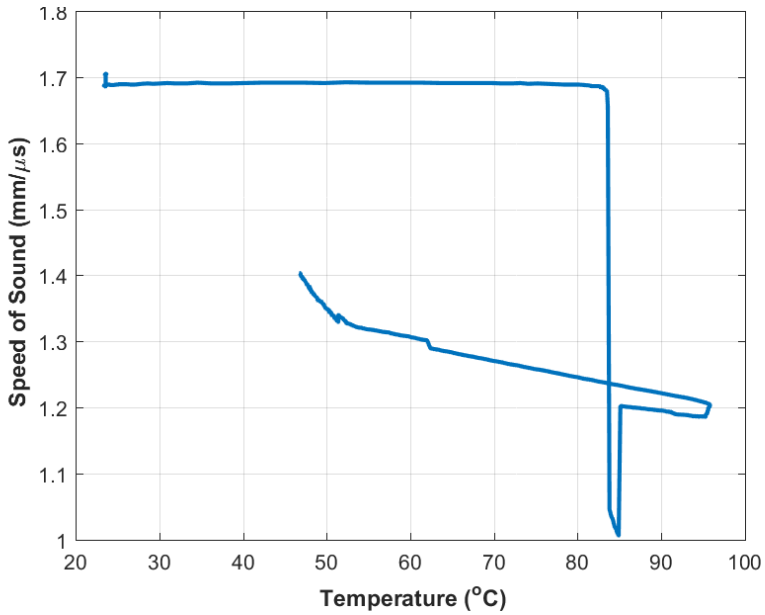

Figure 4. 20: Plot of the speed of sound vs. temperature for ultrasound channel 1 for the duration of the large geometry Ecosoya test.

All of the plots follow a similar trend; immediately after the heater is turned off the temperatures measured by the center thermocouples continue to creep up for a few minutes due to the latent heat of the heater block. At the same time the wax nearer the walls is cooling causing an increase in the speed of sound. The wax continues to cool and a linear relationship between the increasing speed of sound and decreasing temperature is observed until the wax begins to reach a solid state. It is worth noting from Figure 4. 1 that the thermocouples in the box are all nearly at the same temperature, so the observed results for all channels are nearly identical. Once the walls reach a phase change the cooling is no longer uniform, and a noticeable rise in the speed of sound is observed until the wax pulls away from the walls and coupling is lost This relation yields estimates of temperature for a given speed of sound if the material is cooling or in the fully liquid heating stage. The plot also allows the measurement of phase change temperature marked

by the inflection point of the bend at 53°C. This value was confirmed using DSC testing discussed in Chapter Three, Section 4.1 and shown in Figure 3. 35 and Figure 3. 37.

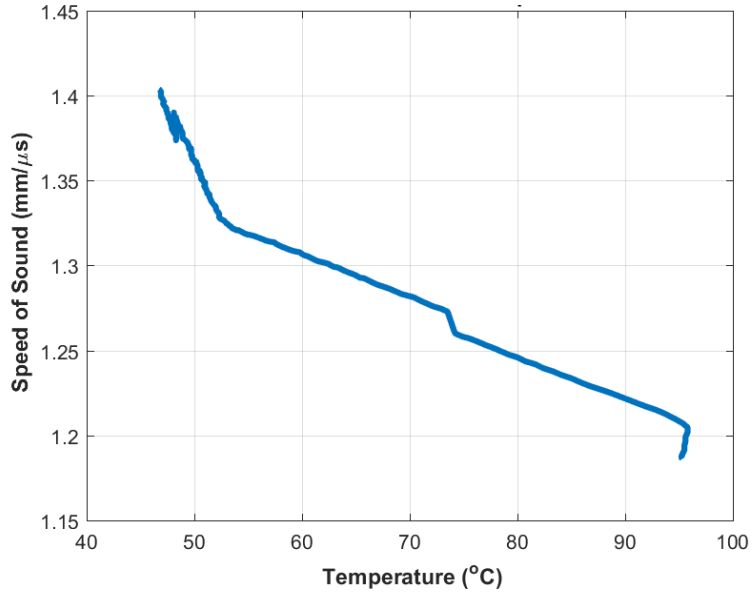

Figure 4. 21: A typical plot of the speed of sound vs. temperature for ultrasound channel 1 during the cooling portion of the large geometry Ecosoya test.

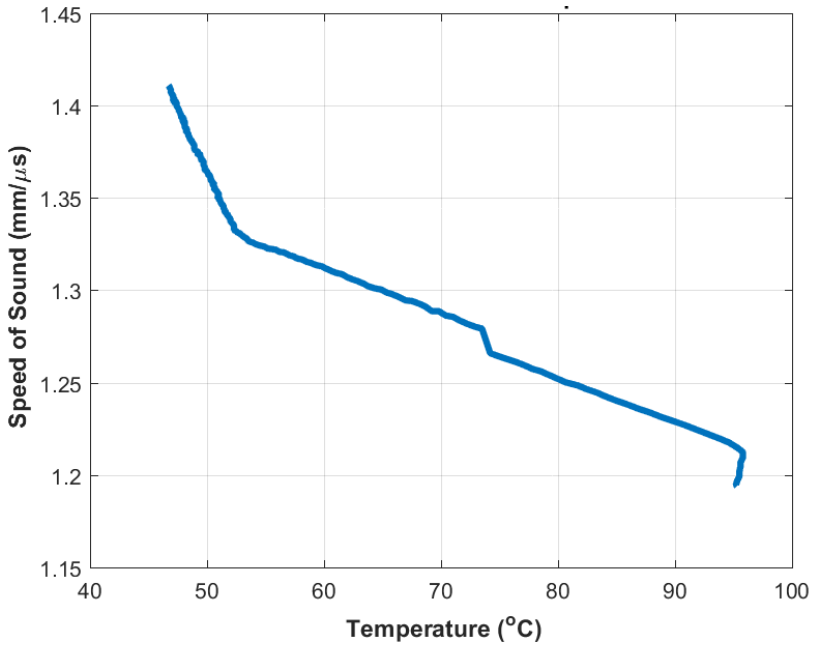

Figure 4. 22: A typical plot of the speed of sound vs. temperature for ultrasound channel 2 during the cooling portion of the large geometry Ecosoya test.

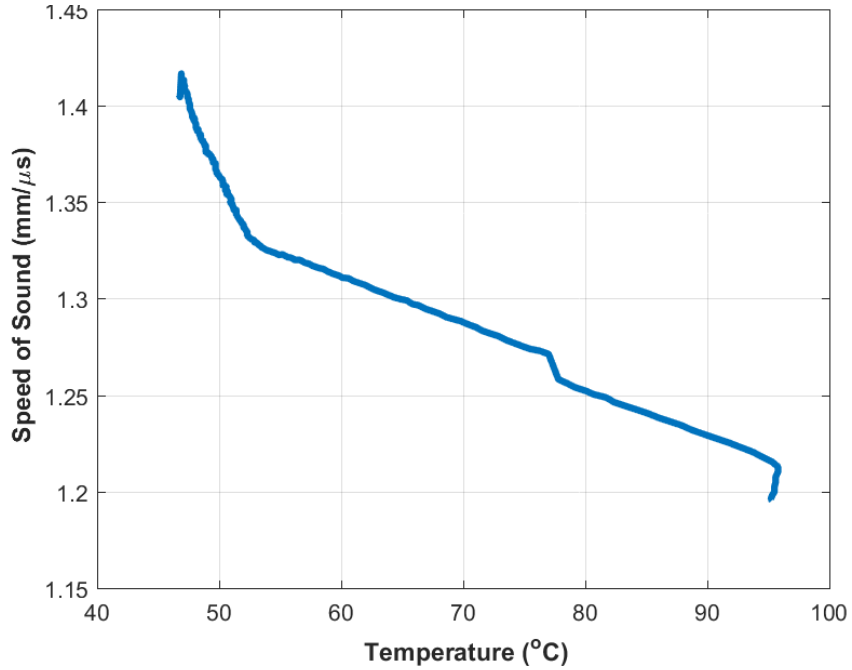

Figure 4. 23: A typical plot of the speed of sound vs. temperature for ultrasound channel 3 during the cooling portion of the large geometry Ecosoya test.

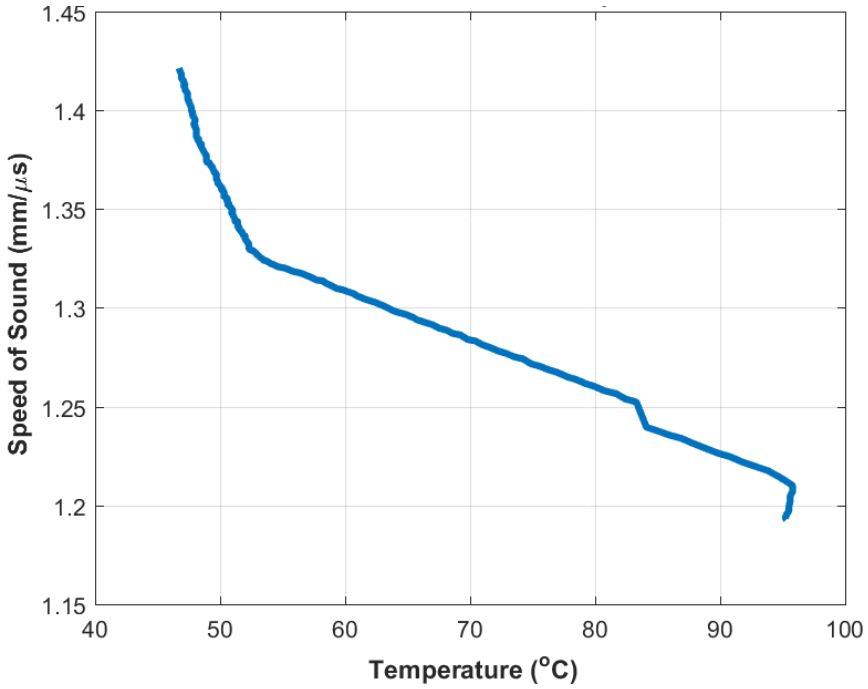

Figure 4. 24: A typical plot of the speed of sound vs. temperature for ultrasound channel 4 during the cooling portion of the large geometry Ecosoya test.

The measured ultrasonic speed of sound provides insight into the temperature and phase of the wax, but in order to accurately estimate the temperature of an unknown material traditional thermocouple probes must be used to first establish the relationship or some physical properties must be known about the material. For example, if it is known how the materials stiffness is affected by heating or cooling the speed of sound can be used to determine what trend is occurring. In the case of the wax as it heats it melts and becomes less stiff decreasing the speed of sound, conversely the stiffness increases as the wax cools resulting in an increased speed of sound. From this it can be determined whether the wax is heating or cooling from only a few minutes of observation. Phase changes are easier to detect since the drastic change in stiffness results in a significant change in the speed of sound over a short period of time.

Chapter Four, Section 1.4 Test Repeatability

This test was repeated five times over five separate days to ensure accuracy and that no phenomena were mistaken as physical reactions, such as air pockets causing temperature spikes or gain changes causing the point selected for time of flight measurement to move from signal peak to signal peak. Figure 4.23 shows the ultrasound channel 01 speed of sound results for all five tests. The results correspond with each other in that there is a sudden drop in the speed of sound as the melt front crosses the signal path, and when the heater is turned off the speed of sound increases quickly over the first 80 minutes and transitions to a more linear slope for the remainder of the test. The main difference between the tests is the timing of events such as melt, when the heater is turned off, and when the wax pulled off of the wall, which can all be caused by small changes in room temperature and humidity from day to day or by the configuration and

amount of voids formed during the previous cooling of the wax. Another key difference is seen in the initial solid speed of sound ranging from 1.66 to 1.78mm/µs. Similar trends are observed for all ultrasound channels. Table 4. 1 shows the average speed of sound and the standard deviation of the speed of sound in fully solid or fully liquid wax. Data points were selected at the 30th, 150th and 300th minutes because at these points the wax is either fully solid, fully liquid, or steadily cooling respectively across all tests. The solid wax speed of sound has the most variation likely due to small voids forming in different areas each time the wax cools as discussed in Chapter Three, Section 4. The average speeds of sound in liquid and solid wax are consistent for all channels, and standard deviations for the liquid and cooling wax are low.

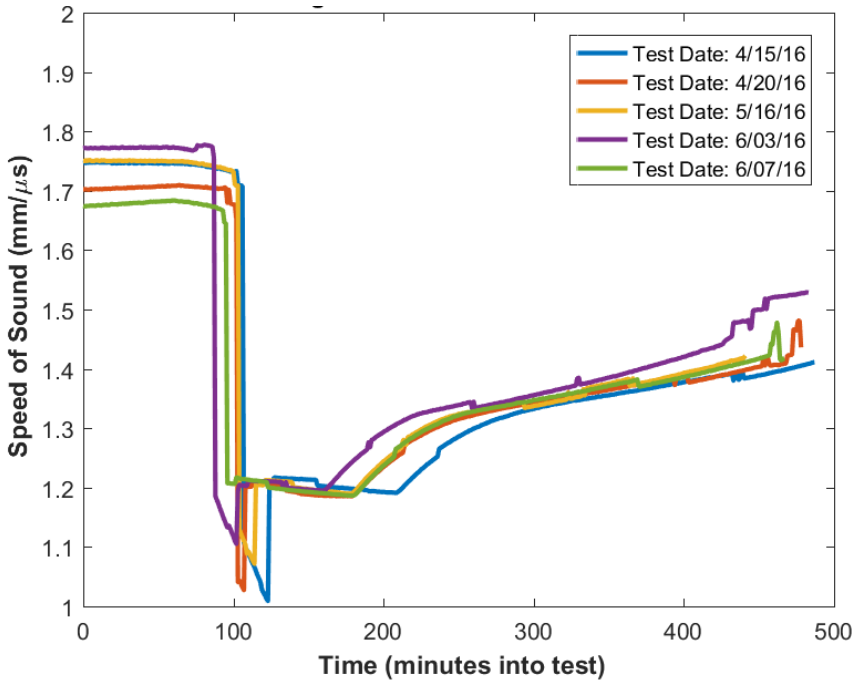

Figure 4. 25: A comparison of the speed of sound vs. time plots recorded from ultrasound channel 1 for all large geometry Ecosoya wax tests.

Table 4. 1: The average speed of sound measured at each ultasound channel for all large geometry Ecosoya wax tests during the solid, liquid, and cooling phases, and their associated standard deviations.

Ultrasound Channel	Average SoS Solid wax (mm/μs)	SoS Standard Deviation solid	Average SoS liquid wax (mm/μs)	SoS Standard Deviation Liquid	Average SoS Cooling wax (mm/μs)	SoS Standard Deviation Cooling
01	1.73	0.038	1.21	0.006	1.34	0.009
02	1.72	0.048	1.20	0.010	1.34	0.005
03	1.71	0.044	1.21	0.010	1.34	0.009
04	1.71	0.035	1.20	0.006	1.34	0.008

Figure 4. 26 shows a plot of the measured temperature vs. the speed of sound for all large geometry Ecosoya tests. All tests follow similar trends with the main difference being a slight vertical shift which may be attributed to slightly different changes in gain made during testing. All plots still have a slope change at 53°C marking the phase change temperature discussed in Chapter Three, Section 4.2 Figure 3. 35 and Figure 3. 37. Table 4.2 shows the standard deviation for the temperature. Using this method the temperature can be estimated to within about ±4°C given a speed of sound measurement.

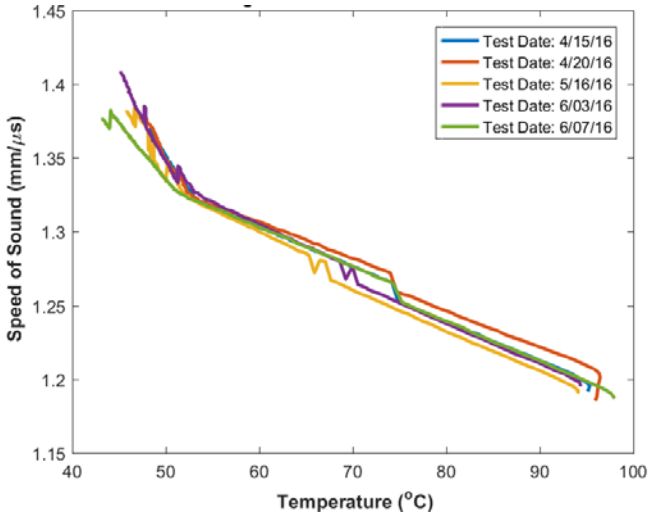

Figure 4. 26: A comparison of the speed of sound vs. temperature plots recorded from ultrasound channel 1 for all large box Ecosoya tests.

All plots still have a slope change at 53°C marking the phase change temperature discussed in Chapter Three, Section 4.2 Figure 3. 35 and Figure 3. 37. Table 4.2 shows the standard deviation for the temperature. Using this method the temperature can be estimated to within about ±4°C given a speed of sound measurement.

Table 4. 2: The average temperatures predicted by ultasound channel 1 from all large geometry Ecosoya wax tests at 1.2, 1.25, 1.3, and 1.35mm/μs and their associated standard deviations.

Speed of Sound (mm/μs)	Average Temperature (°C)	Standard Deviation (°C)
1.2	92.5	3.83
1.25	74.6	3.27
1.3	60.6	1.98
1.35	50.0	0.99

Chapter Four, Section 2: Small Geometry Testing Ecosoya Wax

A second wax container was created with a smaller geometry (see Figure 3. 23 - Figure 3. 25 for geometry specifics) to confirm results from the large geometry container. The change in geometry did not change the speed of sound results although both the melt and the cooling cycles were accelerated. Due to the smaller geometry box and the larger heater geometry the set temperature was decreased to 121°C (250°F) so that the wax was not over heated and the sealant would not be over stressed causing leaking.

Chapter Four, Section 2.1 Speed of Sound Results

The channel 1 A-scans for the small geometry container Ecosoya testing are shown below in Figure 4. 27 - Figure 4. 30. The first A-scan image, shown in Figure 4. 27 is taken 4 minutes into the test while the wax is still completely solid. The scan shows a signal with a time of flight of 45μs with the signal maximum occurring at the third peak and a steady decay through 80μs. The resulting speed of sound calculated at this time is

1.7mm/µs, which matches the speed of sound recorded from the large geometry testing shown in Table 4. 1. This signal is much stronger and more defined than the signal from the large geometry experiment shown in Figure 4. 10. A second smaller signal is recorded at approximately 135µs. This signal is the echo from the original pulse traveling across the container and echoing off of the interior of the acrylic wall back toward the pulsing transducer, then echoing off the interior of the original wall, and finally arriving at the receiving transducer after traveling the length of the box three times, resulting in a time of flight that is about three times that of the original signal.

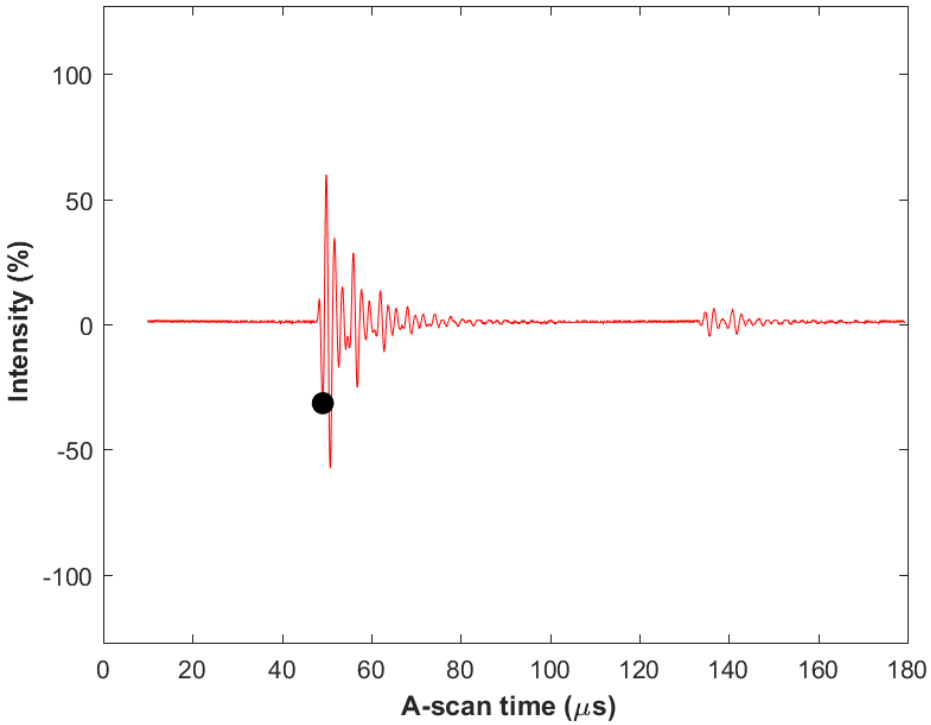

Figure 4. 27: Typical A-scan for the solid Ecosoya wax recorded at channel 1 at 4 minutes into the small geometry test. The time of flight is marked by a black dot.

Figure 4. 28 shows the A-scan image taken 56 minutes into the test. At this time three distinct signals can be observed at 45µs, 65µs, and 85µs, respectively. This indicates that the melt front has arrived at the transducer pair (similar to the melt point

shown in Figure 4. 3) and the material is in transition from solid to liquid in the same fashion as in the large geometry set up shown in Figure 4. 12. At this time the solid region signal is still strong and is selected as the measurement point for speed of sound which is calculated to be 1.7mm/µs. Unlike the large geometry tests the slower signal never reaches a higher intensity than the solid region signal and is never selected as the time of flight for use in calculating speed of sound. This is likely due to the melt front progressing faster across the acoustic path than in the large geometry testing. The small echo signal from Figure 4. 27 has died out as the material has transitioned and the gain has decreased.

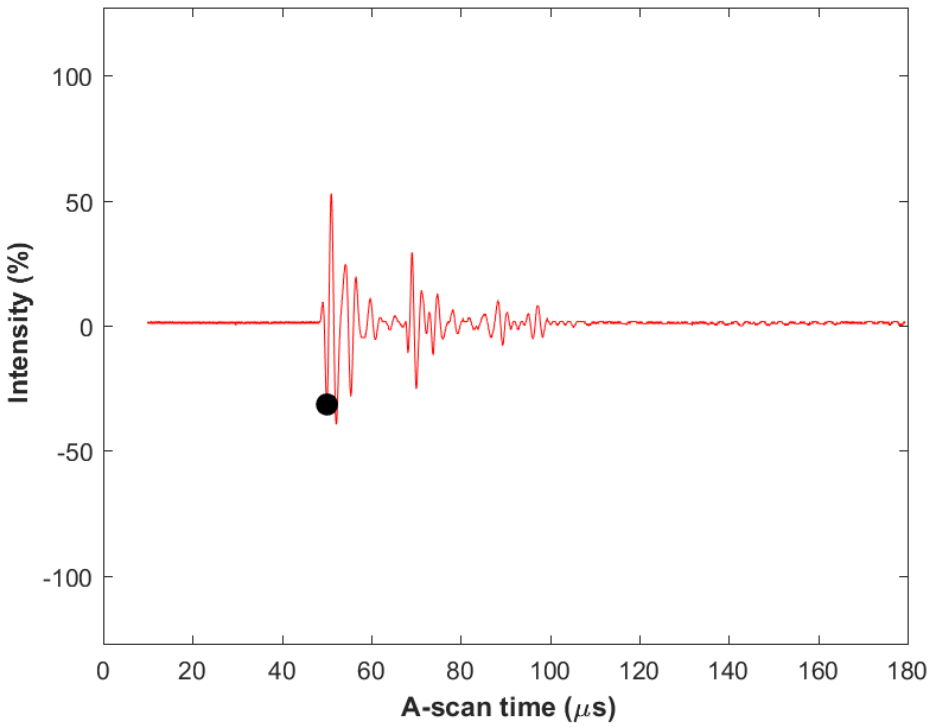

Figure 4. 28: Typical A-scan for the transitioning Ecosoya wax recorded at ultrasound channel 1 at 56 minutes into the small geometry test. The time of flight is marked by a black dot.

By the 80 minute mark the transition has ended and only the liquid signal remains with a time of flight of 65μs as shown in Figure 4. 29. At this time the speed of sound is calculated to be 1.3mm/μs, computed as shown in (4.1). This value matches the speed of sound values from the large geometry testing shown in Table 4. 1. The signal at this time is similar in shape to the all solid signal shown in Figure 4. 27, but has a faster decay.

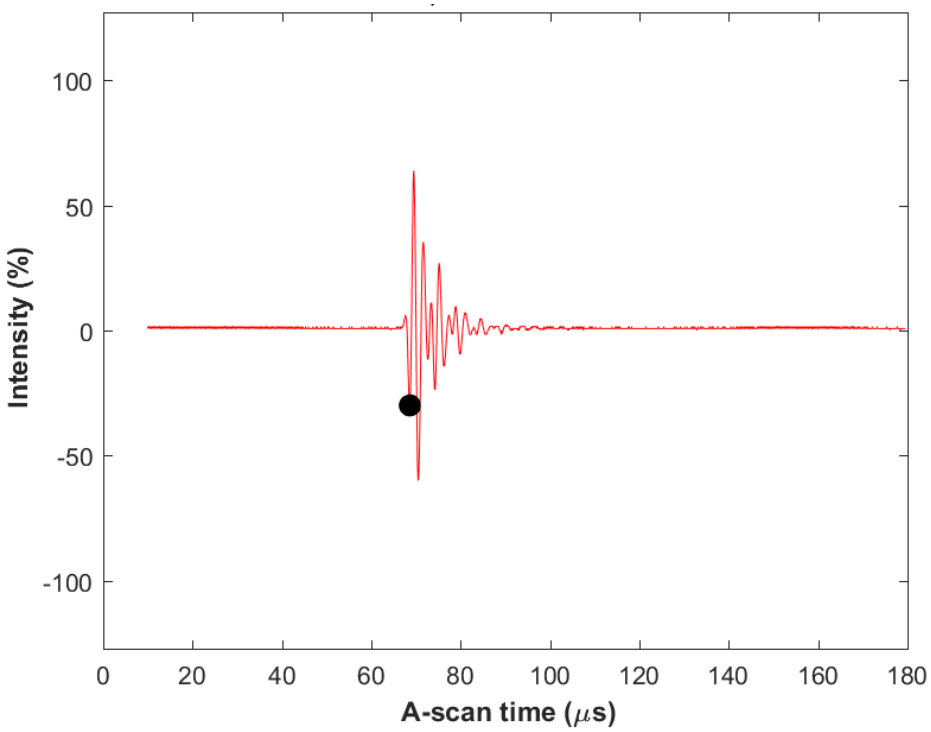

Figure 4. 29: Typical A-scan for the liquid Ecosoya wax recorded at channel 1 at 80 minutes into the small geometry test. The time of flight is marked by a black dot.

Figure 4. 30 shows the A-scan taken 329 minutes into testing. At this time the wax has had several hours to cool and the signal now has a time of flight of approximately 57μs.This time of flight results in a speed of sound of 1.5mm/μs. The signal shape has not changed much from the all liquid signal shown in Figure 4. 29 though the decay has lengthened and the small echo signal from Figure 4. 27 has returned at around 160μs.

The plots of speed of sound vs. time for the small geometry container ultrasound channels 1 and 2 are shown in Figure 4. 31 and Figure 4. 32. Refer to Chapter Three, section 2.2 Figure 3. 23 and Figure 3. 25 for container design and channel layout. Both channels begin at an initial speed of sound of 1.7mm/μs until the melt front passes the ultrasound path.

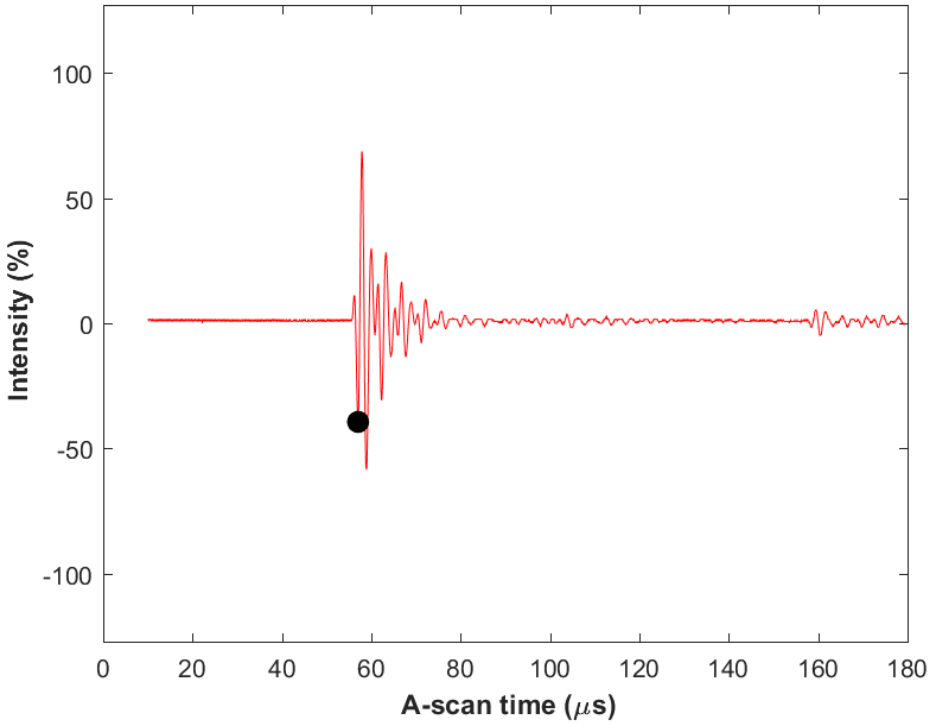

Figure 4. 30: Typical A-scan for the cooling Ecosoya wax recorded at channel 1 at 329 minutes into the small geometry test. The time of flight is marked by a black dot.

This occurs at 60 minutes for channel 1 and at 40 minutes for channel 2. At this point the liquid signal, shown in Figure 4. 29, dominates the solid signal and the measured speed of sound drops to 1.2mm/μs. Both the solid and liquid region speed of sound values agree with those of the large geometry testing shown in Figure 4. 15 - Figure 4. 18 and Table 4. 1. At that point the liquid wax cools over a 300 minute span and the speed of sound increases steadily from 1.3 to 1.4mm/μs over the first 70 minutes.

During this time the wax is beginning to form a solid exterior while the interior remains liquid as is shown in Figure 4. 5. The speed of sound then increases linearly to 1.5mm/μs until the wax pulls away from the box. The temporary drop to a speed of sound of 1mm/μs seen in Figure 4. 15 is not observed during the small geometry testing because that signal is never large enough to be selected as the time of flight (see Figure 4. 28). The return path ultrasound channels 3 and 4 (as shown in Figure 3. 25) are not pictured because their plots are identical to the channel 1 and 2 plots.

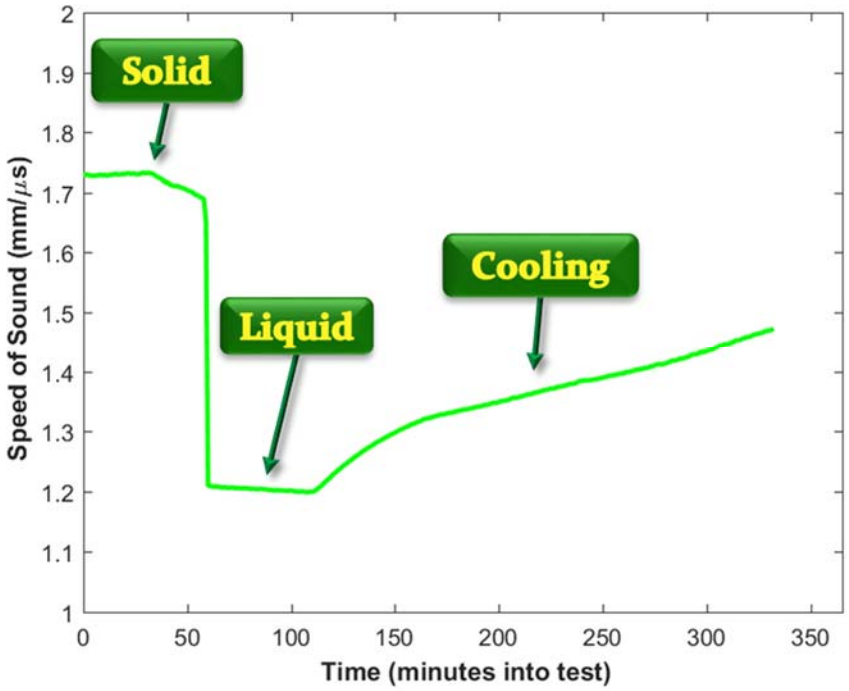

Figure 4. 31: Typical plot of the speed of sound vs. time at ultrasound channel 1 recorded for the duration of the small geometry Ecosoya testing. Major events are labeled.

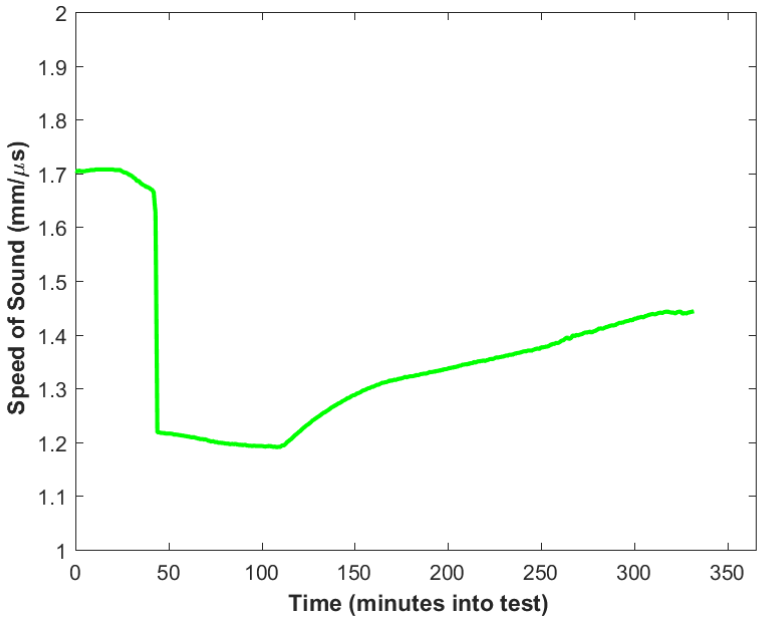

Figure 4. 32: Typical plot of the speed of sound vs. time at ultrasound channel 2 recorded for the duration of the small geometry Ecosoya testing.

Chapter Four, Section 2.2 Predicting the Temperature Using Speed of Sound

Just as in Chapter Four, Section 1.3 plots of temperature vs. speed of sound were created in order to estimate the temperature and phase of the wax during cooling. The plots shown in Figure 4. 33 and Figure 4. 34 follow the same trend from the large geometry testing shown in Figure 4. 21 - Figure 4. 24 and Figure 4. 26 with a linear speed of sound increase from 1.2mm/μs at 98°C to 1.33mm/μs for the phase change at 53°C where the slope changes and the speed of sound increases faster until the wax pulls away from the walls with a final speed of sound at 1.44mm/μs. The ultrasound channel 2 plot in Figure 4. 34 experiences some issues with gain changes toward the end of the test which unfortunately cannot be corrected by the current experimental methods, but a possible solution is proposed in Chapter 5.

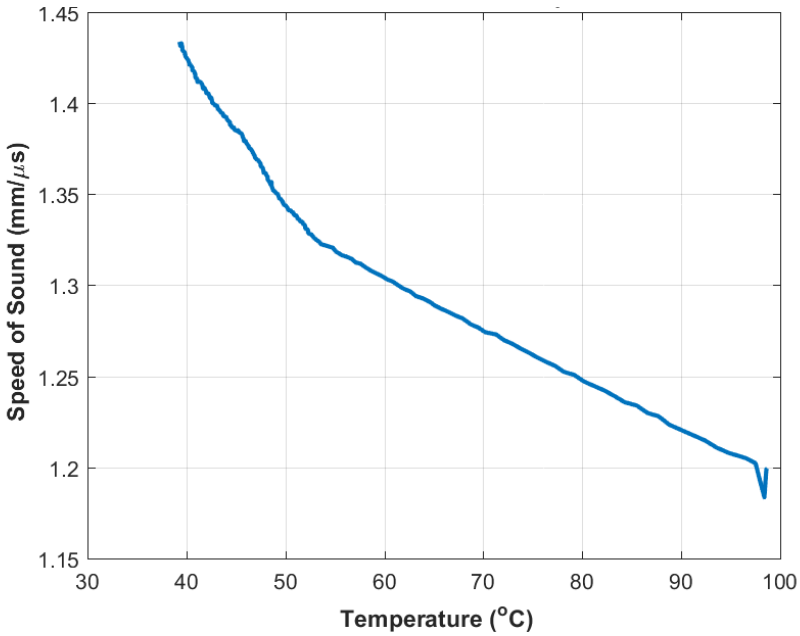

Figure 4. 33: A typical plot of the speed of sound vs. temperature for ultrasound channel 1 during the cooling portion of the small geometry Ecosoya test.

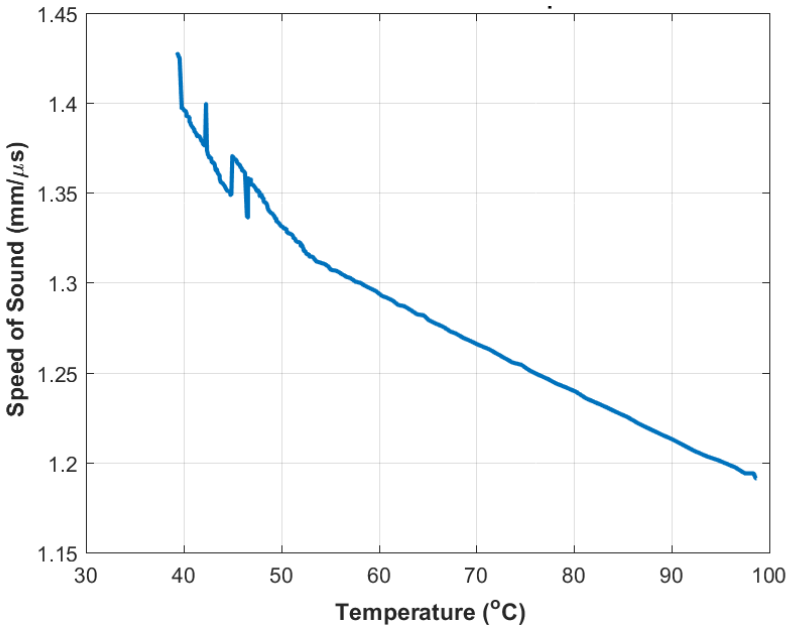

Figure 4. 34: A typical plot of the speed of sound vs. temperature for ultrasound channel 2 during the cooling portion of the small geometry Ecosoya test.

From these plots along with the speed of sound vs. time plots shown in Figure 4. 31 and Figure 4. 32 the phase changes and temperature profiles for the material can be estimated. To demonstrate the estimation method the speed of sound results for ultrasound channel 1, located between thermocouple bars 2 and three as shown in Figure 3. 23, will be observed. By analyzing the speed of sound vs. time plot shown in Figure 4. 31 it can be seen that the material in this acoustic path experiences no change over the first 30 minutes of testing. The slope changes and the speed of sound decreases slightly from 30 to 55 minutes; during this time the wax is melting and the temperature quickly increases from 23°C to above the 53°C melt temperature. With solid to liquid phase change complete the speed of sound continues to decrease slowly to about 1.2mm/μs, indicating that the liquid wax continues to heat to an estimated temperature of 98°C. At about 115 minutes the speed of sound begins to increase as shown in Figure 4. 31, indicating that the material is now cooling. From this point the speed of sound increases linearly as the temperature decreases such that given a speed of sound measurement the temperature can be estimated. For example, a speed of sound reading of 1.25mm/μs corresponds to a temperature of approximately 80°C at about 135 minutes, and a speed of sound reading of 1.4mm/μs corresponds to a temperature of 43°C at about 270 minutes. From these observations a temperature profile that starts at around 23°C (room temperature) will then experience rapid heating from 30 to 50 minutes followed by a steady increase in temperature until the 110th minute where the material rapidly cools for about 60 minutes from 98 to 53°C followed by a slower cooling. These estimations of temperature are accurate to within ±4°C based on measurements made in the large geometry testing listed in Table 4. 2.

Chapter Four, Section 2.3 Temperature Profile Confirmation

The temperature profiles from the small geometry Ecosoya testing are shown in Figure 4. 35 - Figure 4. 37. The thermocouples are arranged as described in Chapter Three, section 2.2 and pictured in Figure 3. 23. Temperature for all thermocouples begins at 23°C and rises quickly as the melt front approaches the thermocouple bar. This occurs at 15 minutes for bar 1, at 25 minutes for bar 2, and at 35 minutes for bar three. This is followed by a slower heating region where the liquid wax continues to heat. For the experiment illustrated in Figures 4.35 – 4.37 the heater is turned off at 110 minutes where upon the wax begins to cool. For the first 60 minutes the wax cools quickly from 98 to 53°C where the wax begins to solidify and the rate of cooling slows. The block continues to cool until the material contracts and pulls away from the walls at around 35°C. This trend matches the estimates of phase change times and the general temperature profile made from the speed of sound measurements in Chapter Four, Section 2.2 demonstrating how the speed of sound can estimate temperature.

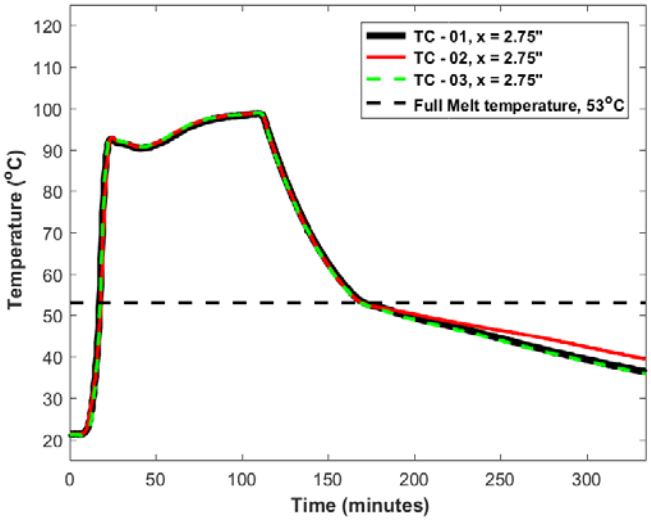

Figure 4. 35: Typical temperature profile measured by the bar 1 thermocouples during a small geometry Ecosoya wax test.

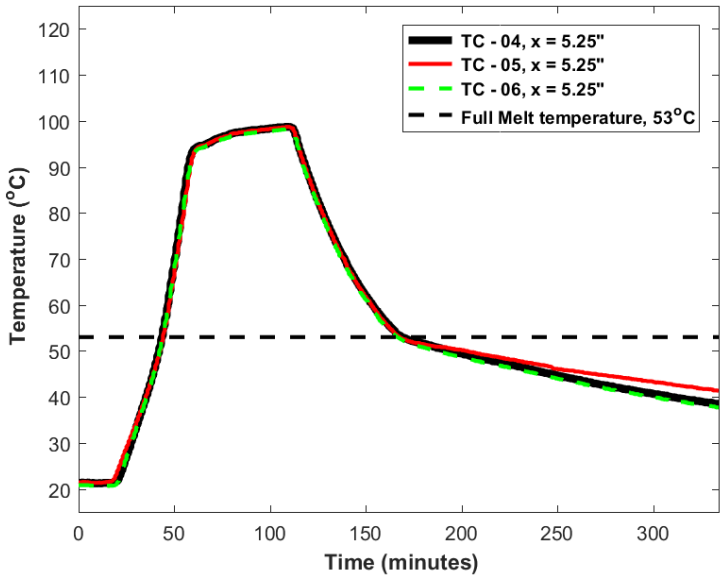

Figure 4. 36: Typical temperature profile measured by the bar 2 thermocouples during a small geometry Ecosoya wax test.

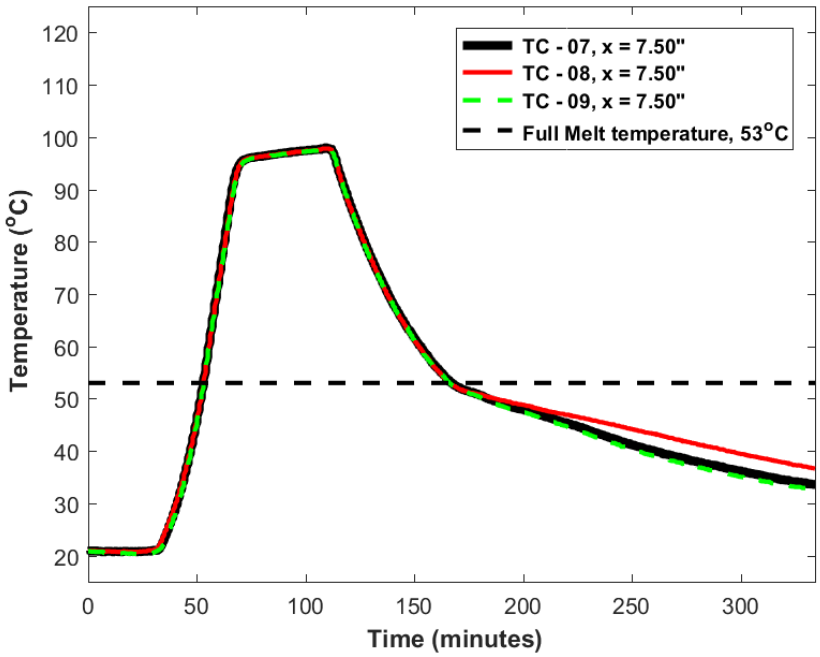

Figure 4. 37: Typical temperature profile measured by the bar 3 thermocouples during a small geometry Ecosoya wax test.

Chapter Four, Section 2.4 Test Repeatability and Relation to Larger Geometry

This test was repeated five times over five separate days to ensure accuracy and that no phenomena were mistaken as temperature or phase change events, such as air pockets causing temperature spikes or gain changes causing the point selected for time of flight measurement to move from signal peak to signal peak. Figure 4. 38 shows the ultrasound channel 01 speed of sound results for all five tests. The results show good agreement with each other in that there is a sudden drop in the speed of sound as the melt front crosses the signal path, and when the heater is turned off the speed of sound increases quickly over the first 60 minutes and transitions to a more linear slope for the remainder of the test. The main difference between the tests is the timing of events such as melt, when the heater was turned off, and when the wax pulled off of the wall, which can all be caused by small changes in room temperature and humidity from day to day or by the configuration and amount of voids formed during the previous cooling of the wax. Similar trends are observed for all ultrasound channels. Table 4. 3 shows the average speed of sound and the standard deviation of the speed of sound in fully solid or fully liquid wax. Data points were selected at the 5^{th}, 100^{th} and 250^{th} minutes because at these points the wax is either fully solid, fully liquid, or steadily cooling respectively across all tests. The solid wax speed of sound variation that was present in the large geometry testing discussed in Chapter Four, Section 1.4 is much less pronounced in the small geometry set up where all initial solid speed of sound measurements are within 1.71 to 1.75mm/μs. The average speeds of sound in liquid and solid wax are consistent for all channels, and the standard deviation for all stages is low.

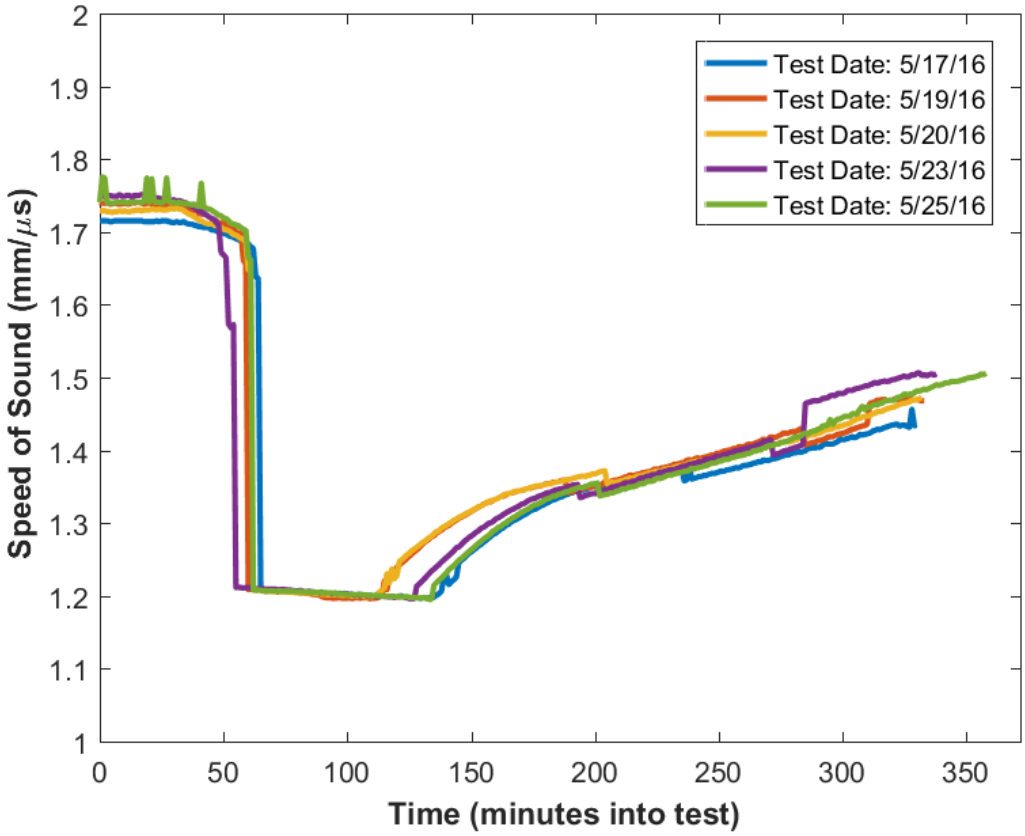

Figure 4. 38: A comparison of the speed of sound vs. time plots recorded from ultrasound channel 1 for all small box Ecosoya wax tests.

Table 4. 3: The average speed of sounds measured at each ultasound channel for all small geometry Ecosoya wax tests during the solid, liquid, and cooling phases, and their associated standard deviations.

Ultrasound Channel	Average SoS Solid wax (mm/μs)	SoS Standard Deviation solid	Average SoS liquid wax (mm/μs)	SoS Standard Deviation Liquid	Average SoS Cooling wax (mm/μs)	SoS Standard Deviation Cooling
01	1.73	0.014	1.20	0.003	1.37	0.008
02	1.72	0.013	1.19	0.008	1.36	0.009

Figure 4. 39 is a plot of the measured temperature vs. the speed of sound for all small geometry Ecosoya tests. All tests follow similar trends with the main difference being a slight vertical shift. All plots show a slope change at 53°C marking the phase change temperature shown in Figure 3. 35 and Figure 3. 37. Table 4.4 shows the standard deviation for the temperature. Notice that the results from the small geometry system have much less deviation from test to test than that of the large geometry testing shown in Figure 4. 26 and are more consistent, being accurate to within ±2°C for temperature estimates of the speed of sound.

Table 4. 4: The average temperatures predicted by ultasound channel 1 from all small geometry Ecosoya wax tests at 1.2, 1.25, 1.3, 1.35, and 1.4mm/μs and their associated standard deviations.

Speed of Sound (mm/μs)	Average Temperature (°C)	Standard Deviation (°C)
1.2	97.4	1.21
1.25	78.2	1.08
1.3	60.5	0.73
1.35	48.3	0.69
1.4	40.4	1.83

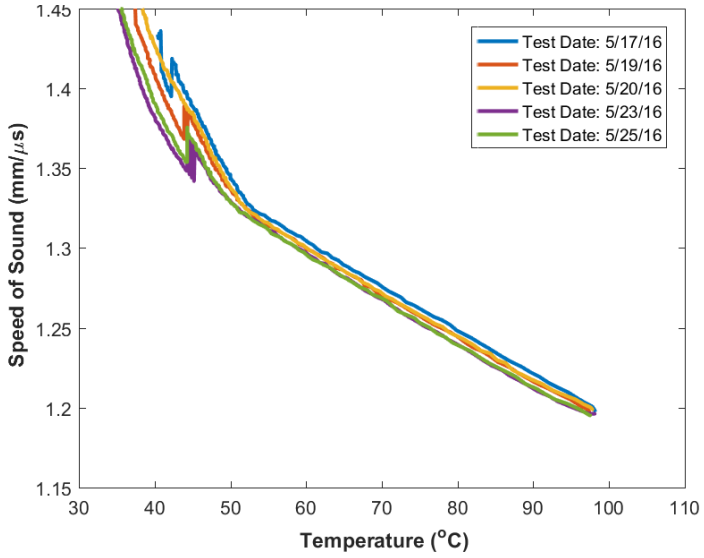

Figure 4. 39: A comparison of the speed of sound vs. temperature plots recorded from ultrasound channel 1 for all small box Ecosoya tests.

Figure 4. 40 and Figure 4. 41 show comparisons of the speed of sound vs. time and the speed of sound vs. temperature data from the large geometry testing preformed on 4/20/16 and the small geometry testing preformed on 5/20/16. It is not expected that the speed of sound vs. time plots will line up with each other because the melt time and solidification times for the two tests are far apart. The plots do agree on the initial speed of sound at 1.70-1.75mm/μs, and the liquid speed of sound at 1.2mm/μs. The trends of each plot also agree with the drop in speed of sound at melt, and the consistent increase in speed of sound during the cooling cycle. Figure 4. 41 Shows the comparison of the speed of sound vs. temperature for the large and small geometry testing. These plots agree very closely with one another as they each have a speed of sound of 1.2mm/μs for the fully liquid wax and a speed of sound of 1.33mm/μs for slope change indicating the phase change at 53°C. One interesting difference is the slope of each curve after the slope change are slightly different with the slope of the large geometry test being steeper than that of the small geometry test. This difference in slope may be due to differences in cooling after the phase change caused by the differences in size. These results indicate that the geometry is irrelevant to the results of the experiment before the phase change so long as the new geometric values of path length and container wall thickness are factored into the speed of sound calculations as is shown in (4.1). After the phase change the difference in slope may be caused by the size of the wax blocks affecting cooling rate. Factoring in the consistency shown in Figure 4. 38 and Figure 4. 39 the small geometry set up is preferable to the large geometry set up.

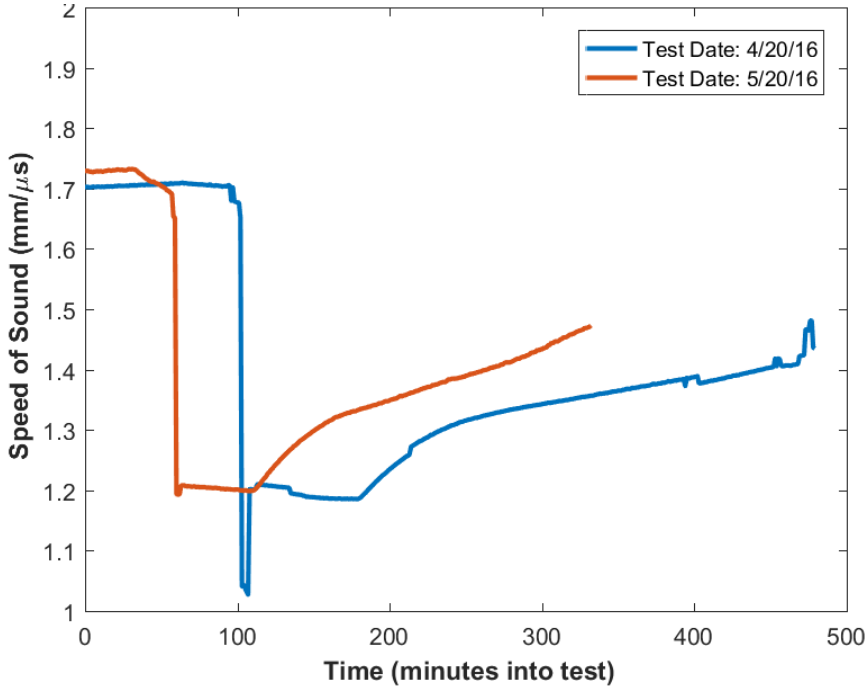

Figure 4. 40: A comparison of the ultrasound channel 1 speed of sound vs. time plots for the large and small geometry tests performed on 4/20/16 and 5/20/16 respectively.

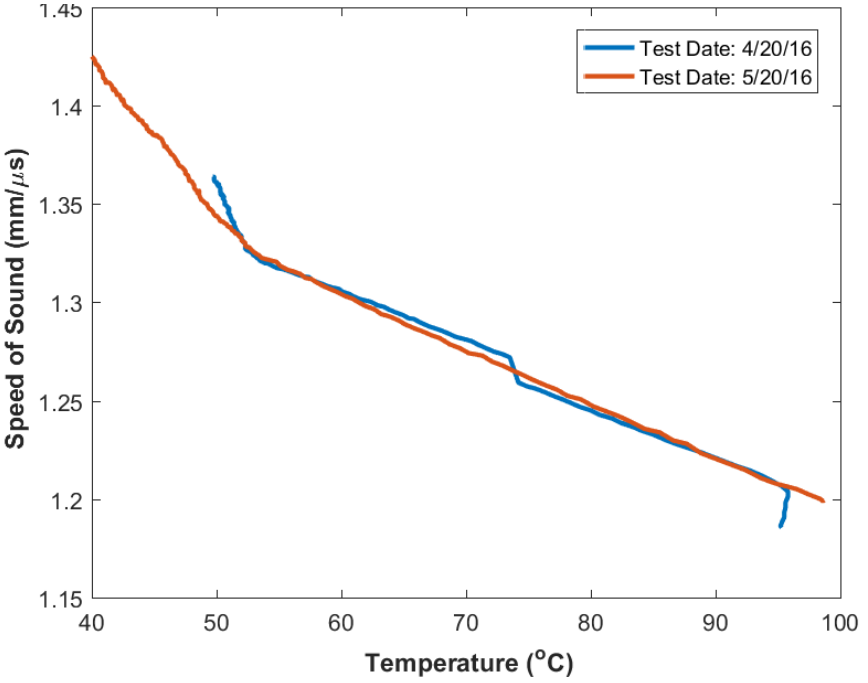

Figure 4. 41: A comparison of the ultrasound channel 1 speed of sound vs. temperature plots for the large and small geometry tests performed on 4/20/16 and 5/20/16 respectively.

Chapter Four, Section 3: Small Geometry Testing Base Paraffin Wax

With the Ecosoya soy based wax well understood there was a desire to extend the testing to other materials. A base paraffin candle wax was selected since it is still similar in that it is a wax, but has a different melting temperature and an intermediate soft wax phase as identified in the DSC testing discussed in Chapter Three, Section 4.3 and shown in Figure 3. 38 and Figure 3. 40. This testing utilized the same small geometry set up shown in Figure 3. 23 and Figure 3. 25 with the heater block set to 121°C (250°F). This wax introduced some interesting challenges such as contracting and forming depressions between the thermocouple bars during cooling that partially cover the transducer path and fill with liquid wax during melting.

Chapter Four, Section 3.1 Speed of Sound Results

The base paraffin wax has some interesting differences in its melt and solidification properties which are highlighted in Figure 4. 42 - Figure 4. 50. A typical A-scan for the solid wax is shown in Figure 4. 42 taken from ultrasound channel 1 located as diagramed in Figure 3. 23 and Figure 3. 25. The signal has an odd shape with the signal maximum sitting farther off the front of the signal than seen in the Ecosoya testing (Figure 4. 27), and a long decay. This is likely caused by the presence of depressions located in the acoustic path as shown in Figure 4. 43 blocking part of the signal from reaching the receiving transducer. The time of flight was about 40μs, resulting in a speed of sound of 2.1mm/ μs. This value is slightly faster than the time of flight for the Ecosoya wax which would indicate that the base paraffin wax is a stiffer material.

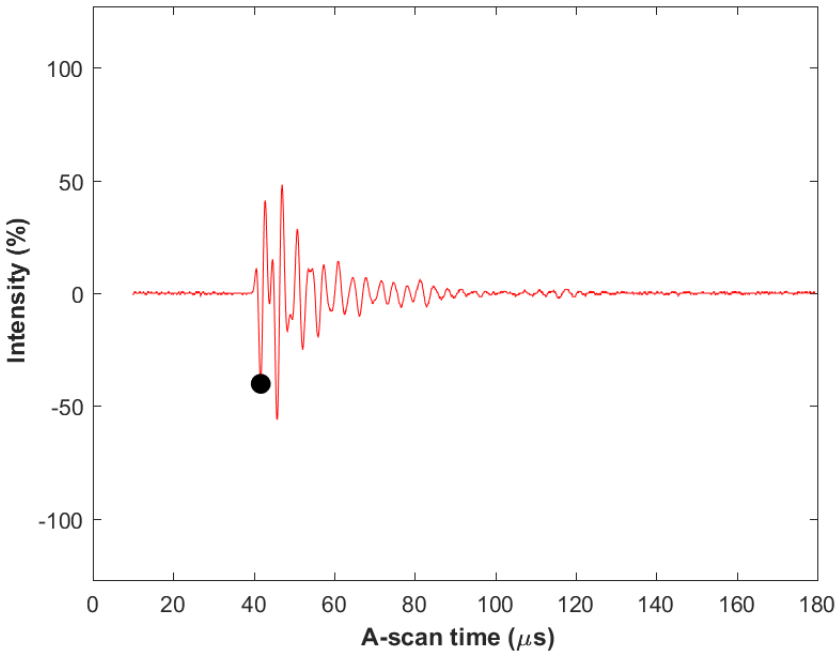

Figure 4. 42: Typical A-scan for the solid base paraffin wax recorded at ultrasound channel 1 at 4 minutes into the small geometry test. The time of flight is marked by a black dot.

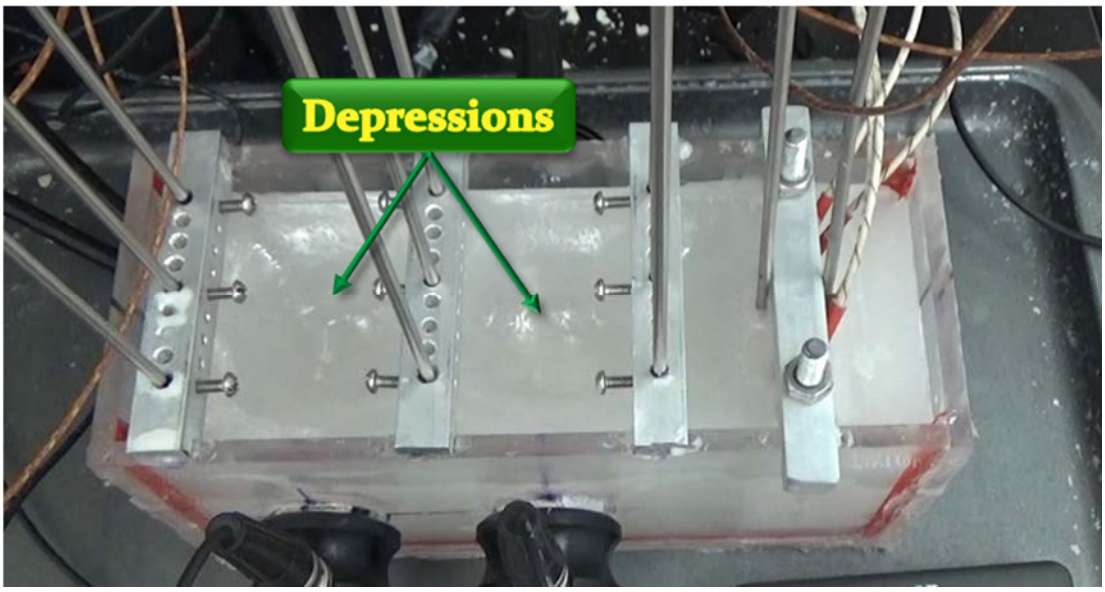

Figure 4. 43: Image of the solid base paraffin wax in the small geometry container with the depressions formed during cooling indicated.

As the wax melts the hot liquid wax flows into the depressions marked in Figure 4. 43 causing pools of liquid wax to form in the transducer paths as shown in Figure 4. 45. These pools also make it difficult to maintain an acoustic coupling as the water that was between the container walls and the solid wax can now flow beneath the heater as the liquid wax flows into the pools. The ultrasound channel 1 A-scan at this time in the test is shown in Figure 4. 44. The plot shows the solid signal with a time of flight at 40µs followed by a chaotic mix of signals from the new path created by the pools of wax, ranging from 60µs to 130µs. Because the solid signal has become weak the measured speed of sound is taken from the front of the mixed signals at about 65µs, resulting in a measured speed of sound of 1.1mm/µs. This stage does not last long because the liquid wax expands the pool and begins to melt the solid wax from the top down clearing solid material out of the acoustic path.

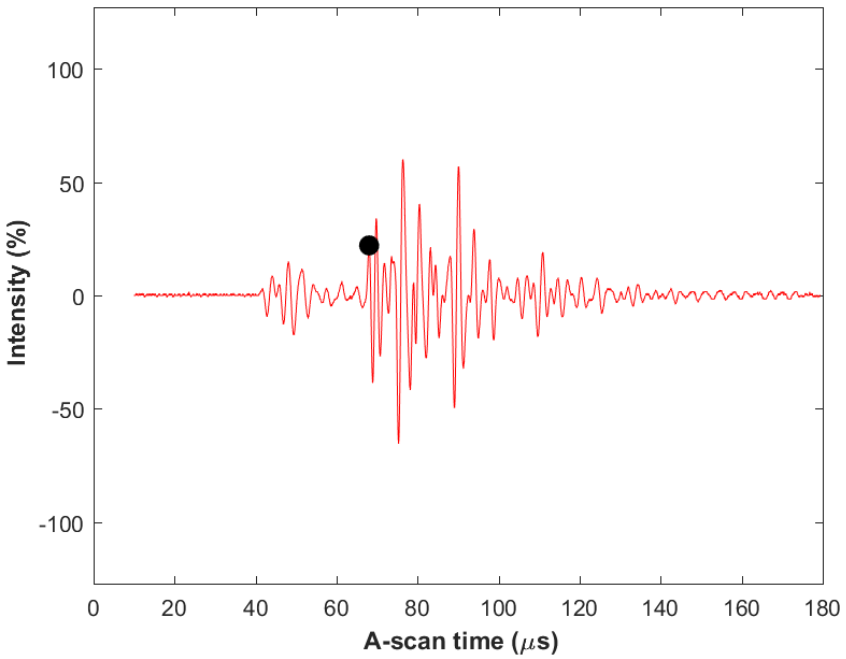

Figure 4. 44: Typical A-scan for the transitioning base paraffin wax recorded at ultrasound channel 1 at 47 minutes into the small geometry test. The time of flight is marked by a black dot.

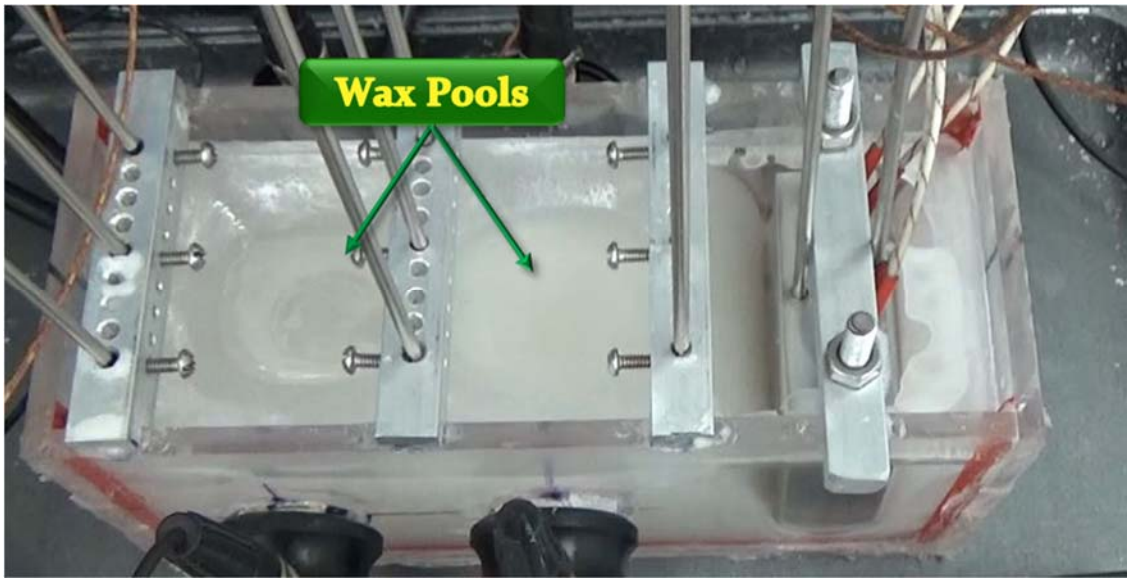

Figure 4. 45: Image of the solid base paraffin wax in the small geometry container with the liquid wax pools formed during initial heating indicated.

Figure 4. 46 shows the A-scan image of the wax as the melt front is passing through the ultrasound path. At this time the fully solid signal has died out and two distinct signals are present at 70μs and 85μs respectively. The signal at 70μs, the liquid signal, is the measured time of flight and the speed of sound is calculated to be 1.15mm/μs. The second slower signal is similar to the slower signal seen in the Ecosoya testing in Figure 4. 12 and Figure 4. 28 where there are two signals apparent, the slower of which may be a decaying Rayleigh wave propagating near the solid-liquid boundary (see Chapter Five, Section 2). Figure 4. 47 shows the melt front progressing across the acoustic paths. Notice that because of the hot wax pools melting the wax around them the melt for this material is more from the top of the container downwards than the Ecosoya which melts primarily across the container from the heater block.

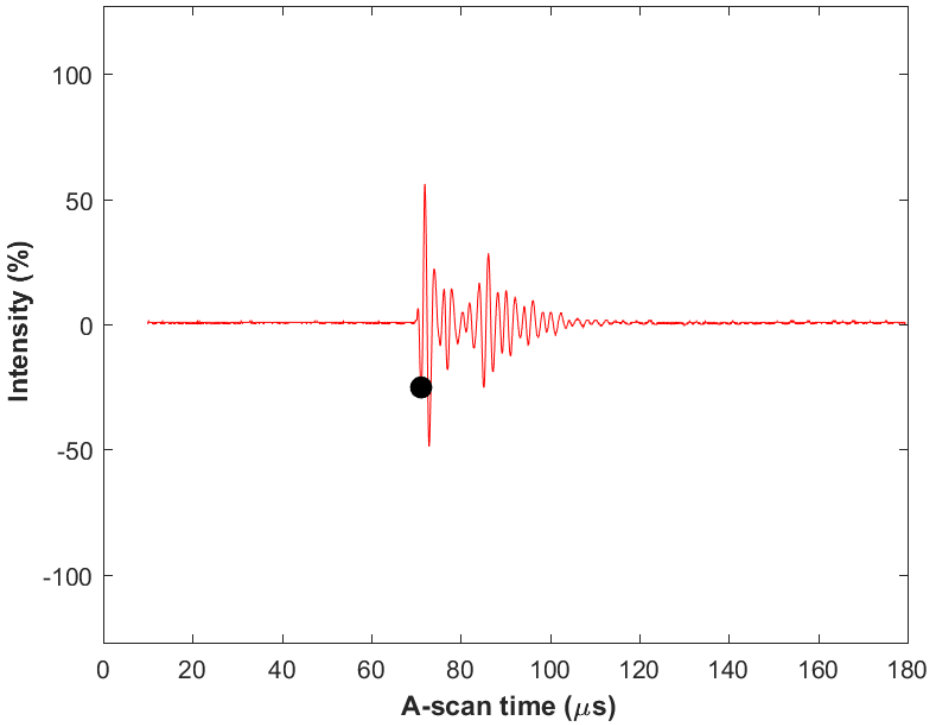

Figure 4. 46: Typical A-scan for the transitioning base paraffin wax recorded at ultrasound channel 1 at 65 minutes into the small geometry test. The time of flight is marked by a black dot.

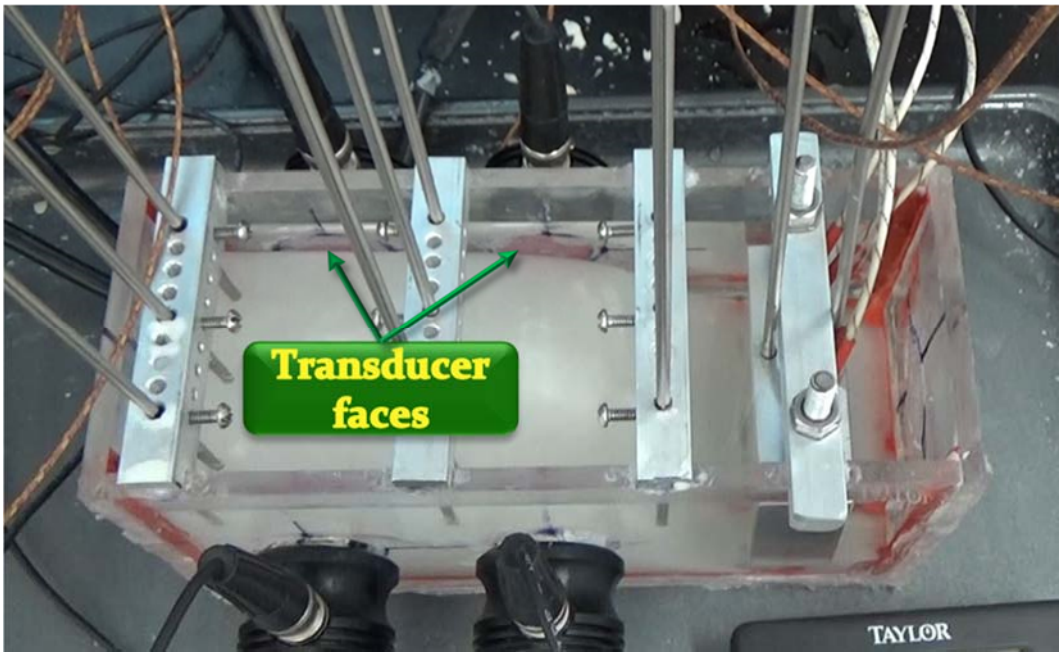

Figure 4. 47: Image of the progressing melt front partially uncovering the acoustic paths during the heating cycle of a small geometry base paraffin wax test

With the wax completely melted the slower signal dies off and only the liquid signal at 70µs remains as shown in Figure 4. 48. The signal shape at this time is more regular at this time with the signal max near the front of the signal followed by a steady decay. The calculated speed of sound at this time is 1.15mm/µs which remained constant until the heater is turned off. This value is slightly slower than the Ecosoya wax which had a liquid speed of sound of 1.2mm/µs indicating that the base paraffin is less stiff than the Ecosoya in the liquid phase. Figure 4. 49 shows the fully melted base paraffin wax.

The heater for this test was turned off at 130 minutes and the wax began to cool. Figure 4. 50 shows the A-scan measured at 369 minutes into the test. At this time the wax has cooled and a small signal has appeared at 50µs just ahead of the larger signal at 55µs and is measured as the time of flight resulting in a jump in the speed of sound to 1.6mm/µs.

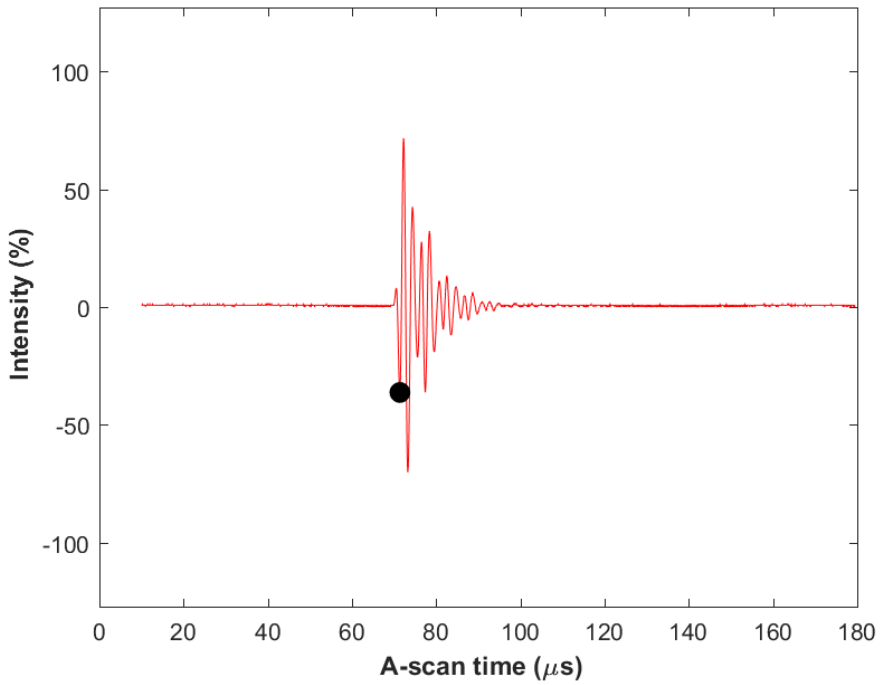

Figure 4. 48: Typical A-scan for the liquid base paraffin wax recorded at ultrasound channel 1 at 80 minutes into the small geometry test. The time of flight is marked by a black dot.

Figure 4. 49: Image of a small geometry base paraffin wax test at full melt.

This smaller signal is a result of some of the wax in the acoustic path hardening from a soft solid to the harder solid as is discussed in Chapter Three, Section 4.3. This smaller signal will continue to grow as the wax hardens and the slower signal dies off resulting in a single solid signal as is shown in Figure 4. 51.

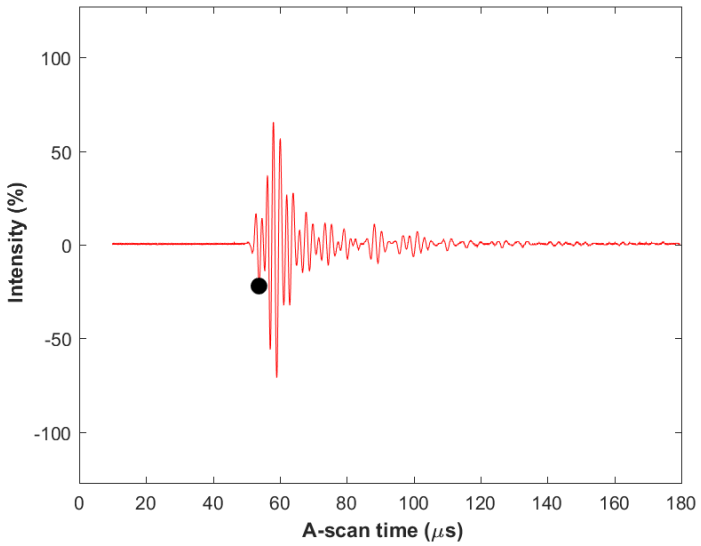

Figure 4. 50: Typical A-scan for the cooling base paraffin wax recorded at ultrasound channel 1 at 369 minutes into the small geometry test. The time of flight is marked by a black dot.

Figure 4. 52 and Figure 4. 53 show the speed of sound plots over the length of the test for the base paraffin wax. The general trends of the plots are similar to the results from the Ecosoya wax shown in Figure 4. 31 and Figure 4. 32 with the exception of the jump in speed of sound for the base paraffin wax near the end of the test caused by the soft solid to hard solid transition.

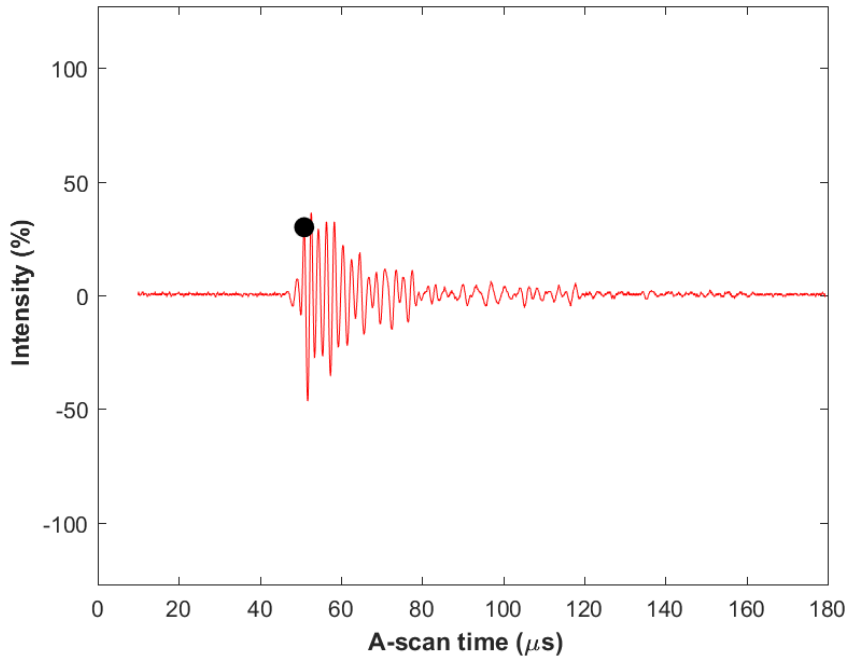

Figure 4. 51: Typical A-scan for the cooling base paraffin wax recorded at ultrasound channel 1 at 417 minutes into the small geometry test. The time of flight is marked by a black dot.

The speed of sound is initially between 2.0 and 2.1mm/μs then decreases slightly until dropping at about 50 minutes for channel 1 and about 40 minutes for channel 2 to near 1mm/μs as the melt front crosses the ultrasound path. With the wax fully melted the speed of sound settles at about 1.15mm/μs until the heater is turned off and the speed of sound steadily increases to 1.3mm/μs over the first 60 minutes and to 1.4mm/μs over the first 200 minutes. At approximately 200 minutes after the heater is turned off the speed of

sound increases to 1.6mm/μs as the wax hardens from a soft solid to a hard solid. The speed of sound continues to increase steadily until the wax contracts and pulls away from the wall. The base paraffin covers a wider range of speeds of sound with a fully solid value at 2.1mm/μs and a fully liquid value of 1.1mm/μs as compared to 1.7 and 1.2mm/μs respectively for the Ecosoya testing.

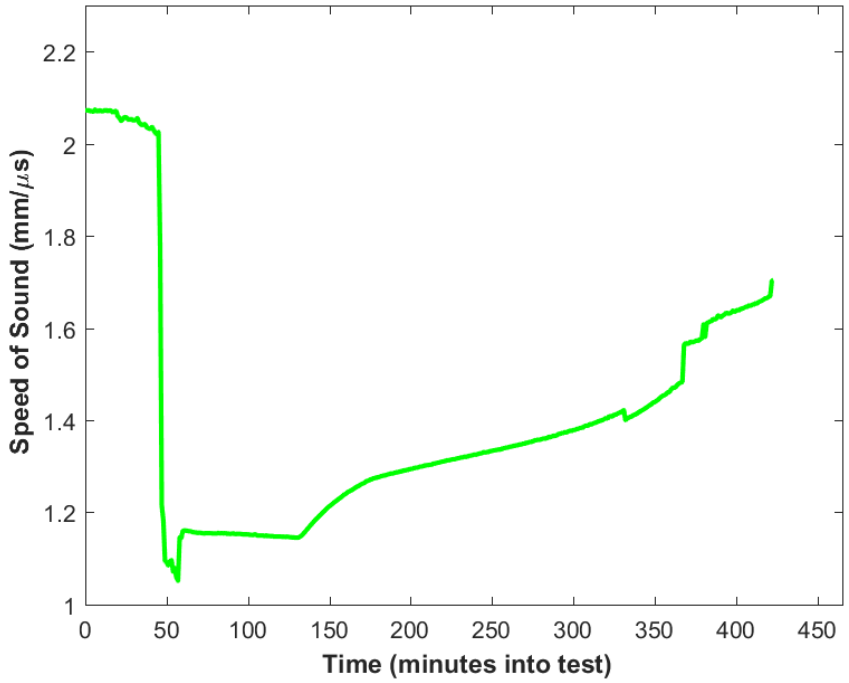

Figure 4. 52: Typical plot of the speed of sound vs. time at ultrasound channel 1 recorded for the duration of the small geometry base paraffin wax testing.

Chapter Four, Section 3.2 Predicting the Temperature Using Speed of Sound

Figure 4. 54 and Figure 4. 55 relate the speed of sound of the base paraffin wax to its temperature during cooling for ultrasound channels 1 and 2. Cooling begins with the heater being turned off with the hot liquid wax at 100°C and the speed of sound at 1.15mm/μs.

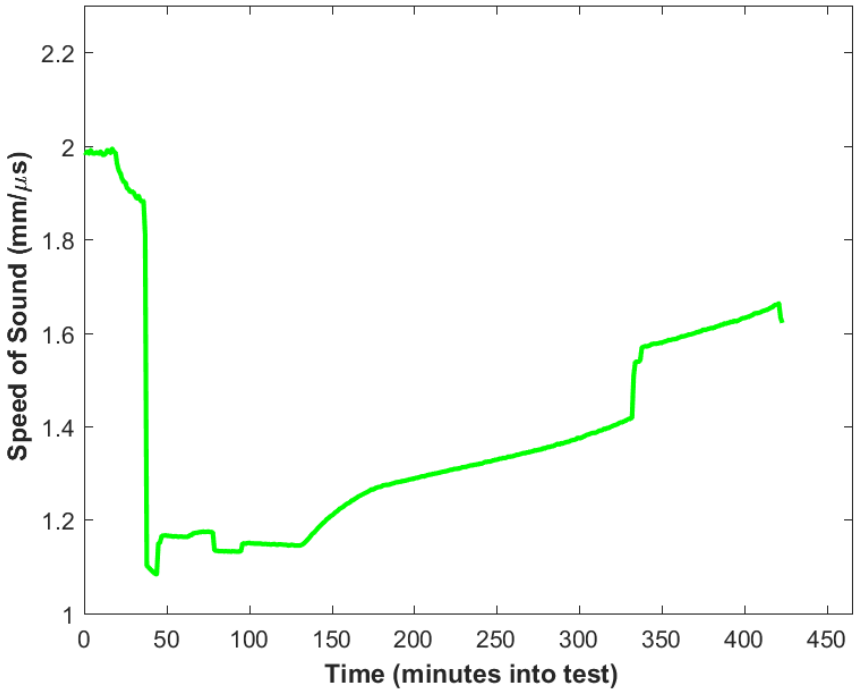

Figure 4. 53: Typical plot of the speed of sound vs. time at ultrasound channel 2 recorded for the duration of the small geometry base paraffin wax testing.

The speed of sound steadily increases to 1.28mm/μs as the material cools to 55°C at which time the wax begins to harden and the speed of sound increases quickly to 1.34mm/μs. The speed of sound then returns to a more steady increase to 1.42mm/μs at 40°C followed by another steep jump in the speed of sound to 1.60mm/μs at 35°C. The speed of sound then continues to increase for a short time until acoustic coupling is lost. The large jumps in speed of sound at 55 and 40°C respectively match the solidification and glass transition temperatures from the DSC testing shown in Chapter Three, Section 4.3 Figure 3. 38 and Figure 3. 40.

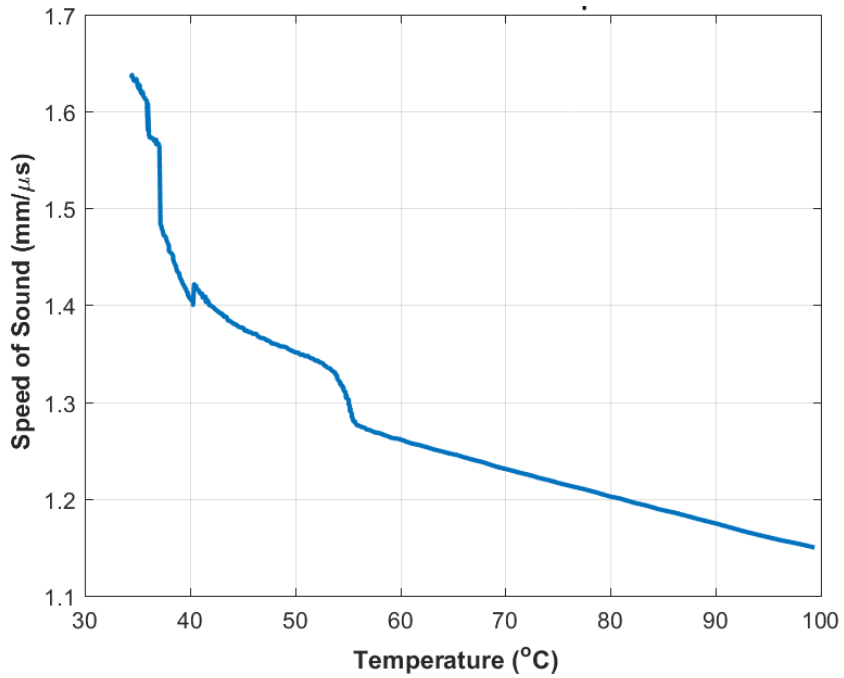

Figure 4. 54: A typical plot of the speed of sound vs. temperature for ultrasound channel 1 during the cooling portion of the small geometry base paraffin test.

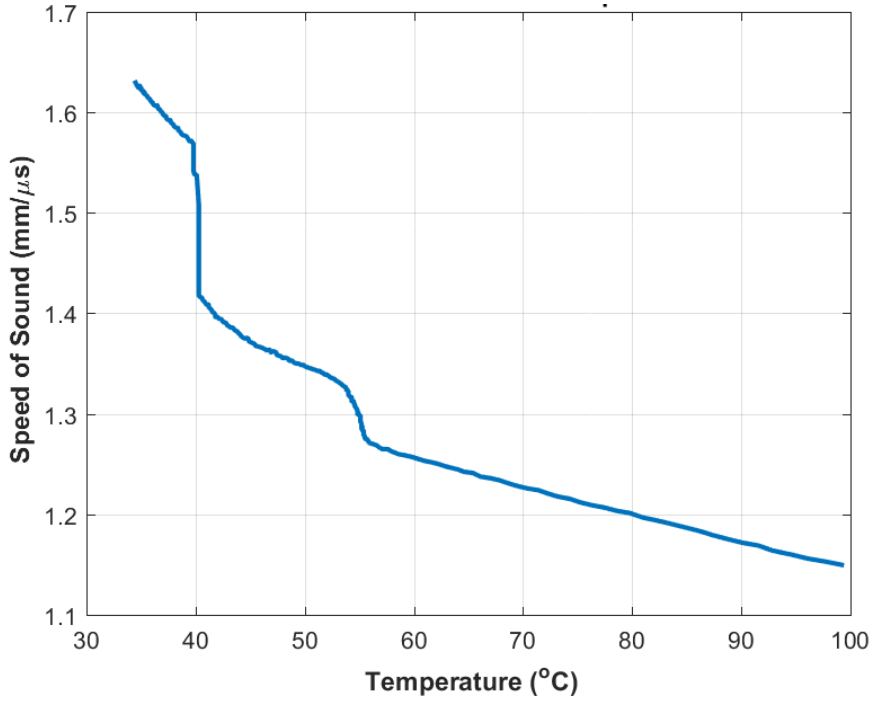

Figure 4. 55: A typical plot of the speed of sound vs. temperature for ultrasound channel 2 during the cooling portion of the small geometry base paraffin test.

From these plots along with the speed of sound vs. time plots shown in Figure 4. 52 and Figure 4. 53 the phase changes and temperature profile of the material can be estimated. To demonstrate the estimation method the speed of sound results for ultrasound channel 1, located between thermocouple bars 2 and 3 as shown in Figure 3. 23, will be observed. First by observing the speed of sound vs. time plot shown in Figure 4. 52 it can be seen that the material in this acoustic path experiences little change over the first 30 minutes of testing. The speed of sound decreases slightly from 30 minutes until the speed of sound drops at 50minutes, during this time the wax is beginning to melt and the temperature increases quickly from 23°C to above the 56°C melt temperature. With solid/liquid phase change complete the speed of sound continues to decrease to a value of 1.15mm/μs indicating that the liquid wax is continuing to heat to an estimate temperature of 100°C. At about 130 minutes the speed of sound begins to increase as shown in Figure 4. 52 indicating that the material is cooling. From this point the speed of sound increases as the temperature decreases such that given a speed of sound measurement the temperature can be estimated. For example, a speed of sound reading of 1.2mm/μs corresponds to a temperature of approximately 80°C at approximately 150 minutes, or a speed of sound reading of 1.4mm/μs corresponds to a temperature estimation of 42°C at approximately 325 minutes. From these observations a temperature profile that starts at around 23°C (room temperature) will then rapidly increase from the 30 to 50 minutes to 90°C followed by a steady increase in temperature to 100°C until the 110^{th} minute where the material begins to cool quickly for about 60 minutes from 100 to 56°C where the cooling stalls for a period of time as indicated from Figure 4. 54. The temperature then stalls at about 56°C as the material transitions to the solid state, it is

difficult to determine how long this stall lasts from Figure 4. 52, though there appears to be slope changes at about 180 minutes where the plot takes on a linear trend and at 275 minutes where the linear trend ends and the speed of sound begins to increase faster. This stall is followed by another cooling period from 56°C to 40°C from about 275 minutes to 340 minutes, and finally, steady cooling until the end of the test. These estimations of temperature are accurate to within ±1.5°C based on measurements made in the large geometry testing listed in Table 4. 2.

Chapter Four, Section 3.3 Temperature Profile Confirmation

The temperature profiles from the small geometry base paraffin wax testing are shown below in Figure 4. 56 - Figure 4. 58. The thermocouples are arranged as described in Chapter Three, section 2.2 and pictured in Figure 3. 23. Temperature for all thermocouples begins near room temperature at 23°C and rises quickly as the melt front approaches the thermocouple bar. This occurs at 20 minutes for bar 1, at 30 minutes for bar 2, and at 40 minutes for bar three, and is followed by a period of steady heating in which the now liquid wax reaches a temperature of 100°C. The heater was turned off at 130 minutes and the wax began to cool. For the first 60 minutes the wax cooled quickly from 100°C to 56°C where the wax begins to solidify and the cooling rate decreases. This decreased cooling rate lasts for about 80 minutes and is followed a temperature decrease to about 40°C over about 50 minutes. The wax cools steadily until the material contracts and pulls away from the walls at around 35°C. This trend matches the estimates of phase change times and general temperature profile made from the speed of sound measurements in Chapter Four, Section 3.2 demonstrating how the speed of sound can estimate temperature.

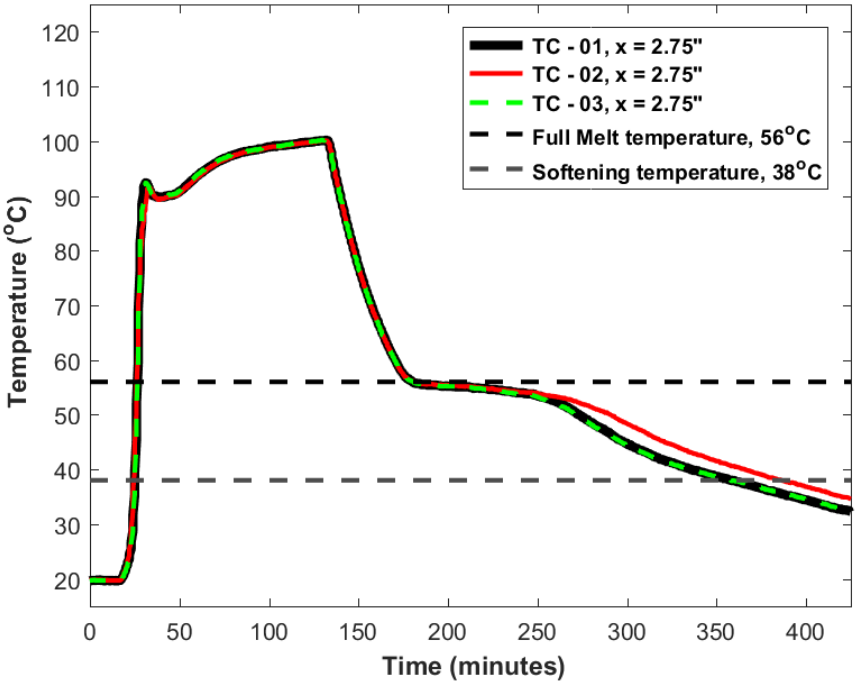

Figure 4. 56: Typical temperature profile measured by the bar 1 thermocouples during a small geometry base paraffin wax test.

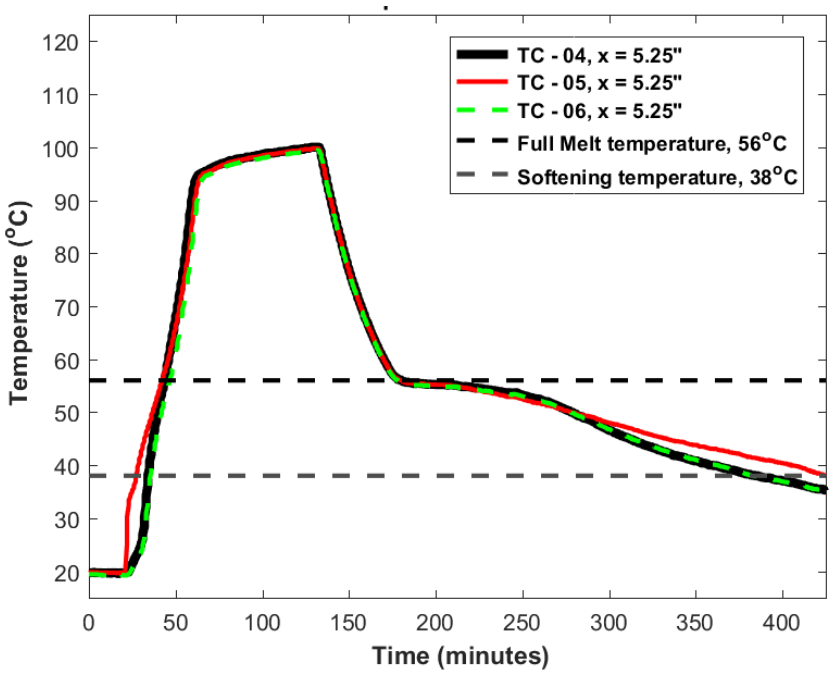

Figure 4. 57: Typical temperature profile measured by the bar 2 thermocouples during a small geometry base paraffin wax test.

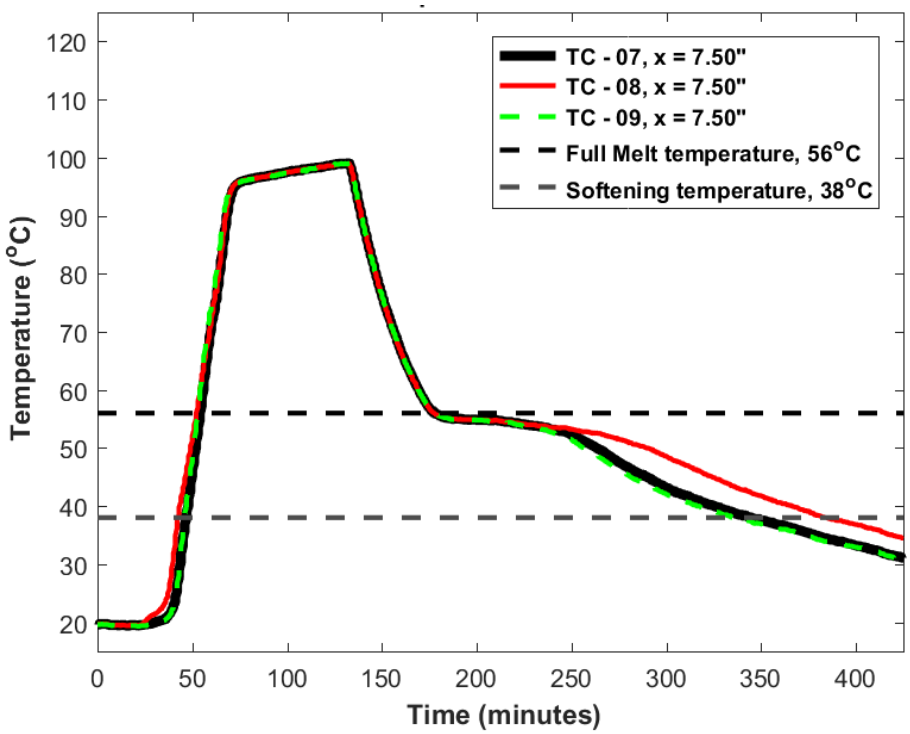

Figure 4. 58: Typical temperature profile measured by the bar 3 thermocouples during a small geometry base paraffin wax test.

Chapter Four, Section 3.4 Test Repeatability

This test was repeated five times over five separate days to ensure accuracy and that no phenomena were mistaken as temperature or phase change events, such as air pockets causing temperature spikes or gain changes causing the point selected for time of flight measurement to move from signal peak to signal peak. Figure 4. 59 shows the ultrasound channel 01 speed of sound results for all five tests. The results agree in that there is a sudden drop in the speed of sound as the melt front crosses the signal path, and when the heater is turned off the speed of sound increases quickly over the first 70 minutes and transitions to a more gradual increase until late in the test where there is a jump in speed of sound from about 1.4mm/μs to 1.6mm/μs followed be another steady increase in speed of sound until the end of the test. Each test is also noisy in the speed of

sound measurements as the melt front is arriving with the speed of sound changing often. This is likely due to the wax pooling as shown Figure 4. 45 and weakened acoustic coupling due to the water displacing the wax underneath the heater block. These events yield the varying signal as shown in Figure 4. 44. The main difference between the tests is the timing of events such as melt, when the heater is turned off, and when the wax pulled away from the wall which can all vary due to small changes in room temperature and humidity from day to day or by the configuration and amount of voids formed during the previous cooling of the wax. Similar trends are observed for all ultrasound channels, except for the test preformed on 6/23/16 where around the 300 minute mark instead of showing an instant increase from 1.4 to 1.6mm/μs the speed of sound continues to increase gradually until 360 minutes where it jumps from 1.5 to 1.6mm/μs. This is likely caused by slight differences in gain adjustments made during cooling allowing the measured time of flight to stay at a slower peak of the signal for a longer time than in the other tests shown. Table 4. 5 shows the average speed of sound and the standard deviation of the speed of sound in fully solid or fully liquid wax. Data points were selected at the 5^{th}, 100^{th} and 250^{th} minutes because at these points the wax is either fully solid, fully liquid, or steadily cooling respectively across all tests. The average speeds of sound in liquid and solid wax are consistent for all channels, and the standard deviation for all stages is very low.

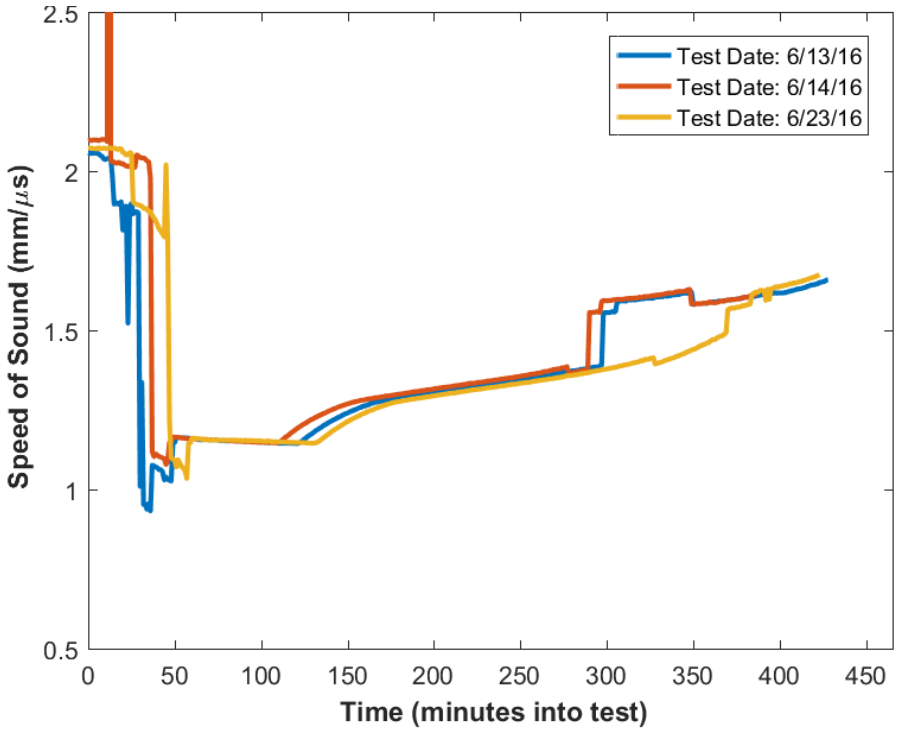

Figure 4. 59: A comparison of the speed of sound vs. time plots recorded from ultrasound channel 1 for all small box base paraffin wax tests.

Table 4. 5: The average speeds of sound measured at each ultasound channel for all small geometry base paraffin wax tests during the solid, liquid, and cooling phases, and their associated standard deviations.

Ultrasound Channel	Average SoS Solid wax (mm/μs)	SoS Standard Deviation solid	Average SoS liquid wax (mm/μs)	SoS Standard Deviation Liquid	Average SoS Cooling wax (mm/μs)	SoS Standard Deviation Cooling
01	2.08	0.020	1.15	0.003	1.34	0.011
02	2.05	0.052	1.14	0.011	1.34	0.011

Figure 4. 60 shows a plot of the measured temperature vs. the speed of sound for all base paraffin wax tests. All tests follow similar trends with a bend at 55°C marking the phase change temperature to a soft solid followed by another sharp increase in speed of sound at about 45°C as shown in Chapter Three, Section 4.3 Figure 3. 38 and Figure 3.

40. The test performed on 6/23/16 has a smoother transition from soft solid to hard solid around 45°C, whereas the other tests have a sharp jump in speed of sound. This may be due to slightly different cooling conditions such as a warmer room temperature or better acoustic coupling resulting in fewer sudden gain changes allowing the measured time of flight to stay at a slower peak of the signal for a longer time than in the other tests shown. Table 4. 6 shows the standard deviation for the temperature. Using this method the temperature can be estimated to within about ±4°C given a speed of sound measurement at the worst points.

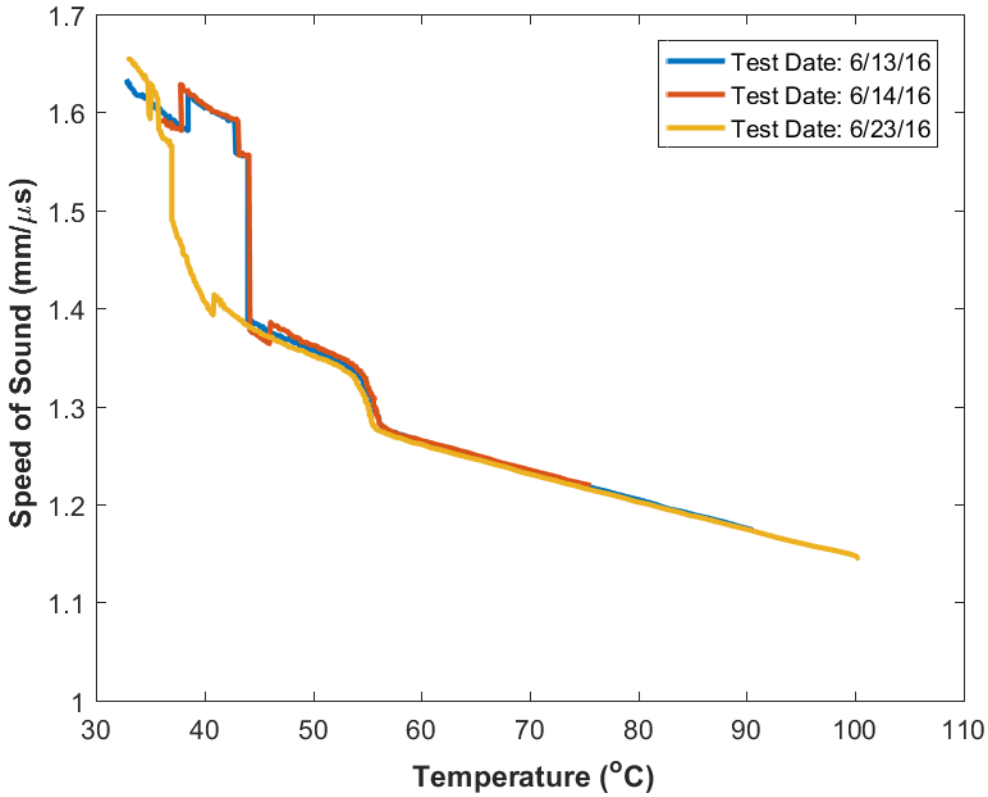

Figure 4. 60: A comparison of the speed of sound vs. temperature plots recorded from ultrasound channel 1 for all small geometry base paraffin wax tests.

Table 4. 6: The average temperatures predicted by ultasound channel 1 from all small geometry base paraffin wax tests at 1.2, 1.3, 1.4, and 1.5mm/μs and their associated standard deviations.

Speed of Sound (mm/μs)	Average Temperature (°C)	Standard Deviation (°C)
1.2	79.4	0.30
1.3	55.4	0.28
1.4	43.3	1.30
1.5	41.7	4.07

Chapter Four, Section 4: Small Geometry Testing Chocolate

Baker's chocolate was selected as another material for study for its ability to melt and re-solidify and to expand the scope of the materials tested. Chocolate is v different from the waxes tested due to its inclusion of small solid particulates of cacao and sugar as well as a tendency to separate the oils from the material when exposed to elevated temperatures. Also the chocolate did not transfer the heat from the heater bock as well as the waxes only melting half of the chocolate as shown in Figure 4. 61 with the set up used for the waxes (see Figure 3. 23 for container diagram). For this reason a new test was designed where the chocolate was melted in a convection furnace at 60°C overnight and the cooling was monitored in a room temperature environment. The container used for this test is described in Chapter Three, section 2.2 and shown in Figure 3. 26 and Figure 3. 27.

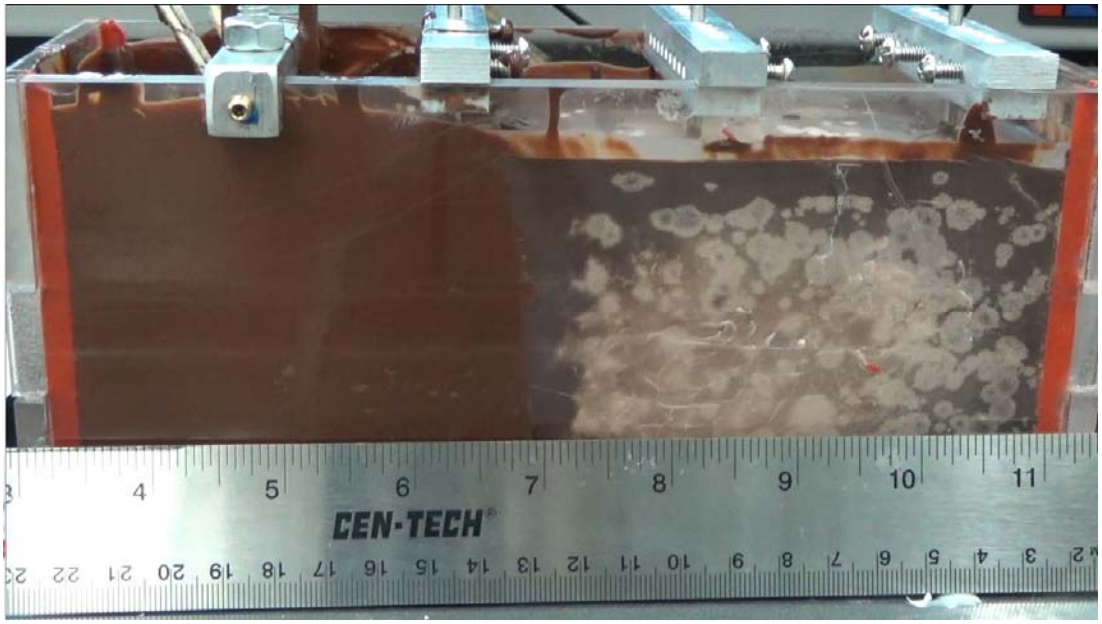

Figure 4. 61: Image of the failed attempt to melt chocolate with the standard small geometry container set up.

Chapter Four, Section 4.1 Speed of Sound Results

The A-scan images from the beginning and end of cooling are shown in Figure 4. 62 and Figure 4. 63 respectively. For the signals seen in both A-scans the signal maximum is located at the third peak near the front of the signal followed by a short delay of about 15μs. The signal taken at the beginning of the test has a time of flight of about 58μs resulting in a speed of sound of 1.46mm/μs. As the chocolate cools the time of flight steadily decreases to about 50mm/μs at about room temperature resulting in a calculated speed of sound of 1.65mm/μs.

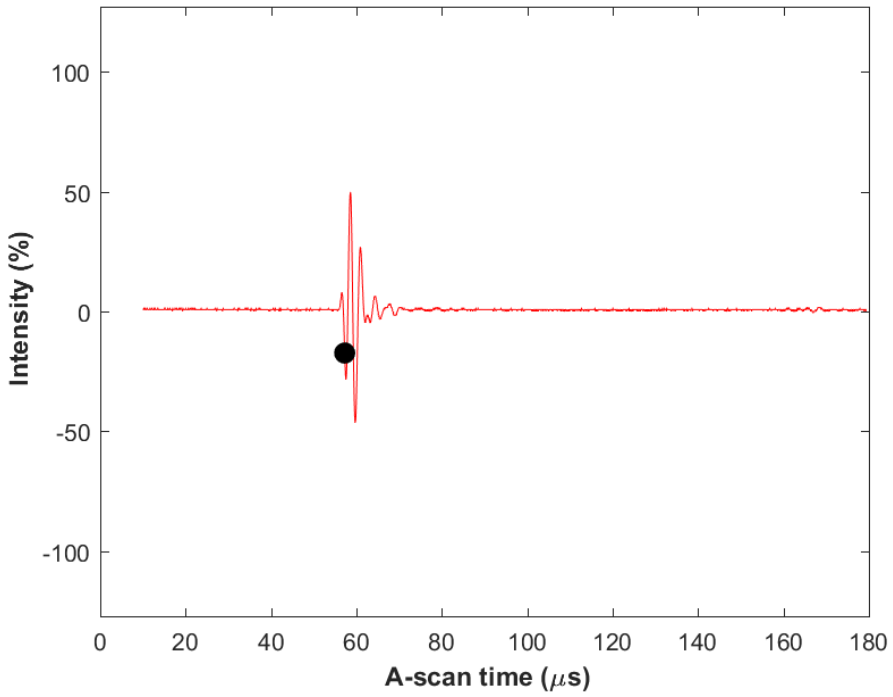

Figure 4. 62: Typical A-scan for the liquid chocolate recorded at ultrasound channel 1 at the start of the small geometry test. The time of flight is marked by a black dot.

Figure 4. 64 - Figure 4. 66 show the plot of the measured speed of sound over the course of the test for the three ultrasound channels. All three plots follow the same trend with an initial speed of sound at about 1.46mm/μs followed by a steady increase over the first 100 minutes of cooling where the slope of the curve decreases to a linear increasing speed of sound for another 150 minutes.

The slope speed of sound then increases for the final 70 minutes of the test as the chocolate approaches room temperature. The final speed of sound is at 1.65mm/μs. There is no major phase change event observed during the cooling of this material because the full solidification of chocolate occurs below room temperature as is discussed in Chapter Three, Section 4.4 and shown in Figure 3. 42 and Figure 3. 44.

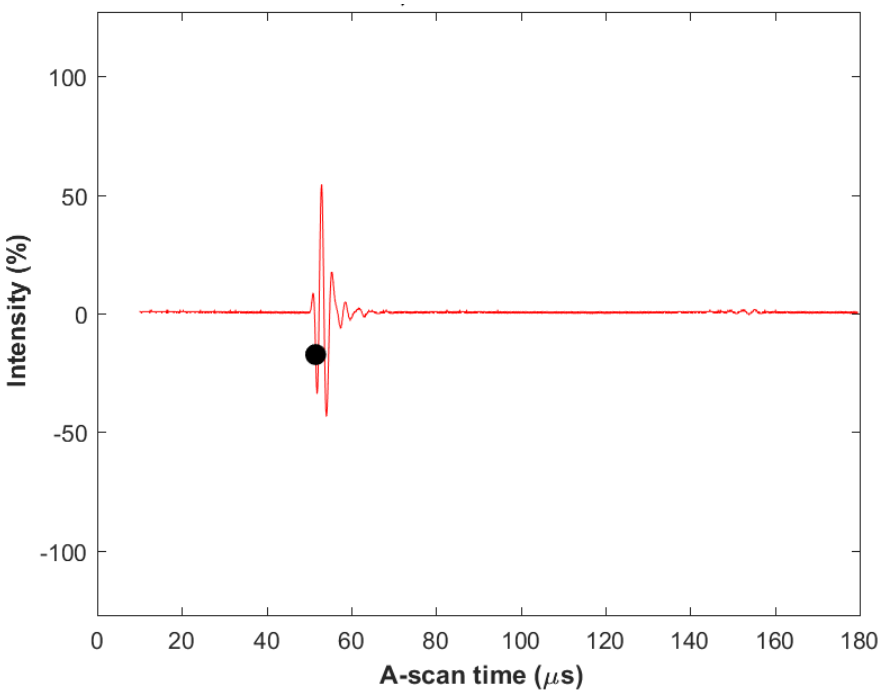

Figure 4. 63: Typical A-scan for the cooling chocolate recorded at channel 1 at 319 minutes into the small geometry test. The time of flight is marked by a black dot.

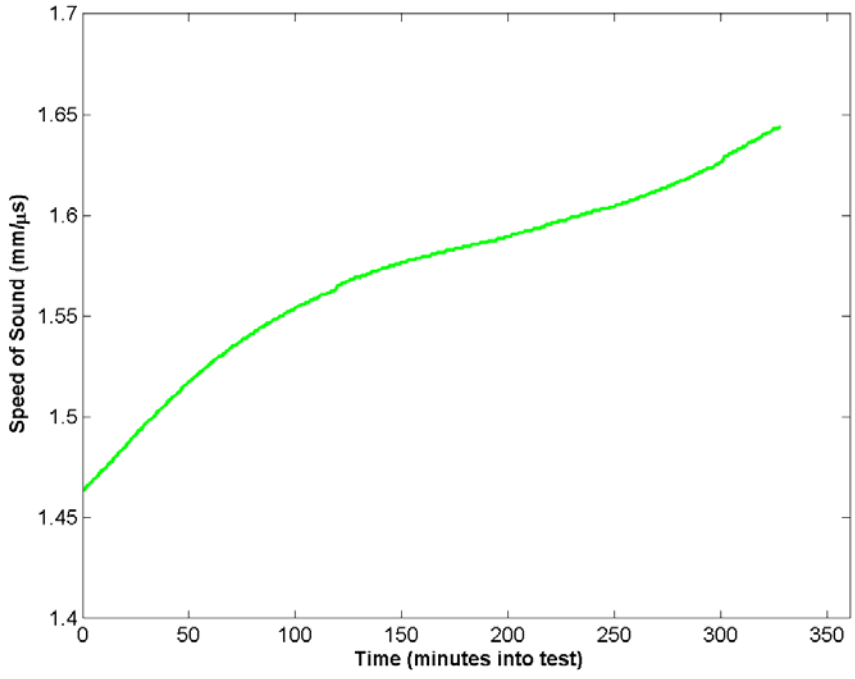

Figure 4. 64: Typical plot of the speed of sound vs. time at ultrasound channel 1 recorded for the duration of the small geometry chocolate testing.

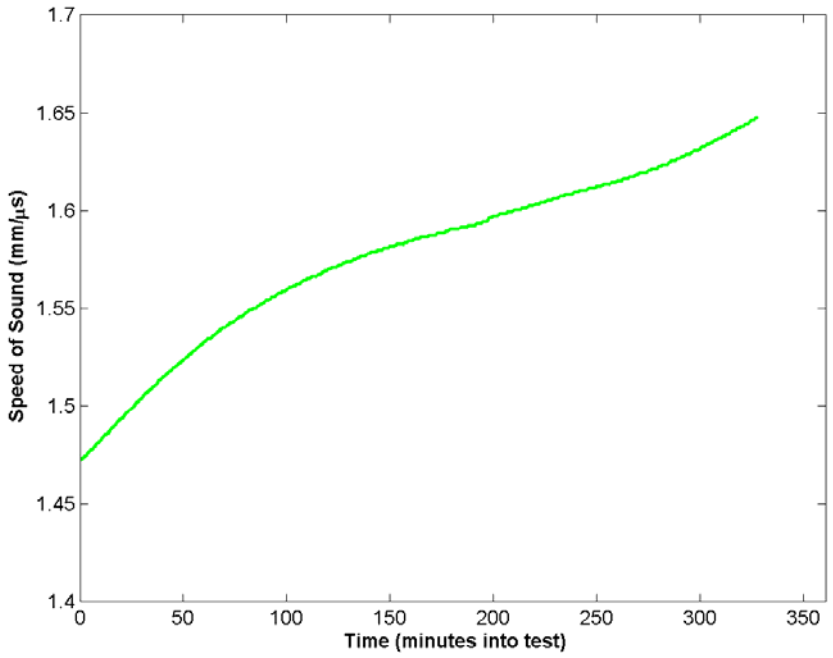

Figure 4. 65: Typical plot of the speed of sound vs. time at ultrasound channel 2 recorded for the duration of the small geometry chocolate testing.

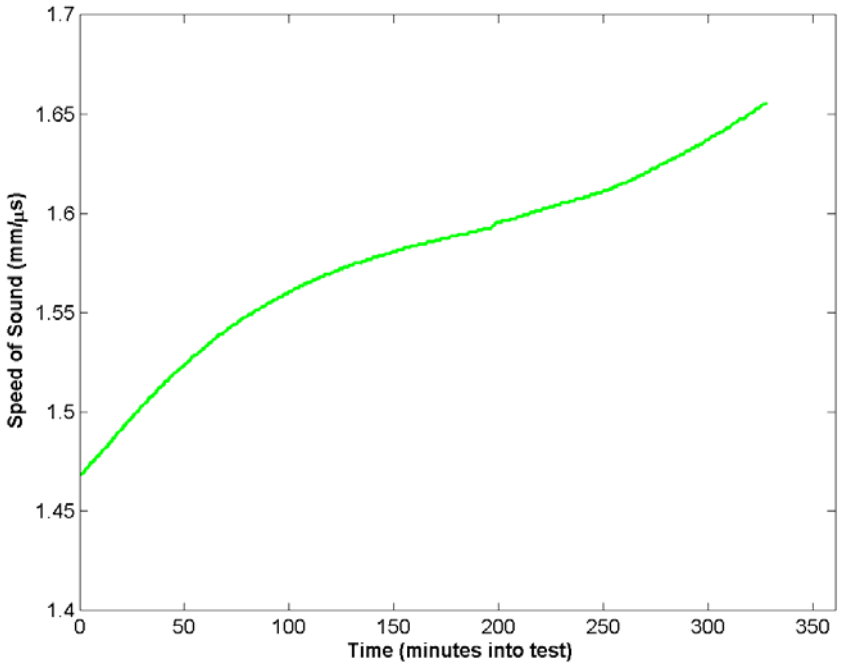

Figure 4. 66: Typical plot of the speed of sound vs. time at ultrasound channel 3 recorded for the duration of the small geometry chocolate testing.

Chapter Four, Section 4.2 Predicting the Temperature Using Speed of Sound

The plot of speed of sound vs. temperature for ultrasound channel 1 is shown in Figure 4. 67. The speed of sound begins at 1.45mm/μs at 58°C and increases linearly as the chocolate cools to 1.58mm/μs at 25°C. At this point the chocolate has reached room temp at thermocouple depth but the speed of sound continues to increase as some of the warm chocolate in the middle of the container continues to cool. Just as with the speed of sound vs. time plots shown in Figure 4. 64 - Figure 4. 66 the speed of sound vs. temperature plots for the other channels are identical to the channel 1 plot as shown in Figure 4. 67 and Figure 4. 68.

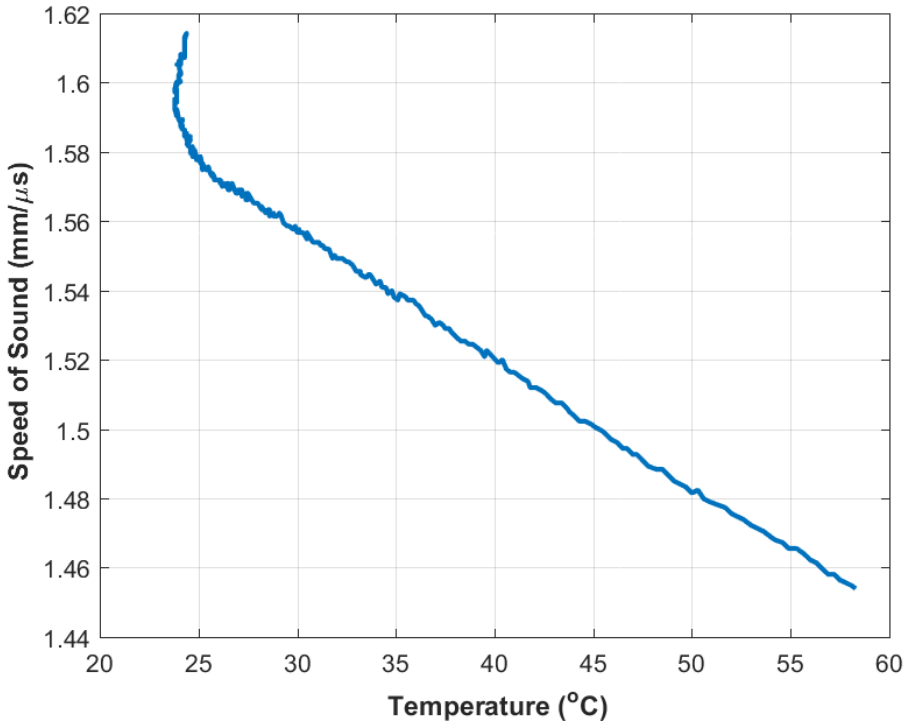

Figure 4. 67: The plot of the speed of sound vs. temperature for ultrasound channel 1 during the cooling portion of the small geometry chocolate test.

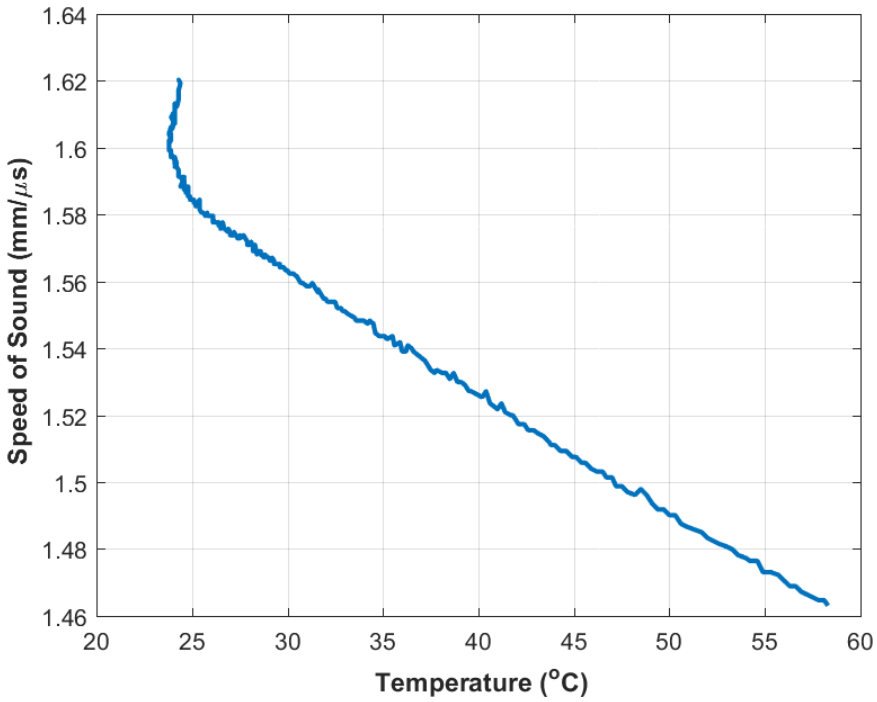

Figure 4. 68: The plot of the speed of sound vs. temperature for ultrasound channel 2 during the cooling portion of the small geometry chocolate test.

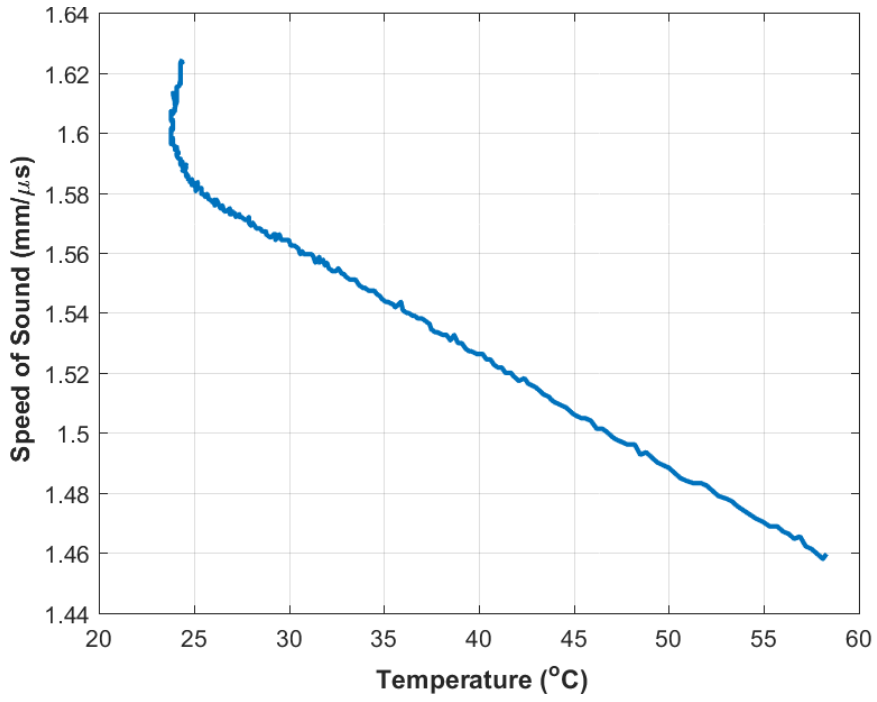

Figure 4. 69: The plot of the speed of sound vs. temperature for ultrasound channel 3 during the cooling portion of the small geometry chocolate test.

Using the speed of sound vs. time plot shown in Figure 4. 64 and the speed of sound vs. temperature plot shown in Figure 4. 67 a temperature profile can be estimated for the ultrasound channel 1 region. The speed of sound begins at 1.45mm/μs which would correspond to a temperature of about 60°C. The initial slope of the speed of sound indicates a quick decrease in the temperature transitioning to a more steady decrease at around 125 minutes at about 30°C. The speed of sound then continues to increase as the internal material continues to cool until the chocolate reaches room temperature.

Chapter Four, Section 4.3 Temperature Profile Confirmation

The temperature profiles for all thermocouple bars are shown in Figure 4. 70 - Figure 4. 72. The temperature profiles for all thermocouple bars are identical. The temperature begins at 60°C and drops to about 30°C in 125 minutes. After that the plot levels out and the temperature decreases to 25°C for the remaining 200 minutes of the test. This profile matches the prediction from Chapter Four, Section 4.2, demonstrating the abilities of the speed of sound to estimate temperature. Considering the accuracy of the small geometry Ecosoya testing shown in Table 4. 4 and the nearly identical trends in the speed of sound vs temperature plots shown in Figure 4. 66 - Figure 4. 69 it is reasonable to estimate the temperature within ±1.5°C for a given speed of sound value.

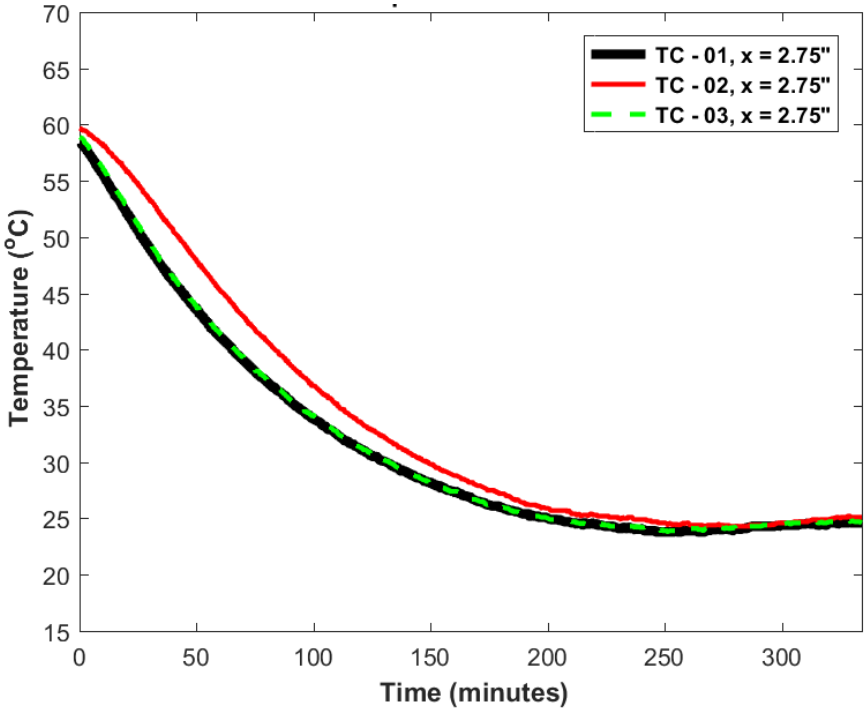

Figure 4. 70: The temperature profile measured by the bar 1 thermocouples during a small geometry chocolate test.

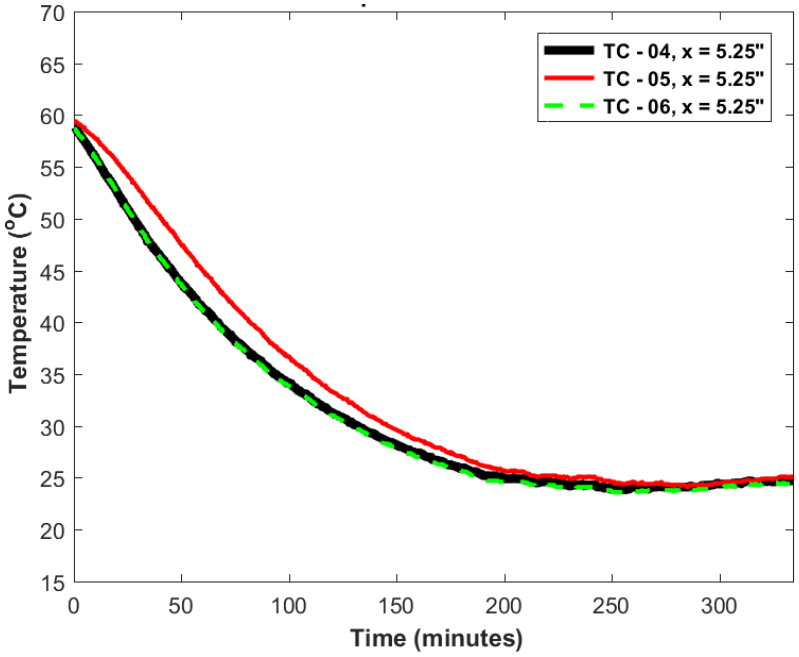

Figure 4. 71 The temperature profile measured by the bar 2 thermocouples during a small geometry chocolate test.

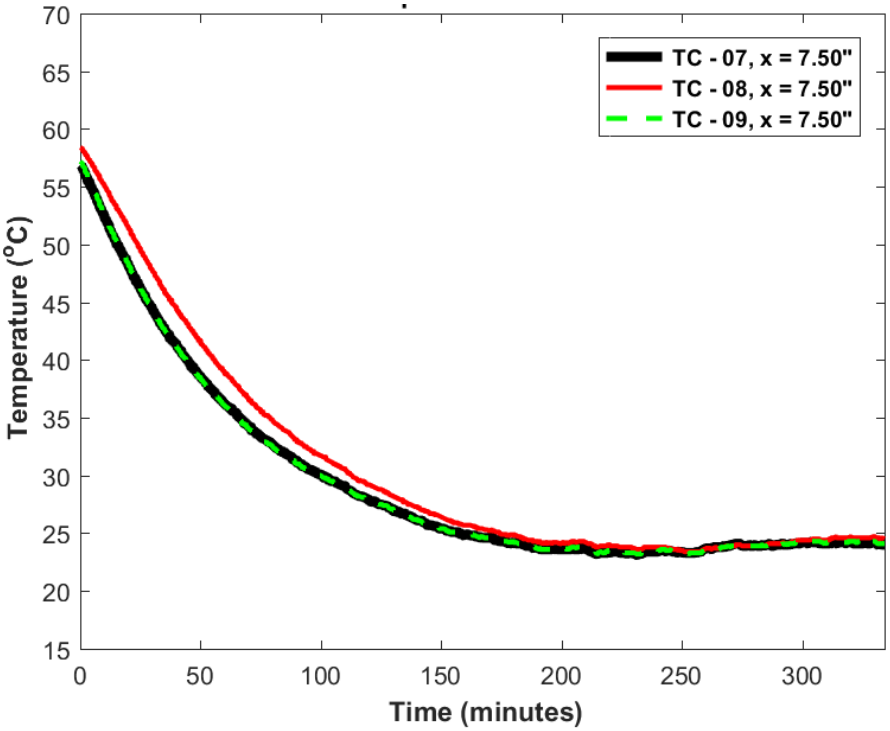

Figure 4. 72 The temperature profile measured by the bar 3 thermocouples during a small geometry chocolate test.

CHAPTER FIVE

Conclusions and Future Work

The goal of this thesis was to demonstrate the effectiveness of using through transmission ultrasound methods to estimate the temperature of a material within a confined vessel and to detect the occurrence of phase changes. In order to accomplish this a custom experiment was built using an array of up to eight one inch diameter 0.5MHz ultrasound transducers to measure the time of flight of a soy based candle wax (Ecosoya), a base paraffin wax, and baking chocolate as they were melted and then cooled. From the observed changes in speed of sound with temperature it was found that the temperature could be estimated within 4°C as was shown in Tables 4.2, 4.4, and 4.6.

Chapter Five, Section 1: Scientific Contributions

The main scientific contribution of this thesis is the proposed method for using through transmission ultrasound measurements of speed of sound to non-invasively estimate temperatures and detect phase changes for Ecosoya, a soy based candle wax, within a confined vessel. Measured times of flight were used to calculate the instantaneous speed of sound of the material at different temperatures and across different physical phases. An array of up to 29 thermocouples was used to confirm temperature estimates from the speed of sound measurements. Plots of the speed of sound vs. temperature were used with the speed of sound vs. time plots to estimate the material's temperature given a measured speed of sound. Phase changes were marked by large changes in the speed of sound during the melting process and by a change in the slope of

the speed of sound vs. temperature plots during the cooling process. It was found that the temperature estimates from the ultrasound measurements were accurate to within 4°C as shown in Table 4. 2.

A second experimental set up with a smaller geometry was created (diagram shown in Figure 3. 23 to speed up the 9 hour tests as well as confirm that the results from the larger geometry tests were not geometry dependent. This set up used four ultrasound transducers and 10 thermocouples. The temperature estimates from the small geometry experiments proved to be accurate within 1.5°C, more accurate than the large geometry testing as shown in Table 4. 4.

The same methods were then applied to samples of base paraffin wax and baking chocolate. These different materials have their own complications such as two detectable material property changes with the base paraffin wax (see the DSC testing in Figure 3. 38 and Figure 3. 40) or the chocolate not sufficiently transferring heat to melt across the box (see Figure 4. 61). Despite the differences in the materials, the temperature estimates were accurate within 4°C for the base paraffin wax (see Table 4. 6), and within 1.5°C for the chocolate. The ultrasound measurements were also able to detect multiple phase changes in the base paraffin wax.

The proposed method for estimating temperature and detecting phase change could be used in several applications across multiple industries. One possible application is in food and beverage production where monitoring the temperature of materials during production by contact with temperature probes or detecting the phase of the material by opening the container for visual observation may introduce contamination. The method could also apply in thermoset composite manufacturing by monitoring the temperatures

and phase of the thermoset resin during the curing process of composite materials in real time by monitoring the speed of sound through the metal tooling without the need for an internal temperature probe. The method is viable in most situations where an internal temperature measurement for a contained material is needed, but it is undesirable to breach the container.

Chapter Five, Section 2: Future Work

One improvement that could be made to the experiment is to automate the manual gain changes and eliminate the need for continuous operator presence. This could be done by creating a program that monitors the signal intensity of the A-scans in real time and adjust the gain such that the maximum signal intensity would remain at a pre-set value. This would allow the speed of sound plots to be smoothed and eliminate the time of flight measurement point from jumping from signal peak to signal peak causing the measured speed of sound to change. This would improve the accuracy of the temperature estimates and the detection of phase change.

Further investigation is needed to determine the source of the slowest signal which appears in Figure 4. 12 and Figure 4. 28 for the Ecosoya as the melt front is in the acoustic path. A possible explanation for this signal is a Rayleigh or surface wave formed as the signal impacts the interface of the solid and liquid wax. To test this hypothesis the Rayleigh wave speed was estimated using the Poisson's ratio (ν) and shear speed of sound (c_s) [1] in the Ecosoya as:

$$c_R = \frac{0.862 + 1.14\nu}{1 + \nu} * c_s \tag{5.1}$$

Because the Poisson's ratio and shear speed of sound for Ecosoya are not known they are estimated as 0.3 to 0.4 for Poisson's ratio (a standard range covering many materials), and a range of 40% to 70% of the longitudinal speed of sound for the shear speed of sound. The estimated Rayleigh wave speed is then used to predict a time of flight for both the large and small geometry systems. This time of flight over the ranges for the Poisson's ratio and shear speed of sound are shown by the surface plots in Figure 5.1 and Figure 5.2. The measured time of flights for the signals are 140μs for the large geometry setup and 90μs for the small geometry setup. This would indicate shear speeds of sound of 1mm/μs for the large geometry system and 0.8mm/μs for the small geometry system. Due to the discrepancy in the shear speeds of sound it is not certain that the signal is that of a Rayleigh wave, but it is in the correct range for time of flight to possibly be a Rayleigh wave. Further study into the shear speed of sound is needed to confirm the source of these signals.

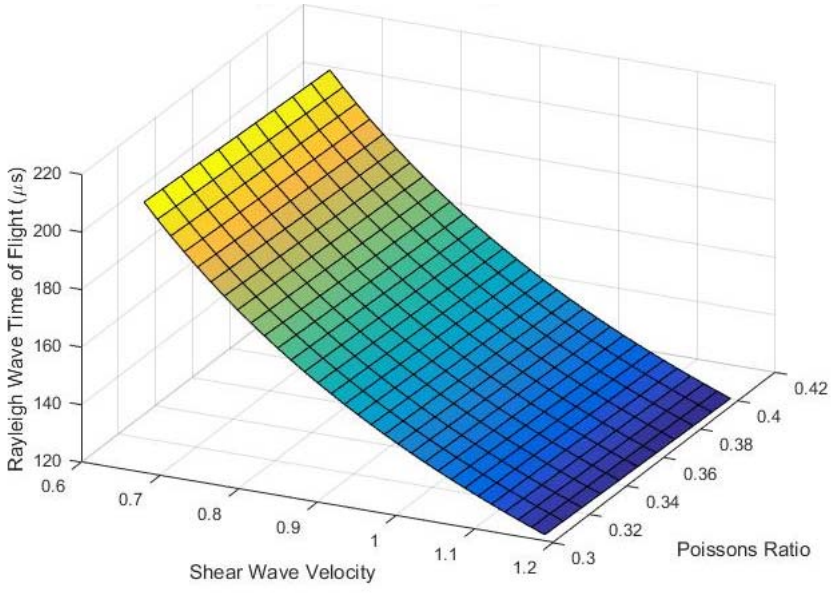

Figure 5. 1: Estimated time of flight for a Rayleigh wave, large geometry set up.

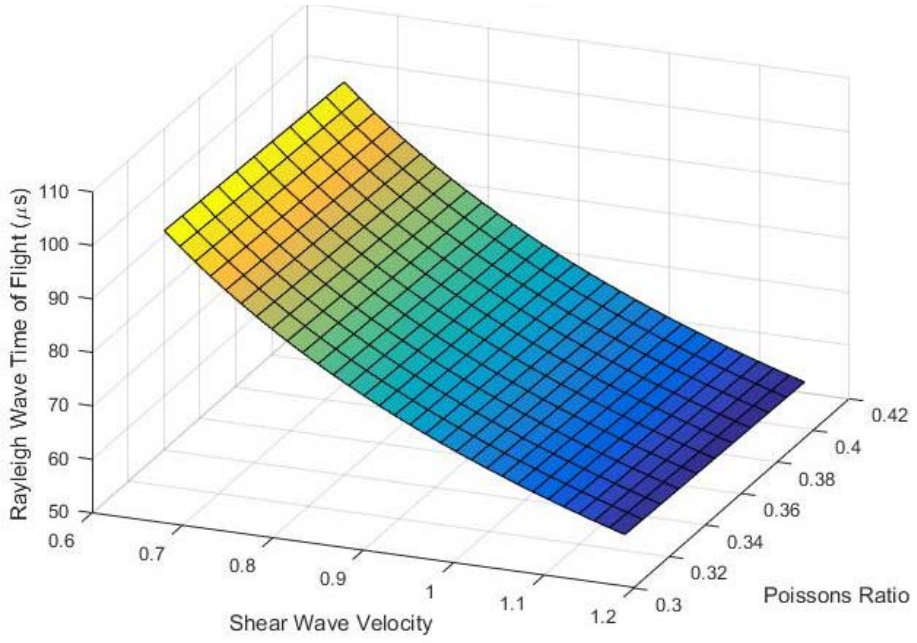

Figure 5. 2: Estimated time of flight for a Rayleigh wave, small geometry set up.

The temperature estimates presented in this thesis were obtained from the speed of sound of the materials measured during cooling due to the material within the acoustic path melting too quickly for changes of the speed of sound for the heating solid wax to be captured. Due to the hysteresis seen in the melt temperature during DSC testing for all materials (see Chapter Three, Section 4) it is possible that the heating side of the speed of sound as a function of temperature plot shifted vertically from the cooling side. A Quasi-static test of the materials in their solid state from room temperature to just below the melt temperature where the speed of sound is measured at each set temperature could be used to test this hypothesis.

The ability to cool the material past room temperature would allow for testing more materials like the bakers chocolate which have a phase change below room temperature. This would require a small temperature controlled chamber to encase the container while allowing the wiring to be run to the computer. This would allow for

further studies of materials that are oils or liquids at room temperature but harden when chilled, such as water freezing or coconut oil hardening.

The continued testing of materials with varying melt, solidification, and acoustic properties is vital to determining what the limits of the method are and what modifications can be made to account for these limitations. For example, modifying the method to use pulse-echo ultrasound techniques could allow the estimate of part temperature and the degree of cure for composite laminates manufactured using vacuum bagging methods. A contact transducer could be adhered to the bottom of the metal tool such that changes in the time of flight can be measured from the signal reflected off of the far side of the composite laminate as the resin hardens. A method for eliminating the ringing of the ultrasound signal caused by the metal tool such as the multi-layer transducer method [5] or signal subtraction would also need to be implemented.

Composite materials that consist of small particles suspended in another material may also be of interest. Initial testing of this type of material might be done by adding in aggregate to the Ecosoya wax such as glass micro-spheres. This would require some testing to determine how the newly introduced aggregate effects the ultrasound signal. It is likely that due to increased attenuation from ultrasound waves reflecting off of the particulates a shorter acoustic path or a higher intensity signal will be required. This testing would be the first step toward analyzing materials such as curing concrete which generally contains a large amount of aggregate material or possibly the polymer melt of fiber reinforced thermoplastics.

REFERENCES

[1] L. W. Schmerr, Fundamentals of ultrasonic nondestructive evaluation: a modeling approach. New York: Plenum Press, 1998.

[2] "Community College Ultrasonic Testing." [Online]. Available: https://www.nde-ed.org/EducationResources/CommunityCollege/Ultrasonics/cc_ut_index.htm. [Accessed: 27-Oct-2016].

[3] T. Tuziuti, A. Tsuge, M. Nishida, and W. Kanematsu, "Measurement of speed of sound in poly(lactic acid)-clay composite," Ultrasonics, vol. 54, no. 4, pp. 1010–1014, Apr. 2014.

[4] P. j. Rae and E. n. Brown, "Some Observations on Measuring Sound Speeds in Polymers Using Time-of-Flight," Exp. Tech., p. n/a-n/a, Aug. 2015.

[5] T. Rommetveit, T. F. Johansen, and R. Johnsen, "Using a multi-layered transducer model to estimate the properties of paraffin wax deposited on steel," Ultrasonics, vol. 51, no. 1, pp. 85–93, Jan. 2011.

[6] E. C. Brown, P. Olley, and P. D. Coates, "In line melt temperature measurement during real time ultrasound monitoring of single screw extrusion," Plast. Rubber Compos., vol. 29, no. 1, pp. 3–13, Jan. 2000.

[7] B. Praher, K. Straka, and G. Steinbichler, "An ultrasound-based system for temperature distribution measurements in injection moulding: system design, simulations and off-line test measurements in water," Meas. Sci. Technol., vol. 24, no. 8, p. 84004, Aug. 2013.

[8] K. Christidis and G. P. P. Gunarathne, "Temperature compensation for ultrasound measurements and characterization of materials," IEEE Trans. Instrum. Meas., vol. 52, no. 5, pp. 1520–1527, Oct. 2003.

[9] Y. Jia, V. Chernyshev, and M. Skliar, "Ultrasound measurements of segmental temperature distribution in solids: Method and its high-temperature validation," Ultrasonics, vol. 66, pp. 91–102, Mar. 2016.

[10] Y. Jia and M. Skliar, "Noninvasive Ultrasound Measurements of Temperature Distribution and Heat Fluxes in Solids," Energy Fuels, vol. 30, no. 5, pp. 4363–4371, May 2016.

[11] A. A. El-Sariti, J. A. Evans, and J. G. Truscott, “The temperature dependence of the speed of sound in bovine bone marrow at 750 kHz,” Ultrasound Med. Biol., vol. 32, no. 6, pp. 985–989, Jun. 2006.

[12] G. Benedetto, R. M. Gavioso, P. A. G. Albo, S. Lago, D. M. Ripa, and R. Spagnolo, “Speed of Sound in Pure Water at Temperatures between 274 and 394 K and at Pressures up to 90 MPa,” Int. J. Thermophys., vol. 26, no. 6, pp. 1667–1680.

[13] S. Hoche, M. A. Hussein, and T. Becker, “Critical process parameter of alcoholic yeast fermentation: speed of sound and density in the temperature range 5–30 °C,” Int. J. Food Sci. Technol., vol. 49, no. 11, pp. 2441–2448, Nov. 2014.

[14] D. Zou, K. L. Williams, and E. I. Thorsos, “Influence of Temperature on Acoustic Sound Speed and Attenuation of Seafloor Sand Sediment,” IEEE J. Ocean. Eng., vol. 40, no. 4, pp. 969–980, Oct. 2015.

[15] P. A. Oliveira, R. M. B. Silva, G. C. Morais, A. V. Alvarenga, and R. P. B. C.-Félix, “Speed of sound as a function of temperature for ultrasonic propagation in soybean oil,” J. Phys. Conf. Ser., vol. 733, no. 1, p. 12040, 2016.

[16] F. Yebra, J. Troncoso, and L. Romaní, “Fully automatized apparatus for determining speed of sound for liquids in the temperature and pressure interval (283.15–343.15) K and (0.1–95) MPa,” J. Chem. Thermodyn., vol. 104, pp. 102–109, Jan. 2017.

[17] A. Kon, K. Mizutani, and N. Wakatsuki, “Noncontact Measurement of Humidity and Temperature Using Airborne Ultrasound,” Jpn. J. Appl. Phys., vol. 49, no. 4, p. 46601, Apr. 2010.

[18] T. M. Whitney and R. E. Green, Jr., “Nondestructive Characterization of Cure Enhancement by High Power Ultrasound of Carbon Epoxy Composites,” Mater. Sci. Forum, vol. 210–213, pp. 695–702, 1996.

[19] S. Thomas, C. Bongiovanni, and S. R. Nutt, “In situ estimation of through-thickness resin flow using ultrasound,” Compos. Sci. Technol., vol. 68, no. 15–16, pp. 3093–3098, Dec. 2008.

[20] L. Svilainis, A. Rodriguez, D. Liaukonis, and A. Chaziachmetovas, “Assessment of Ultrasound Velocity Application for Chemical Process Monitoring,” Elektron. Ir Elektrotechnika, vol. 21, no. 4, Aug. 2015.

[21] F. Lionetto and A. Maffezzoli, “Monitoring the Cure State of Thermosetting Resins by Ultrasound,” Materials, vol. 6, no. 9, pp. 3783–3804, Sep. 2013.

[22] M. Jaunich and W. Stark, “Monitoring the vulcanization of rubber with ultrasound: Influence of material thickness and temperature,” Polym. Test., vol. 28, no. 8, pp. 901–906, Dec. 2009.

[23] N. H. Abu-Zahra, “Real-time viscosity and density measurements of polymer melts using dielectric and ultrasound sensors fusion,” Mechatronics, vol. 14, no. 7, pp. 789–803, Sep. 2004.

[24] N. H. Abu-Zahra, “Measuring melt density in polymer extrusion processes using shear ultrasound waves,” Int. J. Adv. Manuf. Technol., vol. 24, no. 9–10, pp. 661–666, Nov. 2004.

[25] D. Wang and K. Min, “In-line monitoring and analysis of polymer melting behavior in an intermeshing counter-rotating twin-screw extruder by ultrasound waves,” Polym. Eng. Sci., vol. 45, no. 7, pp. 998–1010, Jul. 2005.

[26] C.-C. Cheng, H. Banakar, B.-T. Ooi, and C.-K. Jen, “Melting Quality of Polymers in Internal Mixer Diagnosed by Ultrasound,” Int. Polym. Process., vol. 24, no. 5, pp. 375–383, Nov. 2009.

[27] L. Zhao, Y. Lai, C. Pei, C.-K. Jen, and K.-D. Wu, “Real-time diagnosing polymer processing in injection molding using ultrasound,” J. Appl. Polym. Sci., vol. 126, no. 6, pp. 2059–2066, Dec. 2012.

[28] E. Walker, D. Reyes, A. Krokhin, and A. Neogi, “Anomalous temperature dependence of speed of sound of bulk poly(N-isopropylacrylamide) hydrogels near the phase transition,” Ultrasonics, vol. 54, no. 5, pp. 1337–1340, Jul. 2014.

[29] A. Mizrach, “Determination of avocado and mango fruit properties by ultrasonic technique,” Ultrasonics, vol. 38, no. 1–8, pp. 717–722, Mar. 2000.

[30] P. Llull, S. Simal, A. Femenia, J. Benedito, and C. Rosselló, “The use of ultrasound velocity measurement to evaluate the textural properties of sobrassada from Mallorca,” J. Food Eng., vol. 52, no. 4, pp. 323–330, May 2002.